The Effect of Nanobubble and Nanodroplet Interfaces on Protein Stability and Aggregation in Therapeutic Protein Formulations

By

Jared Richard Snell

B.S., Worcester Polytechnic Institute, 2013

M.S., University of Colorado-Boulder, 2016

A thesis submitted to the

Faculty of the Graduate School of the

University of Colorado in partial fulfillment

of the requirements for the degree of

Doctor of Philosophy

Department of Chemical and Biological Engineering

2019

This thesis entitled:
The Effect of Nanobubble and Nanodroplet Interfaces on Protein Stability and Aggregation in Therapeutic Protein Formulations
written by Jared Richard Snell
has been approved by the Department of Chemical and Biological Engineering

Dr. Theodore W. Randolph

Dr. John F. Carpenter

Date_____

The final copy of this thesis has been examined by the signatories, and we find that both the content and the format meet acceptable presentation standards of scholarly work in the above mentioned discipline

Jared Richard Snell (Ph.D., Chemical and Biological Engineering)

The Effect of Nanobubble and Nanodroplet Interfaces on Protein Stability and Aggregation in Therapeutic Protein Formulations

Thesis directed by Professor Theodore W. Randolph

Interfaces presented by subvisible particulate contaminants may reduce protein stability potentially compromising the efficacy and safety of therapeutic protein formulations. However, minimal guidelines are provided for the characterization and control of particulates smaller than 10 μm in therapeutic protein formulations. In this work we investigated generation of nanobubbles and bis(2-ethylhexyl) phthalate (DEHP) droplets in therapeutic protein formulations and their effect on protein stability and aggregation.

Nanobubbles generated upon reconstitution of lyophilized protein formulations not only serve as a source of subvisible particles but also reduce protein stability, promoting aggregation and particle formation. We show that Interluekin-1 receptor antagonist (IL-1ra) adsorbs readily to the nanobubble air-water interface resulting in significant changes in nanobubble surface charge. Further, incubating IL-1ra in nanobubble suspensions resulted in rapid particle formation and monomer loss. These results suggest nanobubbles generated during reconstitution of lyophilized protein formulations may compromise protein stability.

To develop a strategy for minimizing nanobubble formation and its associated protein aggregation we evaluated the mechanism responsible for nanobubble formation upon reconstitution of lyophilized protein formulations. We hypothesized that nanobubble formation was dependent on nano-sized voids which may originate from small ice crystals generated within the freeze concentrated liquid during freezing. Correlations between nanobubble concentrations following reconstitution of lyophilized formulations and excipient crystallinity in the lyophilized solid suggests excipient crystallization could contribute to nano-void formation. Inhibiting

excipient crystallization was an effective strategy for minimizing nanobubble generation in lyophilized formulations. This strategy for decreasing nanobubble formation also reduced the formation of insoluble protein particle during reconstitution.

Finally, we showed that DEHP droplets shed from polyvinyl chloride (PVC) IV bags could serve as a source of subvisible particulate contaminants in therapeutic protein formulations diluted and administered using these products. Intravenous immunoglobulin (IVIG) adsorbed readily to droplets of emulsified DEHP. Adsorbed protein formed viscoelastic films at the DEHP-water interface which may contribute increased aggregation rates observed in rotated samples of IVIG containing DEHP. Activation of the complement system by IVIG formulations containing DEHP droplets suggests DEHP droplets could contribute to the frequency of infusion reactions following administration of therapeutic protein formulations.

Dedicated to Wesley G. Chadbourne

Acknowledgements

First, I would like to thank my advisor, Dr. Ted Randolph, for the opportunity to conduct research in his lab over the past 5 years. He was always available for a discussion no matter what the research problem might be. Also, I would like to thank my committee members, Dr. Joel Kaar, Dr. Andrew Goodwin, Dr. Jerome Fox and Dr. John Carpenter. I would especially like to thank Dr. Carpenter, as his extensive knowledge of the biopharmaceutical industry was extremely helpful in the development of my research projects.

I spent countless hours using the particle characterization instruments in the Carpenter Lab and I am extremely grateful for help from the graduate students and postdocs there including; Dr. Aaron Krueger, Maraline Adarsha, Dr. Aditya Gandhi, Dr. Cheng Her, Dr. Chen Zhou and Dr. Vaida Linkuviene. In addition, I would like to thank past and present members of the Randolph lab for always being available for a discussion or for trouble shooting an instrument problem. I am especially indebted to Hao Wu, Austin Daniels, James Weltz and Dr. Ben Barthel for all their help and advice during my graduate career.

While it seems like I spent most of my 5 years in Boulder working in lab there are a few people who made my graduate experience infinitely more enjoyable. Dr. Joe Plaks and Sam Summers for always being someone to complain with or to about graduate school. Ryan Smyth for always being willing to organize a happy hour.

Lastly, I would like to thank my family for all their encouragement and support over the past five years. Especially, my parents, Richard and Suanne Snell, for fostering my interest in science from a young age. I could not have gotten to this point without them.

Table of Contents

List of Tables

List of Figures

Chapter 1 Introduction

1.1 Proteins as Therapeutic Agents

Proteins are highly complex biological macromolecules which accomplish diverse and highly specific functions within the human body. Protein functions within the human body range from catalysis of biochemical reactions to the formation of receptors and channels within cell membranes.[1] The capability of proteins to accomplish diverse biological functions results from the complex relationship between protein structure and function. All proteins are composed of the same 26 amino acids. However, the exact sequence of amino acids in the primary sequence will dictate the higher order three-dimensional structure of the protein and ultimately the protein's function. This relationship between structure and function of proteins make these biomolecules ideal candidates for therapeutic applications. Proteins provide distinct advantages over small molecule-based drugs based on their highly complex and specific functions. This specificity helps to lower the potential for interference with normal biological functions reducing the probability of adverse side effects compared to small molecule drugs.

Therapeutic proteins are currently used to treat a variety of human diseases and disorders with applications ranging from the replacement of deficient native proteins, such as insulin for treatment of diabetes, to altering diseases processes including treatment of multiple sclerosis, hepatitis and cancer.[2] Resulting from their diverse potential applications, therapeutic proteins are a rapidly growing area of the pharmaceutical industry. Since the approval of the first therapeutic protein manufactured with recombinant DNA technology by the U.S. Food and Drug administration in 1982, the use of therapeutic proteins has been rapidly expanding. By 2005 there were over 160 biopharmaceutical products on the market with annual sale exceeding 30 billion dollars.[3] Following the introduction of the first therapeutic protein products in the 1980s, protein has been engineered to further increase their clinical potential by increasing efficacy while

reducing the possibilities for adverse immune responses. In addition, engineered proteins have expanded the use of therapeutic proteins from replacement of endogenous proteins to the development of proteins which provide novel functions such as interfering with molecules or organisms or delivering payloads such as cytotoxic drugs.[4] Despite significant advances resulting in the development of new biological products significant challenges still surround the production of safe and efficacious therapeutic protein products.

1.2 Stability of Therapeutic Proteins

One of the most significant challenges associated with the development of therapeutic proteins is their marginal stability and propensity to aggregate when stressed. This marginal stability is attributed to the minimal difference in free energy between native and unfolded protein states which are typically on the order of only 50 kJ/mol.[5,6] A protein's native structure results from a delicate balance between stabilizing and destabilizing forces. Intramolecular interactions between amino acid residues dictate the higher order protein structure and stabilize a protein's native structure. These interactions include hydrophobic interactions, electrostatic interactions, hydrogen bonding, and van der waals forces.[7] These stabilizing forces are opposed by losses in conformational entropy resulting from significant reductions in translation, rotational and vibrational degrees of freedom in the protein's native state compared to the unfolded state.[8] This balance of destabilizing and stabilizing forces is highly dependent on the protein's local environment including pH, ionic strength, excipients and temperature.[9,10] Therefore, proper formulation and storage conditions are crucial for maintaining a protein in its native conformation.

When administered to patients, therapeutic protein products must be chemically as well as conformationally pure.[11] Therapeutic proteins native conformation must be maintained throughout manufacturing, shipping, and storage. For a therapeutic protein to be economically viable, it must

remain stable for 18-24 months when stored as the final drug product.[11] Loss of native protein structure or aggregation and particle formation during storage or handling can have severe clinical implications ranging from reduced biological efficacy to severe immune responses potentially leading to anaphylaxis and even death.[11–13]

Maintaining a protein's native structure and inhibiting aggregation from manufacturing to administration is a significant challenge which requires extensive knowledge of stresses which may be incurred during manufacturing, shipping, storage and handling of a therapeutic protein product. The development of a successful therapeutic protein products requires that the product is capable of maintaining conformational stability throughout its shelf life.[14] Achieving a conformationally stable product requires the development of a protein formulation in which a protein will maintain its native secondary, tertiary and quaternary structure when exposed to a wide range of conditions.[15,16] The development of an optimized therapeutic protein formulation requires extensive knowledge of stresses the product will be exposed to prior to administration. Below we have briefly reviewed major stresses encountered by proteins and formulation-based strategies that can be employed to minimize their impact on protein stability.

The thermostability of therapeutic proteins is an important property used in the selection and development of biological drug products. As proteins are only marginally stable, proteins can be destabilized at even moderate temperatures resulting in thermal denaturation.[17,18] Resulting from the nature of the intramolecular interactions stabilizing their high order structure, proteins typically have relatively low melting temperatures and are usually recommended to be stored at a temperature between 4-8 °C. Elevated temperatures will induce local unfolding and subsequent exposure of hydrophobic residues can induce rapid aggregation and particle formation.[14,19,20]

The combination of interfaces and shear is one of the leading causes of structural perturbations and aggregation in protein formulations.[21–23] Protein is amphiphilic molecules with hydrophobic and hydrophilic regions and therefore absorbed readily at interfaces.[5,24] Furthermore protein adsorption to interfaces can result in irreversible denaturation.[25] When proteins adsorb to hydrophobic interfaces such as air-water or oil-water interfaces, hydrophobic region previously buried within the protein interior may reorientate to contact the hydrophobic interface resulting in significant structure perturbations.[26,27] Changes in protein structure following adsorption to interfaces may lead to protein aggregation and gelation at interfaces.[28–30] Protein gels layers formed at interfaces resulting from protein-protein intermolecular interaction including hydrogen bonding which may promote formation of non-native intermolecular β-sheet structures.[31,32] Gelled protein layers when disrupted by fluid shear forces can be shed into the bulk solutions resulting in the generation of insoluble protein particles and significant monomer loss.[23,33,34]

Between various processing steps during manufacturing, therapeutic proteins may be frozen to reduce rates of protein degradation as the protein is immobilized in the frozen matrix.[14] In addition, during storage therapeutic proteins may be intentionally or unintentionally frozen. While protein stability is typically improved in a frozen state, a number of destabilizing events can occur during freezing including solute concentration, phase separation, pH changes and formation of ice-water interfaces.[35] During freezing protein and formulations components will be concentrated in the non-ice phase.[14] Increases in solute concentrations combined with pH shifts induced by crystallization of buffer components, such as phosphate buffers, can result in significant perturbations in protein structure.[36] Furthermore, during freezing excipient crystallization can separate protein from stabilizing additives.[35] As well as changes in the protein

local environment, freezing can also generate damaging ice-water interfaces which may induce protein structure perturbation and aggregation upon adsorption.[37]

Proper handling of therapeutic proteins is crucial for maintaining a conformationally pure product as well as preventing protein aggregation and particle formation. As discussed above, interfacial shear caused by agitation of protein formulations can induce particle formation. In addition, mechanical shock caused by dropping vials can also promote protein aggregation. Cavitation results from the violent collapses of cavities generated by high-pressure shockwave during mechanical shock.[38] During the collapse of these cavities, regions of extremely high temperature and pressure are generated as well as reactive hydrogen and hydroxyl radicals.[39,40] The conditions generated during these cavitation event caused by dropping can induce protein aggregation as well as oxidative damage. However, cavitation events are concentrated to an extremely small volume, and therefore negligible changes in protein concentration were observed.[41] However even a small number of protein aggregates and oxidized species induced by cavitation could compromise product safety and efficacy.

To minimize structural perturbations and aggregation in protein formulations various strategies may be employed to minimize the impact of various environmental stresses. The first strategy is often to minimize the occurrence of each stress. For example, biological manufacturers will minimize the number of freeze-thaw cycles protein are submitted to during manufacturing and provide clear package labeling regarding the recommended storage temperatures. However, not all stresses can be avoided entirely, and manufacturers have limited control over the handling and storage of their products after shipping.[42]

Formulation based strategies are also employed to minimize the destabilizing effect of various stresses and to maintain product quality and integrity throughout manufacturing, shipping

and storage.[7] To limit the extent of damage incurred by interfaces such as during agitation or freezing many protein formulations include surfactants. Surfactants will compete with proteins for adsorption at interfaces reducing the degree of protein aggregation, and gelation.[28,43,44] For thermally unstable proteins stabilizing excipient are often added to increase the free energy of protein unfolding.[14] Common stabilizing excipients include sugars which are excluded from adsorbing to the protein surface. This negative adsorption increases the free energy of the unfolded state making increases in surface area caused by protein unfolding energetically unfavorable.[45,46] Finally, rates of protein aggregation can be reduced by optimizing formulation conditions such as pH and ionic strength. Proteins are typically formulated as far from their isoelectric points as possible to increase net charge and therefore electrostatic repulsions between proteins. While a variety of methods have been developed to improve the robustness of protein conformation stability, not all stresses can be solved through formulation strategies. Therefore, maintaining a conformationally pure product is also dependent on ensuring the protein is handled and stored correctly.

1.3 Immunogenicity of Therapeutic Protein Formulations

One of the most significant factors impacting the efficacy and safety of therapeutic proteins is the potential for immune responses targeting administered products.[47–49] Immune responses typically involve the generation of neutralizing antibodies which target the therapeutic protein significant reducing the product half-life and altering pharmacokinetics.[47] In addition to reduced efficacy immune response can result in severe complications if neutralizing antibodies also target the patient's endogenous proteins with non-redundant functions. Furthermore, adverse immune responses can result in anaphylaxis and in severe cases fatalities.[50] As nearly all therapeutic proteins have been shown to have the capability of inducing immune responses, which may

compromise both product efficacy and safety, minimizing the immunogenicity of the therapeutic protein product is a significant goal biological manufactures and regulators.[51–54]

In modern therapeutic protein products using recombinant DNA technology, the frequency of immune response are low compared to early animal-derived products and immune response are often not associated with severe clinical consequences.[2] However, there have been multiple recent examples of immune response elicited against administered therapeutic protein products including interferon-α, recombinant human erythropoietin (EPO), factor VIII.[53] The clinical consequences of immunogenicity have varied from reduced efficacy in the case of interferon-α to life-threatening adverse responses in the case of EPO. One of the most widely used examples of the severe clinical implications resulting from the immunogenicity of marketed therapeutic protein products occurred following administration of EPO. Erythropoietin based products were first approved in 1988 to treat patients with anemia associated with a deficiency in endogenous erythropoietin. However, it was later found that immune response targeting this product could induce pure red cell aplasia resulting from the generation of neutralizing antibodies following administration of EPO which targeted not only the drug product itself but the patient's endogenous erythropoietin. This generation of anti-erythropoietin antibodies resulted in undetectable levels of erythropoietin in patients and the development of transfusion-dependent anemia.[53] The serious clinical consequences of immune response highlight the importance of understanding and minimizing the immunogenicity of therapeutic protein products.

Minimizing immunogenicity is a major goal of biological manufactures and regulators to assure both the safety and efficacy of therapeutic protein products.[49] The immunogenicity of early therapeutic protein products derived from animal source was first explained based upon differences in structure between human and animal proteins. However, it was later found that while

proteins derived from human tissues and plasma exhibited lower frequencies of immune responses, immune response was still observed.[55] Even recombinant proteins with structures nearly identical to native protein are capable of inducing an immune response.[56] As new therapeutic product begin to be developed with structures significantly different from those of native proteins it will become even more important to understand factors contributing to immunogenicity and develop strategy for minimizing immune responses. To attempt to reduce the immunogenicity of foreign protein several strategies have been implemented including pegylation, site-specific mutagenesis, exon shuffling and humanization of monoclonal antibodies.[57] It can be difficult to evaluate the effectiveness of these strategies as the immunogenicity of proteins are typically monitored using animal models in early stages of product development, however conventional animal models have been shown to have limited use for predicting immunogenicity in humans.[57,58] Therefore the actual frequency of immune response in humans for a therapeutic protein product is often not determined until the later stages of clinical trials or after the product is launched.[59]

Product quality, such as the extent of aggregation, deamination, and oxidation, contribute to the frequency of immune responses following administration of therapeutic protein products.[49,52,56,60–67] While many studies have established a connection between protein aggregation and immunogenicity, questions remain regarding what properties of protein aggregates promote interaction with immune cells and if all protein aggregates are inherently immunogenic. It has been shown that immunogenicity of protein aggregates may be dependent on various properties including size and protein structure within the aggregate.[59,68] Generation of neutralizing antibodies against a therapeutic product is dependent on the protein maintaining a near-native conformation upon aggregation.[56] The highly ordered and repeating arrays of native protein aggregates can lead to a strong B cell response and rapid activation of the immune

response.[69] Protein aggregation is also associated with perturbations in protein structures resulting in the exposure of hydrophobic region which promotes protein aggregates. This change in protein secondary and tertiary structure may cause the protein to be considered foreign by the immune system.[51]

1.4 Controlling Sub-Visible Particulate Contaminants in Therapeutic Protein Formulations

The effect of sub-visible particulate contaminants on the safety and efficacy of therapeutic protein products is of growing concern in the biopharmaceutical industry. Recently it was identified that lack of control of subvisible particulates in marketed biopharmaceutical products which could compromise the safety and efficacy of therapeutic protein products.[70] The primary guidance used by the biopharmaceutical industry for control of particulate matter in therapeutic protein products is provided by the United States Pharmacopeia (USP) chapter 787 and 788. This guidance dictates that upon release particulate matter in therapeutic protein products must not exceed 6000 particles per container larger than 10 µm and 600 particles per container greater than 25 µm.[71] This standard for the levels of particulate matter in released therapeutic protein products may not necessarily ensure product safety.[72] These regulations do not address particle levels in the 0.1 – 10 µm particle range which could have significant consequences for the immunogenicity of protein products.[70]

There is growing evidence showing connections between sub-visible particle in therapeutic protein products and immunogenicity. In an article published in 2013, Barnard et al. found that in marketed Interferon-β products the rate of neutralizing antibody formation during clinical studies correlated closely with the concentration of particles in each formulation.[73] Further evidence of the potential connection between particulate matter and immunogenicity was obtained when an erythropoietin peptide mimic was withdrawn from the market after 49 cases of anaphylaxis

including seven fatalities were reported.[74] During clinical trials, this product was both safe and efficacious contrary to the results observed within 1 year after the product was launched. This increase in immunogenicity was again shown to closely correlate with higher concentrations of sub-visible particles in the marketed multi-use formulation compared to the single-use formulation used during clinical trials. The growing evidence of connections between subvisible particulate matter and immunogenicity has emphasized the importance of controlling protein aggregate levels in therapeutic protein formulations.[75–77]

Particulate matter in therapeutic protein products can originate from a wide variety of sources and are classified as either intrinsic or extrinsic. The major source of intrinsic particulate matter in most protein formulations is aggregation of the drug product itself. Aggregation and particle formation is considered to be an inherent property of proteins and is present in all protein products to some extent.[78,79] Protein aggregates can span a wide size range from oligomers composed of just a few protein molecules to large aggregates up to 100s of μm in length. Aggregates have highly variable structures and morphologies which are often dependent on the type of stress applied and the specific protein. In addition to protein aggregation, non-proteinaceous particles may originate from various manufacturing unit operations or packaging materials.[80] For example, glass lamellae can be shed from glass vials while lubricants such as silicone oil have been found to shed from lubricated prefilled syringes.

While most studies of the immunogenicity of therapeutic formulations have focused primarily on protein aggregates, sub-visible non-proteinaceous particulates can also have a significant impact on product quality and immunogenicity. Particulate matter serves as an additional interface for protein to adsorb in which protein will adsorb typically until the surface is completely coated with a protein monolayer.[81] Even in formulations that are both

thermodynamically and colloidally in the bulk solution the presence of foreign surface can have significant destabilizing effects. Upon adsorption to these interface rearrangements in protein structure can occur resulting in increased rates of both protein degradation and aggregation.[82] Through a heterogeneous nucleation mechanism particulate matter can promote the nucleation of protein aggregation which will then grow into large aggregates can promote significant monomer loss in the bulk solution. For example, Chi et al. showed that silica nanoparticle could induce rapid aggregation of rhPAF-AH, while increase formation of soluble aggregates was observed when a monoclonal antibody was incubated with stainless steel microparticles.[81,82] Eliminating non-proteinaceous particulate matter such as metal or glass particles from a protein formulation may not always be practical as it may require the re-engineering of the material properties of containers, pumps, and tubing to attempt to eliminate particle shedding completely. However, biological manufacturers must be vigilant in monitoring the type of particulate matter present in their products and their impact on product stability.

The impact of sub-visible particle concentration below 10 µm on the safety and efficacy of therapeutic protein products has led to increased calls to better regulate and control particulate matter. However, the characterization of particulate contaminants poses formidable challenges for many existing particle characterization methods originally developed to measure non-proteinaceous particulates. In therapeutic protein products, the greatest source of particulate matter is often aggregation of the protein product itself. Protein particles can be difficult to detect and characterize resulting from significant differences in morphology, density and refractive index between proteinaceous particles and particle standards.

The primary method for characterizing particulate matter described in USP 787/788 is light obscuration.[83] In light obscuration instruments, a beam of light is passed through a flow cell with

a detector on the opposite side.[84] Particles passing through the flow cell obscure light and the reduction in light intensity are used to calculate particle sizes. This method provides data regarding the size and concentration of particles present in a formulation. However, light obscuration does not provide any information regarding particle morphologies and cannot differentiate between protein aggregate and other particulate contaminants. This method has significantly lower sensitivity than other characterization methods especially if the refractive index of a particle is similar to the surrounding media.[85,86], In the example of the erythropoietin mimic described above, light obscuration was not capable of detecting increased particle concentrations in formulations associated with increased immunogenicity.[74]

New particle characterization methods have begun to emerge which may provide opportunities to significantly improve characterization and control of sub-visible particulate contaminants in therapeutic protein products. Improvements in flow imaging technologies developed by Flowcam and MFI allows the acquisition of morphology information as well as concentration and size distribution during characterization of protein formulations.[86] Flow imaging techniques utilize a digital camera to acquire images of individual particles as they pass through a flow cell. Using flow images, proteinaceous particles can be differentiated from extrinsic particulates such as silicone droplets or air droplets.[87]

Flow imaging microscopy-based methods can characterize particles down to approximately 2 µm leaving a significant gap in the nanometer size range. To bridge this gap instruments have begun to be developed to measure particle concentrations and size distribution below 1 µm. Techniques such as nanoparticle tracking analysis allow particles a small as 10 nm to be analyzed. This method utilized as laser beam passed through the samples chamber and the scattering of light by these particles are used to track the movement of each particle individually.

The movement of individual particle can then be used to calculate particle diameters using the Stoke-Einstein equation.[88] Another technique developed to characterize particles below 1 µm is resonant mass measurement (RMM). Using the principal of resonant mass measurement, these instruments not only measure the concentration and size distribution of particles but can also differentiate between different particles base on their buoyancy. RMM can differentiate between particles whose densities are less than or greater than that of the bulk fluid based on changes in resonance frequency as particles pass through a resonating cantilever.[89] This process allows protein aggregates to be easily differentiated from positively buoyant particles such as air bubbles or silicone oil droplets.

While instruments are beginning to be developed which may allow the complete sub-visible particle size range to be characterized most of these instruments are still in early stages of development. Few if any new instruments have been validated for use in quality control applications in manufacturing. For industrial applications, new particle characterization instruments must allow for both high sample throughput and limited sample volumes.[90] These instruments would enable manufacturers to rapidly screen particle concentrations in early-stage product development as well as allows for formulation optimization. However, even when the technology does exist better characterize sub-visible particles in protein formulation questions remaining concerning exactly how particle concentration limits should be set.

While no new regulations have been developed particulate matter in therapeutic protein since USP 787/788 the regulatory perspective on this challenging problem of particle control is beginning to evolve. Regulators such as the FDA are starting to expect manufacturers to count and characterize particles below the 10 µm limit set in USP 787.[86] This push for characterization below 10 µm stems from the recognition that a lack of understanding of how particles impact both product

safety and efficacy constitutes a significant source of uncontrolled risk.[91] As instruments for particle characterization are developed and our knowledge of the effect of particle in-vivo improves we should expect to see substantial change in how the regulation of sub-visible particle in therapeutic protein formulations in the future.

1.5 Stabilization of Therapeutic Proteins in Freeze-Dried Solids

Lyophilization or freeze-drying is a commonly employed strategy to improve the long-term stability of proteins with unsatisfactory stability in aqueous formulations.[92,93] In freeze dried solids, proteins are maintained in a glassy state in which the rate of both physical and chemical degradation are significantly reduced. Inhibition of protein degradation in a lyophilized solid allows proteins with minimal stability in aqueous formulation to achieve acceptable shelf lives.[94] Lyophilization begins with freezing of the protein drug product in its final drug product container. Drug product is placed on the shelves of a freeze dryer, and the shelf temperature is gradually reduced depending on the freezing protocol. Following freezing, the dehydration step of lyophilization is conducted under vacuum and is separated into two separate stages primary and secondary drying. During primary drying, the frozen water is sublimated while the :remaining unfrozen water within the freeze concentrated liquid is removed during secondary drying.[95]

The goal of a lyophilization process is to achieve a final product in which perturbations in protein structure are minimized following drying and in which aggregation is inhibited upon reconstitution. However, loss of protein structure resulting in both aggregation and loss of biological activity is commonly observed in reconstituted lyophilized samples.[92,96–98] To inhibit perturbations in protein structure during lyophilization, both the formulation and lyophilization process must be optimized to minimize stress incurred by the protein during freezing and drying .[92] A well-designed lyophilized formulation and protocol requires an understanding of stresses

incurred through lyophilization and how they can be minimized through both formulation and processing based strategies.

Freezing is a major stress during any lyophilization process. As ice begins to nucleate within the sample, the protein and solutes will be concentrated in the liquid non-ice phase as ice crystals grow. During freeze concentration, the solute concentration can increase as much as 50-fold. Freeze concentration combined with crystallization of formulation components can induce a significant change in the local protein environment potentially impacting protein structure .[96] For example, selective crystallization of buffer components can induce shifts in pH denaturing pH-sensitive proteins.[99] It has been well documented that resulting from its lower solubility, Na_2HPO_4 crystallizes more readily than NaH_2PO_4 causing significant pH shifts during freezing.[100–102] Therefore crystallizing buffers such as phosphate are generally avoided in lyophilized formulations.

During freezing, the formation of an ice water interface can promote protein adsorption and induce perturbations in protein structure.[103] It has been shown that the extent of destabilize correlates with freezing rate. Faster cooling rates will result in greater supercooling before ice nucleation occurs facilitating the formation of smaller ice crystals and increased ice surface area compare to slower cooling rates.[104] This destabilization of proteins at the ice-water interface can be reduced by adding surfactants to compete with protein for adsorption at the ice-water interface.[104]

A significant component of lyophilized formulations is non-reducing sugars such as trehalose or sucrose. These polyhydroxy compounds resist crystallization and instead form amorphous glasses when concentrated. The increased viscosity of the freeze concentrated sugars prevents complete ice crystallization within the sample. However, ice crystallization is inhibited

once the sugar forms a highly viscous amorphous glass. Upon vitrification the non-frozen phase is considered to be maximally freeze-concentrated and typically contains 15-30% unfrozen water by weight.[105] The temperature at which vitrification occurs is the glass transition temperature of the maximally freeze-concentrated phase and is a critical processing parameter.

The glass transition temperature of the freeze concentrated phase dictates the primary drying temperature. To prevent cake collapse and product loss during drying, the product temperature must remain below the glass transition temperature of the freeze concentrated liquid. Typically, primary drying temperatures approximately 2-5 ˚C below the glass transition temperature are chosen to maximize primary drying rates while minimizing the potential for cake collapse and product loss.[92] Selection of a primary drying temperature can be complicated by variations in primary drying rates between vials within a single lyophilization run. This variation often results from the random nature of ice nucleation resulting in differing degrees in supercooling from vial to vials impacting ice crystal size.[106] This heterogeneity may result in large differences in drying rates from vial to vial.[106] To eliminate this heterogeneity an annealing step above the product glass transition temperature can be implemented before the start of primary drying.[107] Above the glass transition temperature Ostwald ripening rates are significantly increased resulting in growth of large ice crystal as the expense of smaller ice crystals.[108] Ostwald ripening process will increase the ice crystal size and simultaneously reduce heterogeneity in ice crystal size allowing for more uniform drying rates.[109,110] In addition to coarsening of ice crystals, annealing can promote crystallization of bulking agents such as mannitol or glycine which may be necessary for providing cakes structure or for ensuring protein stability.[94] Crystallization of bulking agents with low glass transition furthermore combined with further ice crystallization can increase the glass transition of the amorphous phase allowing for higher primary drying temperatures.[92]

Amorphous non-reducing sugars also play an important role in stabilizing proteins during drying and as well as in the dried solid. Multiple studies have shown that amorphous excipients protect against drying related stresses and that crystallization of stabilizing excipients significantly reduces protein stability.[93,111,112] Dehydration of protein during lyophilization results in the removal of the monolayer of water which forms the hydration shell.[113] Loss of hydrogen bonding interactions upon removal of the hydration layer during drying can result in disruption of native protein structure.[113] However, sugars can reduce dehydration related stress and stabilizing therapeutic protein during lyophilization by hydrogen bonding to polar groups and serving as a "water replacements".[114,115]

1.6 Formation of Nano-sized Air Bubbles Following Reconstitution of Freeze-Dried Solids

As mentioned above particle formation may occur readily upon reconstitution of lyophilized formulation resulting from destabilization of proteins induced by the freezing and drying process. While characterizing the formation of sub-visible particles in lyophilized formulations of intravenous immunoglobulin, Zhou et al. discovered that not all particle generated upon reconstitution of the lyophilized formulations were proteinaceous. Rather when the reconstituted solutions were characterized using a resonant mass measurement technique a large number of nano-sized air bubbles called nanobubbles were observed. These nanobubbles could not be removed readily by gassing and remained stable when stored for extended periods up to 11 days.[116]

This report of nanobubble generation upon reconstitution of lyophilized formulations was not the first time that nano-sized air bubbles. There have been multiple papers published reporting the formation of stable air bubbles with diameters of approximately 100 nm.[117–120] Despite multiple published accounts of the existence of nanobubbles, significant controversy surrounds their

reported long-term stability.[121] This controversy originates from the long-term stability of nanobubbles being inconsistent with predictions of nanobubble lifetimes based on thermodynamic considerations.

The controversy surrounding nanobubble stems from the expected internal pressure required to stabilize a nano-sized gas bubble. For a bubble to be stable, the internal pressure within the bubble must balance the external liquid pressure as well as the tendency for surface tension to compress the bubble. As shown in the equation below;

$$\Delta P = 2\sigma/R$$

the Laplace pressure (ΔP), can be calculated from the surface tension of the air-water interface (σ) and the bubble radius R.[122] If we assume that the surface tension of the nanobubble air-water interface is identical to that of the planar air-water interface the Laplace pressure of a nanobubble with a 100 nm radius would be approximately 14 atm.[123] This high internal pressure should provide a large driving force for gas to dissolve into the surrounding liquid results on an expected nanobubble lifetime on the order of 80 μs based on Epstein-Plesset theory.[124]

To explain the unexpected long-term stability of nanobubbles, multiple theories have been postulated throughout the nanobubble literature. Most theories either focus on reducing the driving force for gas to dissolve from the nanobubble into the surrounding bulk liquid by reducing the bubble surface tension or even preventing gas diffusion through some sort of barrier or skin. Reductions in Laplace pressure could be accomplished by completely coating a nanobubble in an organic contaminant or if a large number of nanoparticles adsorbed to the surface resulting in an effective reduction in the radius of curvature of the air-interface.[121,125] Yasui et al. has suggested that a small amount of hydrophobic material adsorbed on a bubble could serve as a source of

additional gas potentially balancing the outflux of gas dissolved into the surrounding solution.[126] Finally, it has been suggested that the commonly reported negative surface of nanobubble air-water interface could contribute to their stability.[127–129] Bunkin et al. postulated that the surface charge of the nanobubble itself could provide a repulsive force countering the Laplace pressure.[130–132]

Despite there being little consensus regarding the stabilizing mechanism of nanobubbles, significant effort has been placed in the development of nanobubble generators and applications for the bubbles. Proposed applications for nanobubble include aquaculture, cleaning and wastewater treatment.[121,133–135]

Chapter 2 Objectives and Specific Aims

2.1 Objectives

The majority of therapeutic protein products have exhibited the potential to induce adverse immune responses with effects ranging from reduced therapeutic efficacy to severe cases of anaphylaxis and even fatalities. While the frequency of severe immune response to therapeutic protein products are low, questions remain regarding factors contributing to adverse immune responses. One relatively uncontrolled factor remains the presence and concentration of sub-visible particles in protein products. Currently, regulatory agencies only provide guidelines for particles concentrations down to 10 µm leaving a significant uncontrolled region below this size range. It has been suggested that both the lack of control and characterization of particles below 10 µm may constitute an uncontrolled risk, potentially compromising the safety and efficacy of therapeutic protein formulations.[70]

Particles in therapeutic protein formulations may originate from a wide variety of sources including aggregation of the protein itself, manufacturing unit operations as well as containers and closures. Past research has shown that interfaces presented by silicone oil lubricants shed from prefilled syringes could promote protein aggregation and enhance the immunogenicity of protein formulations. In this work we have chosen to study two previously unexplored sources of sub-visible particles in protein formulations. First, we evaluated the effect of air-water interfaces presented by nanobubbles generated upon reconstitution of lyophilized solids on the stability of the interleukin-1 receptor antagonist (IL-1ra). In addition, we investigated the potential contribution to subvisible particulate content from plasticized polyvinyl chloride (PVC) bags used for the delivery of therapeutic protein formulations. These studies focused on evaluating if bis(2-ethylhexyl) phthalate (DEHP) droplets shed from PVC bags containing intravenous (IV) saline could reduce protein stability while enhancing immunogenicity

2.2 Specific Aims

2.2.1 Aim 1: Evaluate the effect of nanobubbles generated following reconstitution of lyophilized solids on aggregation and particle formation of IL-1ra.

In 2016, Zhou et al. reported the formation of stable nanobubbles upon reconstitution of lyophilized solids. The formation of stable nanobubbles with diameters of approximately 100 nm had been commonly reported in the literature, but there had been no investigation of how nano-sized air bubbles could impact protein stability. Using the model protein interleukin-1 receptor antagonist (IL-1ra), we investigated interactions between nanobubbles and IL-1ra. We began by measuring the surface charge of nanobubble solutions both with and without IL-1ra as a function of pH to probe potential impacts of IL-1ra adsorption on nanobubble surface charge and colloidal stability. We then employed particle characterization methods including resonant mass measurement and nanoparticle analysis to evaluate the effect of IL-1ra on the formation of nanobubbles and the generation of proteinaceous particles following reconstitution of lyophilized solids. Finally, accelerated stability studies were conducted where the stability of IL-1ra was monitored as a function of nanobubble concentration.

2.2.2 Aim 2: Elucidate mechanism of nanobubble formation upon reconstitution of lyophilized solids and develop strategies for reducing both nanobubble generation and associated protein aggregation.

The second aim of this research was to develop a mechanism by which nanobubbles are formed in lyophilized formulations and to ultimately leverage this mechanism to reduce nanobubble formation and its associated protein aggregation described in Aim 1. We hypothesized that nanobubble generation in lyophilized formulation resulted from the formation of nano-sized voids within glassy lyophilized matrices which formed nanobubbles as the surrounding matrix dissolved away during reconstitution. This generation of nano-sized voids within a glassy matrix would likely be dependent on the physical state of excipients in the final lyophilized solid. To explore this hypothesis, we compared nanobubble generation measured following reconstitution

of lyophilized amorphous formulations of either trehalose or sucrose to formulations of the crystallizing excipient mannitol. We then added mannitol progressively to formulations of either trehalose or sucrose and monitored nanobubble generation as a function of excipient crystallinity in the final lyophilized solid measured using powder X-ray diffractometry. We then monitored the effect of co-lyophilizing a model protein IL-1ra on nanobubble generation and quantified the formation of proteinaceous particles in these lyophilized formulations following reconstitution.

2.2.3 Aim 3: Investigate DEHP nanodroplet formation in PVC IV bags and its effect on the stability and immunogenicity of therapeutic protein formulations.

Bags containing IV saline are regularly used for dilution and administration of therapeutic protein formulations. These bags are often composed of polyvinyl chloride, a material which must have plasticizers added at concentration as higher as 40% by weight to achieve desirable material properties for medical applications. It has been commonly reported that the plasticizer DEHP leaches from plasticized PVC material, but there have been no reports of the generation of insoluble DEHP droplets in PVC IV bags. We began this aim by characterizing particles generated in PVC IV bags using a variety of particle characterization method including nanoparticle tracking analysis, resonant mass measurement, and flow imaging microscopy. Particle contents within bags were characterized either after being shaken to replicate shipping related stress or after being transported using the pneumatic tube system at the Denver Children's Hospital.

Following characterization of particles generated in PVC IV bags we proceeded to characterize the effect of DEHP-water interfaces on the stability of intravenous immunoglobulin (IVIG). Experiments were conducted to allow for direct comparison with silicone oil droplets previously shown to be shed from prefilled syringes. Protein adsorption to DEHP droplets was characterized using a solution depletion method, while changes in protein structure upon adsorption was monitored using 4,4′-Dianilino-1,1′-binaphthyl-5,5′-disulfonic acid dipotassium

salt (bis-ANS). Formation of intermolecular protein networks at the DEHP-water interface was monitored using interfacial shear rheometry. The stability of IVIG in formulation containing DEHP droplets was evaluated by quantifying the extent of IVIG monomer and dimer loss using size exclusion high performance chromatography. Finally, the immunogenicity of DEHP and silicone oil droplet was investigated through complement activation testing.

Chapter 3 Particle Formation and Aggregation of a Therapeutic Protein in Nanobubble Suspensions

This chapter has been published in the Journal of Pharmaceutical Sciences as: Snell, JR., Zhou C., Carpenter JF., & Randolph, TW. (2016). Particle formation and aggregation of a therapeutic protein in nanobubble suspensions. J Pharm Sci 105:3057-3063.

3.1 Abstract

The generation of nanobubbles following reconstitution of lyophilized trehalose formulations has recently been reported.[116] Here, we characterize particle formation and aggregation of recombinant human interleukin-1 receptor antagonist (rhIL-1ra) in reconstituted formulations of lyophilized trehalose. Particle characterization methods including resonant mass measurement and nanoparticle tracking analysis were used to count and size particles generated upon reconstitution of lyophilized trehalose formulations. In addition, accelerated degradation studies were conducted to monitor rhIL-1ra aggregation in solutions containing various concentrations of suspended nanobubbles. Reconstitution of lyophilized trehalose formulations with solutions containing rhIL-1ra reduced nanobubble concentrations and generated negatively buoyant particles attributed to aggregated rhIL-1ra. Furthermore, levels of rhIL-1ra aggregation following incubation in aqueous solution correlated with concentrations of suspended nanobubbles. The results of this study suggest nanobubbles may be a contributor to protein aggregation and particle formation in reconstituted, lyophilized therapeutic protein formulations.

3.2 Introduction

Sub-visible particles within therapeutic protein products have become the focus of increased regulatory concern due to the association of particles with adverse immune responses in patients.[48,73,74,91] This focus has led to significant efforts within the biopharmaceutical industry to count and characterize populations of sub-visible particles within formulations. Recently, a new source of particles in therapeutic formulations was identified by Zhou et al., who showed that large numbers of stable nanobubbles were generated following reconstitution of lyophilized trehalose formulations.[116] Nanobubbles within reconstituted lyophilized formulations will likely contribute to counts of sub-visible particles, but it is not known whether nanobubbles also may promote protein aggregation and particle formation.

Currently, nanobubbles are a growing area of research, with significant focus on understanding the mechanism(s) responsible for the stabilization of the 100-200 nm diameter bubbles[129,136,137] in bulk aqueous solutions. Bubbles with diameters on the nanometer scale might be expected to be unstable due to high internal pressures generated by surface tension at the air-water interface.[138–140] If the surface tension at the nanobubble-water interface were typical of air-water interfaces, the Young-Laplace equation would predict that high pressures within the nanobubbles should result in dissolution and disappearance of the nanobubbles on the order of microseconds.[122] However, studies have reported long-term (meta)stability of nanobubbles, with lifetimes ranging from hours[119] to several months.[136] It has been proposed that nanobubble stability may be dependent on the selective adsorption of anions at the nanobubble interface.[132,139,141] At the nanobubble scale, ions adsorbed to the nanobubble interface could be in close enough proximity to result in repulsive forces strong enough to balance the compressive force from surface tension. The balance of these two forces would be expected to result in a nanobubble with a stable diameter where the dissolution of gas from the bubble would be minimized.

Suspensions of nanobubbles have been explored as cleaning agents to remove proteins from surfaces,[134,142] but there have been no published examples of research on the effect of nanobubbles on protein aggregation and particle formation. It is well-established that protein molecules have a tendency to interact with and adsorb to various interfaces. [143,144] In particular, due to their amphiphilic nature, proteins adsorb readily to air-water interfaces. The tendency of a protein to adsorb to a hydrophobic interface results mainly from the hydrophobic interactions between exposed hydrophobic residues and the air-water interface, although electrostatics may also play a role.[145,146] Following adsorption, reorientation of hydrophilic and hydrophobic residues of protein often occurs, resulting in loss of native structure and production of gel-like protein layers.[44,147] Conformational changes resulting from adsorption to the air-water interface have been associated with reduced efficacy in therapeutic proteins.[144] Adsorption of protein particles to nanobubbles could result in protein particles and/or hybrid protein-air bubble nanoparticles, and potentially nucleate protein aggregation in the bulk solution.

In this study, we investigated whether nanobubbles generated following reconstitution of lyophilized disaccharide formulations could induce protein aggregation and particle formation in formulations containing recombinant human interleukin-1 receptor antagonist (rhIL-1ra). Particles generated following reconstitution of lyophilized disaccharide formulations were characterized using a combination of resonance mass measurement (RMM), nanoparticle tracking analysis (NTA) and zeta potential measurements. Lyophilized trehalose and sucrose samples were reconstituted either with a buffer solution alone or with a buffer solution that contained rhIL-1ra, and the number and characteristics of particles present in the resulting solutions were compared. Accelerated degradation studies in aqueous solution were then conducted to determine if the presence of nanobubbles could induce rhIL-1ra aggregation during extended incubation. In other

studies, polysorbate 20 (PS20) and ethylenediaminetetraacetic acid (EDTA) were added to rhIL-1ra formulations that contained nanobubbles to investigate whether these excipients would alter aggregation of rhIL-1ra in nanobubbles suspensions.

3.3 Materials and Methods

3.3.1 Materials

Recombinant human interleukin-1 receptor antagonist (rhIL-1ra) at a concentration of 100 mg/mL was donated by Amgen (Thousand Oaks, CA). High purity (low endotoxin) grade trehalose was obtained from Pfanstiehl (Waukegan, IL) and EMPROVE® low endotoxin sucrose was purchased from EMD Millipore (Billerica, MA). Urea and PS20 Surfact-Amps detergent solution were obtained from Fisher Scientific (Hampton, NH), and trisodium citrate dihydrate was acquired from Alfa Aesar (Ward Hill, MA). 2-mercaptoethanol and EDTA were purchased from Sigma-Aldrich (St. Louis, MO). Quick Start™ Bradford 1x dye reagent was obtained from Bio-RAD (Hercules, CA).

3.3.2 Sample Preparation

All buffer solutions contained 10 mM sodium citrate, and hydrochloric acid was added to adjust to pH values of 4.6, 5.4 and 6.6. Solutions were filtered with a 0.22 μm Millipore filter prior to use (Billerica, MA) unless otherwise noted. A stock solution containing100 mg/ml rhIL-1ra was dialyzed three times into 10 mM sodium citrate buffer pH 6.6 using 10 kDa molecular-weight cutoff Slide-A-Lyzer cassettes (Pierce, Rockford, IL). Concentrated rHIL-1ra solutions at pH 6.6 were diluted in the respective buffers to obtain 1 mg/mL concentrations of rhIL-1ra at the buffer conditions required for the study.

3.3.3 Lyophilization Procedure

Before use, 20 mL Fiolax glass lyophilization vials purchased from Schott (Lebanon, PA) were soaked overnight in Hellmanex III cleaning solution (Müllheim, Germany). The following

day, vials were rinsed and soaked in tap water to remove the remaining detergent. The vials were then thoroughly rinsed with filtered (0.22 μm) deionized ultrapure water and subsequently rinsed with 0.22 μm-filtered 190 proof ethanol. After vials were allowed to dry for at least 12 hours, 3 mL aliquots of either 10% (w/v) trehalose or sucrose solutions dissolved in deionized ultrapure water were filtered with a 20 nm cutoff Anotop 25 inorganic membrane filter (GE Healthcare Life Sciences, Pittsburgh, PA) were added by pipette. The contents of the vials were frozen by submersing the vials in liquid nitrogen for two minutes and stored at -80 °C prior to lyophilization. Frozen samples were loaded into a FTS Lyostar I lyophilizer on shelves precooled to -40 °C and allowed to equilibrate for 300 minutes. After equilibration, primary drying was initiated at a shelf temperature of -20 °C for 1700 minutes with the chamber pressure set to 70 mTorr. To initiate secondary drying the shelf temperature was raised to 33 °C at a rate of 0.1 °C/min. The shelf temperature was then held at 33 °C for four hours. Upon completion of secondary drying the chamber was back-filled with nitrogen and the vials were sealed.

3.3.4 Reconstitution of Lyophilized Formulations

To reconstitute samples to the original 3 mL volumes to which the vials were filled prior to lyophilization, 2.80 mL of reconstitution solution was pipetted into vials containing lyophilized sucrose or trehalose. Solutions containing 1 mg/mL rhIL-1ra were filtered using a 100 nm Anotop 10 inorganic membrane filter (GE Healthcare Life Sciences, Pittsburgh, PA) prior to reconstituting lyophilized cakes. Particles present in the reconstituted samples were analyzed immediately following reconstitution using the particle characterization methods described below.

3.3.5 Particle Characterization

Particle concentrations and diameters between 50 and 1000 nm were measured using a NanoSight NTA NS300 (Malvern Instruments Ltd, Malvern, UK) instrument. Prior to acquisition, shutter and gain values were optimized for analysis of the nanobubble samples and these settings

were held constant for all samples. Sample solutions were continuously injected using a 1 mL silicone oil-free syringe while 30-second videos were recorded in triplicate. Videos were analyzed for particle concentration and diameter using NanoSight NTA 3.0 software, with particle diameter calculated using a solution viscosity of 1.3 centipoise.

An Archimedes instrument (Malvern Instruments Ltd, Malvern, UK) that relies on the principle of RMM was used to measure particle size distributions for populations of particles differentiated by their respective densities. Concentrations and diameters of negatively and positively buoyant particles were measured for particles with sizes between approximately 0.1 and 5 µm. For calculation of particle diameters, the density of air and rhIL-1ra were provided as 0.00123 g/cm^3 and 1.3 g/cm^3 respectively. Samples were filtered with a 5 µm filter needle (BD, Franklin Lakes, NJ) prior to loading approximately 150 µL of sample volume. Samples were analyzed for 10 minutes and between samples the sensor was flushed with deionized ultrapure water for 60 seconds.

Zeta potentials were measured using a Zetasizer® (Malvern Instruments Ltd, Malvern, UK) using the procedure described by Zhou et al.[116]

3.3.6 Accelerated rhIL-1ra Degradation Studies in Nanobubble Suspensions

To determine whether nanobubbles are capable of inducing protein aggregation in formulations containing rhIL-1ra, accelerated degradation studies were conducted using nanobubble suspensions. For degradation studies, nanobubble suspensions were generated immediately before use by reconstituting lyophilized formulations of trehalose with 2.80 mL of 10 mM sodium citrate buffer pH 6.6. For initial studies, nanobubble suspensions generated from reconstitution were used directly or diluted with a filtered (0.22 µm) nanobubble-free control solution consisting of 10% (w/v) trehalose, 10 mM sodium citrate pH 6.6 by factors of 2, 3, 6 and

20. Aliquots (225 μL) of undiluted and diluted nanobubble suspensions as well as the nanobubble-free control solution were combined with 25 μL aliquots of 10 mg/ml rhIL-1ra formulated in 10 mM sodium citrate buffer pH 6.6 to obtain samples containing 1 mg/mL rhIL-1ra and a final volume of 250 μL. Samples were then placed in a 40 °C incubator and after 23 hours rhIL-1ra aggregation was quantified with a Bradford protein assay using the procedure described below. Additional degradations studies utilized the same procedure for sample preparation described above unless otherwise specified. All subsequent studies were conducted with nanobubble suspensions generated directly from reconstitution of lyophilized formulations without dilution.

To monitor the time-dependent aggregation of rhIL-1ra in nanobubble suspensions, nanobubble suspensions containing 1 mg/mL rhIL-1ra were incubated at a 40 °C and sampled at various time points over a 23 hour period. Following an initial time point, samples were removed from a 40 °C incubator every 3 hours for the first 12 hours and at the completion of the study after 23 hours. Samples were stored at 4 °C until completion of the study and then were analyzed simultaneously. Previous studies indicated negligible rhIL-1ra aggregation occurred in nanobubble suspensions stored at 4 °C for at least 23 hours.

To evaluate how disaccharide excipients influenced rhIL-1ra aggregation in nanobubble suspensions, rhIL-1ra aggregation was compared in nanobubble suspensions generated by reconstitution of lyophilized sucrose and trehalose. Nanobubbles were generated by reconstituting lyophilized formulations of sucrose using the methods described previously for trehalose, and rhIL-1ra aggregation in the nanobubble-containing reconstituted samples was quantified following 23 hours of incubation at 40 °C.

To determine how other common excipients such as surfactants or chelators might alter rhIL-1ra aggregation in formulations containing suspended nanobubbles, samples containing

either PS20 or EDTA were studied. Solutions of 0, 0.05, 0.5, 2.5, 5, 7.5 and 10% (w/v) PS20 were prepared by diluting 10% (w/v) PS-20 solution with 10 mM sodium citrate buffer pH 6.6. Aliquots (5 μL) of these PS20 solutions were added to 225 μL of nanobubble suspensions previously generated by reconstitution of lyophilized trehalose cakes with 10 mM sodium citrate buffer. 20 μL of a 12.5 mg/mL solution of rhIL-1ra were added to these solutions to obtain a final a volume of 250 μL, resulting in a rhIL-1ra concentration of 1 mg/mL and PS20 concentrations of 0, 0.001, 0.01, 0.05, 0.1 0.15 and .2 % (w/v). In a separate study, 5 μL of a 250 mM EDTA solution in 10 mM sodium citrate buffer pH 6.6 was added to 225 μL of nanobubble suspension. Nanobubble and EDTA solutions were combined with 20 μL of 12.5 mg/mL of rhIL-1ra, resulting in a final EDTA concentration of 5 mM. For both studies, rhIL-1ra aggregation was quantified using a Bradford assay following 23 hours of incubation at 40 °C.

3.3.7 Quantification of rhIL-1ra Aggregation

Upon completion of the incubation period, 250 μL samples were centrifuged for 20 minutes at 15,000 x g in an Eppendorf 5424R centrifuge that was maintained at 4 °C. Following centrifugation, a pellet of aggregated rhIL-1ra was observable on the bottom of the centrifuge tube. Resulting from the small quantity of aggregated rhIL-1ra, it was found that aggregation could be quantified most accurately by measuring the amount of pelleted rhIL-1ra directly using the Bradford protein assay. For this method, 150 μL of supernatant were carefully removed to avoid disturbing the pellet and the pellet was washed with 400 μL of 10 mM sodium citrate buffer pH 6.6. The washing step was repeated three times. After each removal 400 μL from the supernatant, the volume was replenished with fresh buffer. Following the washing steps, 400 μL of supernatant were removed and the pellet was solubilized by adding 100 μL of 8 M Urea, 10% (v/v) 2-mercaptoethanol to the pelleted rhIL-1ra and incubating for 1 hour at room temperature. Aliquots of 150 μL of the solubilized pellet were then added to a 96 well plate. Standards for rhIL-1ra were

prepared in the same plate using a stock solution containing 10 mg/ml rhIL-1ra to obtain rhIL-1ra concentrations between 0.0 to 50 μg/mL in 10 mM sodium citrate, 4 M urea and 5% (v/v) 2-mercaptoethanol at a volume of 150 μL. In this concentration range a plot of absorbance versus rhIL-1ra concentration was linear (data not shown) as required by the Bradford protein assay. 150 μL of Bradford reagent were added to each well and the solutions were mixed thoroughly using a pipette. After a 10 minute incubation period at room temperature the absorbance of each well was measured at 595 nm using a plate reader (Molecular Devices, Sunnyvale California). Using the standard protein solutions, a standard curve of absorbance versus rhIL-1ra concentration was constructed from the absorbance at 595 nm. Using this standard curve, the quantity of rhIL-1ra present in each well could be calculated.

3.4 Results

3.4.1 Characterization of Particles Generated Following Reconstitution

To confirm the previously reported generation of nanobubbles from lyophilized trehalose cakes, lyophilized formulations consisting of 10% (w/v) trehalose were reconstituted with 10 mM sodium citrate buffer. NanoSight NTA analysis of reconstituted samples detected the generation of a large number of nanoparticles with concentrations on the order of 2×10^9 nanoparticles/mL (Figure 3-1A). The particle diameters were approximately 100 nm (Figure 3-1B). Adjusting the pH of the buffer solution used for reconstitution did not appear to significantly alter the size or concentration of particles generated. RMM analysis of the generated particles confirmed that the particles were nanobubbles because large quantities of positively buoyant particles were measured whereas the counts of negatively buoyant particles were negligible (Figure 3-2). These results are consistent with recently published findings of Zhou et al. which reported the generation of nanobubbles in lyophilized formulations of trehalose after reconstitution.[116]

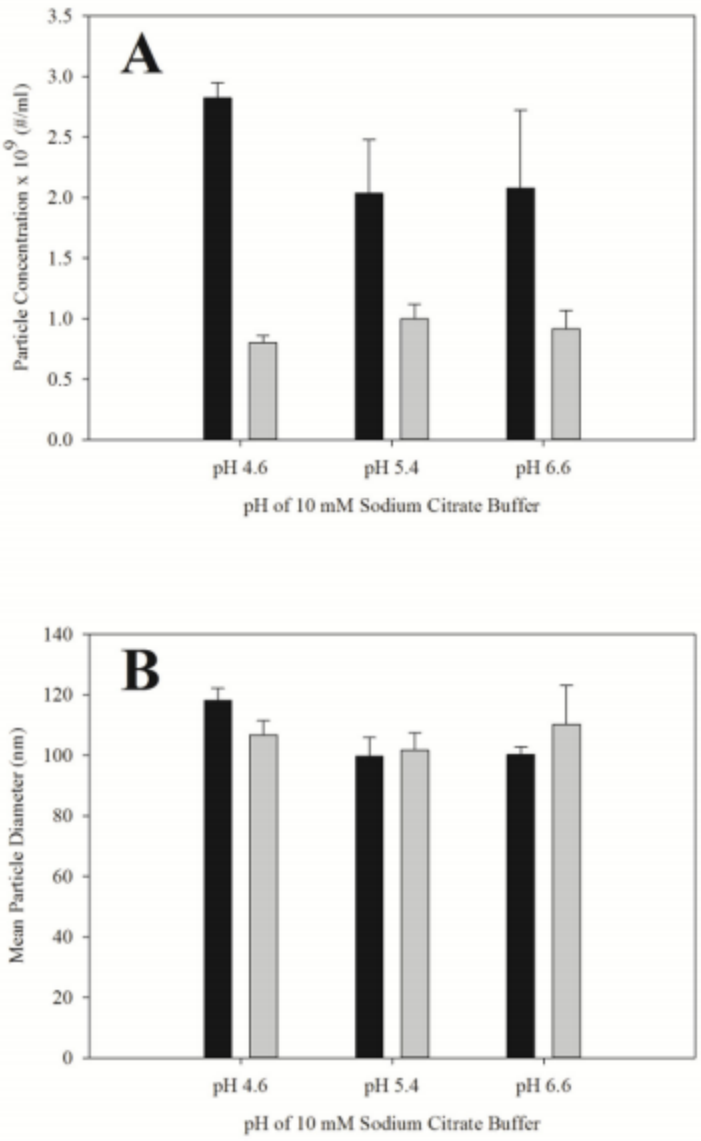

Figure 3-1. NTA Particle characterization of particle concentrations (A) and diameters (B) of particles generated following reconstitution of lyophilized trehalose formulations. Samples were reconstituted using 10 mM sodium citrate buffer either without (Black bars) or with (Gray bars) 1 mg/mL rhIL-1ra.

To investigate the potential effects of rhIL-1ra on nanobubble formation and nanobubbles on rhIL-1ra particle formation, formulations containing 10% (w/v) trehalose were reconstituted with solutions that contained 1 mg/ml rhIL-1ra in 10 mM sodium citrate at pH values of 4.6, 5.4 and 6.6. Reconstitution of lyophilized cakes with the rhIL-1ra solutions resulted in suspensions with reduced nanobubble concentrations (determined by NTA) as compared to suspensions

prepared by reconstitution of lyophilized trehalose cakes with the corresponding rhIL-1ra-free buffer solutions (Figure 3-1B). In contrast, nanobubble diameters were unchanged by the presence of rhIL-1ra (Figure 3-1B). Using RMM, negatively buoyant particles that could be attributed to rhIL-1ra particles were detected following reconstitution with buffer containing rhIL-1ra (Figure 3-2B). The concentration of these negatively buoyant particles was dependent on the solution pH. RhIL-1ra particle formation was minimized (1.7×10^6 particles/mL) at a pH corresponding to rhIL-1ra's isoelectric point of 5.4 and increased at solution pH's above and below the pI of rhIL-1ra (3.4×10^6 and 2.5×10^6 particles/mL at pH 4.6 and 6.6, respectively).

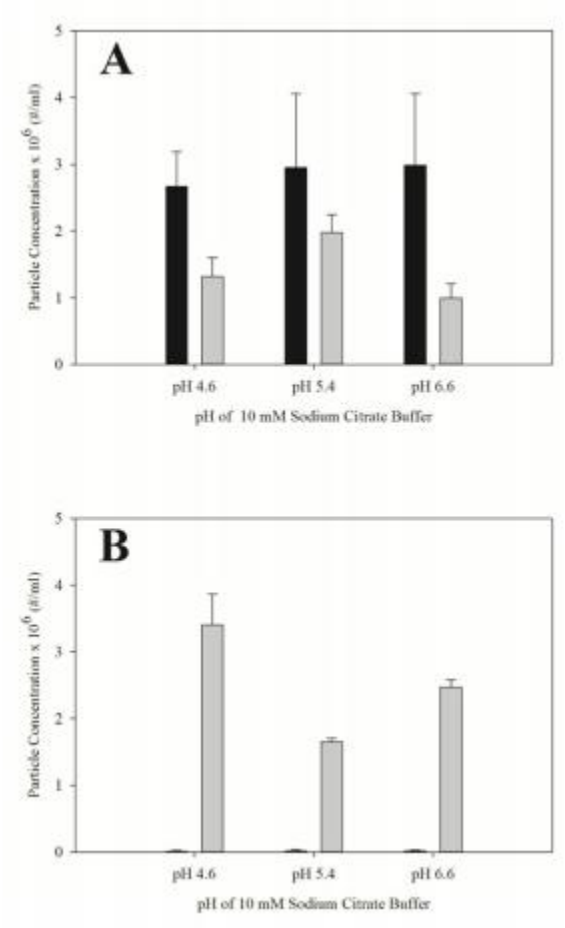

Figure 3-2. Concentration of positively (A) of positively (B) buoyant particles measured by resonant mass measurement. Samples were reconstituted using 10 mM sodium citrate buffer either without (Black bars) or with (Gray bars 1 mg/mL rhIL-1ra.

Zeta potential measurements were used to determine the effective charge at the nanobubble surface. At all pH values tested, zeta potentials of nanobubbles suspensions without rhIL-1ra were negative (Table 1). Reconstitution with rhIL-1ra resulted in significant changes in the magnitude of the zeta potential of the system which were pH dependent. At buffer pH conditions of 4.6 and 5.4 the nanobubble zeta potential closely matched that of the rhIL-1ra alone. At pH 6.6, however, the zeta potential measured in 1 mg/mL rhIL-1ra solutions containing suspended nanobubbles (-20.6 ± 0.6 mV) differed significantly from that of solutions of the rhIL-1ra alone (-3.96 ± 4.7 mV).

Table 3-1. Zeta potential values measured in mV using electrophoretic light scattering. Zeta potentials were measured following reconstitution with buffer either with or without 1 mg/mL rhIL-1ra. The zeta potential of 1 mg/mL rhIL-1ra solutions without nanobubbles were also measured

Solution pH	Nanobubble Suspension	Nanobubbles with 1 mg/ml rhIL-1ra	1 mg/ml rhIL-1ra
4.6	−15.7 ± 1.3 mV	7.0 ± 0.8 mV	6.7 ± 1.8 mV
5.4	−22.3 ± 4.7 mV	−2.2 ± 0.5 mV	−3.1 ± 0.9 mV
6.6	−27.6 ± 4.3 mV	−20.6 ± 0.6 mV	−4.0 ± 4.7 mV

3.4.2 Accelerated rhIL-1ra Degradation Studies in Nanobubble Suspensions

To further study the influence of nanobubbles on rhIL-1ra aggregation, accelerated rhIL-1ra degradation studies were conducted wherein rhIL-1ra was added to suspensions of nanobubbles generated by reconstitution of lyophilized trehalose cakes with 10 mM sodium citrate buffer pH 6.6. Incubation of rhIL-1ra in these nanobubble suspensions for 23 hours at 40 °C yielded rhIL-1ra precipitates that were visible following centrifugation. In contrast, no precipitates were observed when rhIL-1ra was incubated in nanobubble-free solutions of 10% (w/v) trehalose. Quantification of the extent of aggregation indicated that approximately 2.3 ± 0.2% of the rhIL-1ra formed insoluble aggregates in the presence of nanobubbles (Figure 3-3A). Diluting the nanobubble suspensions with nanobubble-free, 10% (w/v) trehalose solutions prior to incubation resulted in decreases in rhIL-1ra aggregation that correlated directly with decreasing nanobubble concentrations. During shorter incubation studies, insoluble aggregates could be detected in

nanobubble suspensions after 3 hours of incubation (Figure 3-3B). The quantity of rhIL-1ra aggregates formed in the presence of nanobubbles increased roughly linearly with time, suggesting a constant rate of rhIL-1ra aggregation.

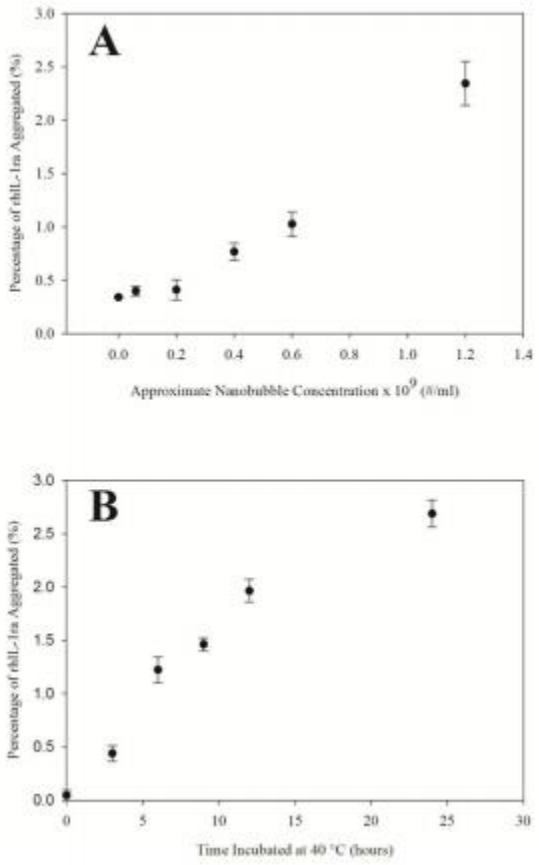

Figure 3-3. (A) Percentage of rhIL-1ra aggregated following incubation for 23 hours at 40 °C with increasing nanobubble concentrations was measured using a Bradford protein assay. (B) The percentage of IL-1ra aggregated in nanobubble suspensions was quantified every three hours for twelve hours and then after 23 hours of incubation at 40 °C.

To determine whether nanobubble generation and subsequent associated effects on rhIL-1ra aggregation were a phenomena specific to trehalose, lyophilized cakes consisting of 10% (w/v) sucrose were prepared using the same lyophilization procedure used to prepare lyophilized trehalose samples. To confirm nanobubble generation, lyophilized sucrose formulations were reconstituted with 10 mM sodium citrate buffer pH 6.6 and particle generation was characterized by NTA. 2.5 x 10^9 nanoparticles/mL were detected, as compared to 2.3 x 10^9 nanoparticles/mL

that had been obtained after reconstitution of the corresponding lyophilized trehalose cakes. Subsequently, accelerated degradation studies were conducted wherein rhIL-1ra was incubated at 40 °C in nanobubble suspensions generated from reconstituted lyophilized sucrose formulations. Similar extents of rhIL-1ra aggregation were observed with the sucrose-generated nanobubble suspensions as had been observed in the trehalose-generated nanobubble suspensions, with 3.0 ± 0.3% and 3.1 ± 0.2% of rhIL-1ra forming insoluble aggregates respectively after 23 hours of incubation at 40 °C.

Addition of PS20 to 1 mg/mL solutions of rhIL-1ra containing suspended nanobubbles suspensions resulted in a small but statistically significant ($p=0.007$) increase in the extent of rhIL-1ra aggregation after incubation for 23 hours at 40 °C for all concentrations above the PS20 critical micelle concentration of ~0.006% (w/v) (Figure 3-4). Without surfactant, slightly less aggregation was observed than in previous studies with 1.9 ± 0.2% of the rhIL-1ra aggregating. The presence of PS20 resulted in increasing aggregation in the solutions with 3.3 ± 0.2% of the rhIL-1ra aggregated at a PS20 concentration of 0.2% (w/v).

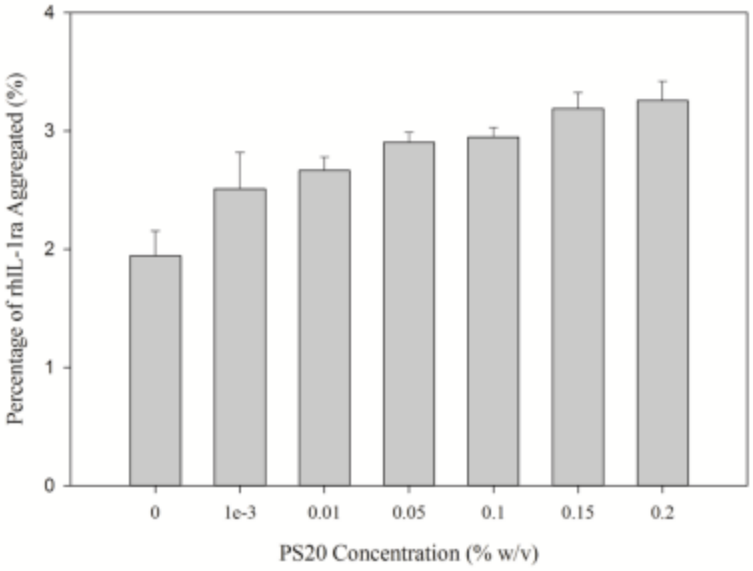

Figure 3-4. Percentage of rhIL-1ra aggregated in nanobubble suspensions containing 0 to 0.2% PS20 after incubating for 23 hours at 40 °C

In nanobubble suspensions in 10% (w/v) trehalose solutions containing 5 mM EDTA, rhIL-1ra aggregation could not be detected either visually or by the Bradford assay following incubation for 23 hours at 40 °C. Particle characterization by NTA confirmed also that the number and size of nanobubbles in the suspension was unaffected by addition of EDTA (data not shown).

3.5 Discussion

Reconstitution of lyophilized formulations of the disaccharides trehalose and sucrose generated suspensions of (meta)stable nanobubbles. The concentration and size of nanobubbles described in this work are consistent with the recently published findings of Zhou et al.[116] Reconstituting lyophilized formulations with a solution that contained 1 mg/ml rhIL-1ra resulted in a decrease in nanobubble concentrations, and the generation of negatively buoyant particles attributed to rhIL-1ra aggregates. At the same time, the presence of rhIL-1ra in the reconstituting medium resulted in suspensions containing fewer nanobubbles. The reduction in nanobubble concentration may result from rhIL-1ra adsorption to the air-water interface, which would reduce

the surface tension at air-water interfaces, reducing the rate at which some of the relatively large bubbles present immediately following reconstitution of lyophilized cakes might shrink to nanobubble dimensions.

It has been postulated that nanobubble stability may be dependent on a negative surface charge resulting from adsorbed anions which may generate a repulsive force sufficient to oppose the force of surface tension.[132,139,141] Consistent with previous reports, [129,141] our zeta potential results confirmed that nanobubbles are negatively charged. Following reconstitution with rhIL-1ra the magnitude and sign of the zeta potentials in this system were dependent on the net charge of rhIL-1ra, as controlled by altering buffer pH. Because zeta potentials measured by electrophoretic light scattering are an average value weighted by the intensity of light scattered by each component, it remains unclear what population of particles would contribute most to this value as rhIL-1ra monomers, rhIL-1ra aggregates and nanobubbles would all be present following reconstitution of lyophilized disaccharide cakes with a rhIL-1ra solution. In all cases, however, the addition of rhIL-1ra resulted in a reduction in the absolute magnitude of the zeta potential. This decrease in zeta potential could reduce electrostatic repulsion between components, potentially inducing nanobubble destabilization and protein aggregation.

The observed changes in zeta potential of these systems could result from adsorption of rhIL-1ra to the nanobubble interface, resulting in nanobubble zeta potentials similar to those of rhIL-1ra alone at the respective pH. Although proteins are surface active and structural perturbations have been described to occur at interfaces,[148] the quantity of aggregation observed is not commensurate with the available nanobubble surface area for aggregation to take place. In our accelerated stability studies following incubation in nanobubble suspensions, up to 3% of rhIL-1ra in these solutions formed insoluble aggregates. This extent of rhIL-1ra aggregation is

significantly greater than the quantity of rhIL-1ra which could adsorb to the available nanobubble surface area present in our solutions. From a simple approximation assuming monolayer formation and hexagonally closest packing, only 0.0001 mg of rhIL-1ra could adsorb per mL of nanobubbles (2×10^9 nanobubbles/mL). However, the quantity of rhIL-1ra that aggregated in nanobubble suspensions was more than 300 times greater, suggesting that a direct mechanism wherein surface layers of adsorbed rhIL-1ra molecules form aggregates at the nanobubble-water interface may not be sufficient to explain the extent of aggregation observed.

Furthermore, addition of PS20 at concentrations both above and below the critical micelle concentration did not inhibit aggregation during incubation studies. The presence of nonionic surfactants such as PS20 would be expected to compete with rhIL-1ra molecules for adsorption at the nanobubble interface or to bind to hydrophobic regions of rhIL-1ra reducing surface activity.[149] If rhIL-1ra aggregation in the solution was dependent on adsorption to the nanobubble-water interface the addition of surfactant would be expected to reduce or inhibit aggregation. This again suggests that another mechanism may be responsible for generating rhIL-1ra aggregates. Other potential mechanisms may be that nanobubbles serve as nucleation sites for aggregation with further aggregation occurring in the bulk solution or nanobubbles could be capable of catalytically generating structurally perturbed rhIL-1ra species.

At a concentration of 5 mM, EDTA was capable of completely eliminating rhIL-1ra aggregation in nanobubble suspensions. As EDTA is a chelator capable of reducing the activity of a variety of cations, this result suggests contaminants such as cations leaching from glass container surfaces may be involved in the generation of rhIL-1ra aggregates in our formulations. Whether nanobubbles may facilitate leaching of contaminants from glass surfaces or may interact with contaminants remains unclear. Potentially, cations may be electrostatically attracted to the

negatively charged nanobubble interface, resulting in locally higher concentrations at the nanobubble interface. Interactions with contaminants near the nanobubble surface could catalyze perturbations in rhIL-1ra structure resulting in an increased propensity for rhIL-1ra aggregation.

The presence of nanobubbles combined with the generation of rhIL-1ra aggregates following both reconstitution of lyophilized formulations and incubation in reconstituted formulations could be a significant source of sub-visible particles in therapeutic protein formulations. Recent work by both Barnard et al. and Kotarek et al. has identified a correlation between increased concentrations of sub-visible particles and immune responses to marketed therapeutic protein products.[74,150] In addition, Rosenberg et al. highlighted the importance of investigating and characterizing sub-visible particles in formulations to develop strategies to mitigate risk and ensure the safety of therapeutic protein products.[91] As a newly identified source of sub-visible particles likely present upon reconstitution of lyophilized protein products, nanobubbles pose an unknown risk to the safety of therapeutic protein formulations requiring additional research to investigate if nanobubbles could alter the efficacy and immunogenicity of therapeutic protein products.

3.6 Conclusions

Nanobubbles generated following reconstitution of lyophilized formulations may induce rhIL-1ra aggregation and particle formation. Following accelerated stability studies we found a correlation between the quantity of insoluble rhIL-1ra aggregates generated and nanobubble concentrations. RhIL-1ra aggregation in nanobubble suspensions was not attenuated upon addition of PS20 while EDTA appeared to completely inhibit formation of rhIL-1ra aggregates. The extent of aggregation observed in these studies combined with the minimal effect of PS20 is not consistent with rhIL-1ra aggregation in these formulations being dependent on the nanobubble-

water interface. While the exact mechanism by which aggregation in these reconstituted formulations occurs remains unclear, preliminary experiments suggest nanobubbles may be capable of reducing protein stability in reconstituted formulations via a mechanism dependent on the presence of metal cations.

3.7 Acknowledgements

This work was supported by a graduate research fellowship from the T32 GM-065103 NIH/CU Molecular Biophysics Training Program (to J.R.S).

Chapter 4 Nanobubbles in Reconstituted Lyophilized Formulations: Interactions with Proteins and Mechanism of Formation

This chapter has been submitted to the Journal of Pharmaceutical Sciences as: Snell, JR., Kumar NS., Suryanarayanan, R., & Randolph, TW. Nanobubbles in reconstituted lyophilized formulations: interactions with proteins and mechanism of formation.

4.1 Abstract

Reconstitution of lyophilized disaccharide formulations results in the formation of nano-sized air bubbles that persist in suspension for weeks. If proteins are present, interactions with nanobubbles may cause loss of monomeric protein and formation of sub-visible particles. The goals of this work are to determine the mechanism(s) by which nanobubbles form in reconstituted lyophilized formulations, and to develop strategies for reducing nanobubble generation. We hypothesize that nanobubbles are created from nano-sized gas pockets within lyophilized solids, which become bubbles when the surrounding matrix is dissolved away during reconstitution. Nano-sized voids may originate from small ice crystals formed within the concentrated liquid during freezing that subsequently sublime during drying. Nanobubble concentrations are correlated with the extent of mannitol crystallization during freezing. Nano-sized ice crystals, induced by the release of water during mannitol crystallization, were responsible for nanobubble formation. The presence of trehalose or sucrose, in formulations with low mannitol concentrations, inhibited excipient crystallization during lyophilization and reduced nanobubble levels following reconstitution. Our results show a correlation between nanobubble formation and concentrations of insoluble IL-1ra aggregates, suggesting that minimizing nanobubble generation may be an effective strategy for reducing protein aggregation following reconstitution.

4.2 Introduction

The effect of sub-visible particulate matter on the safety and efficacy of parenterally administered therapeutic proteins is a growing concern in the pharmaceutical industry.[151] Particulate matter in protein formulations can be generated by aggregation of the protein, and shed from wetted surfaces including those presented by filling pumps and product containers/closures.[70] Another source of particulates was recently identified by Zhou et al.,[116] who found that reconstitution of lyophilized formulations can generate a large number of nano-sized air bubbles. These nanobubbles exhibit long-term stability, remain suspended for more than a week after reconstitution, and are not readily removed by degassing.[116] High nanobubble concentrations in reconstituted lyophilized formulations have been associated with increased rates of protein aggregation.[152]

Because proteins in aqueous formulations typically exhibit high rates of chemical and physical degradation, lyophilization is often employed to increase their long term storage stability.[92,94,153] [43,95,154,155] In lyophilized formulations, proteins typically are dehydrated and stabilized in glassy matrices composed of non-reducing disaccharides such as trehalose or sucrose. Using these formulations, long term storage stability (e.g., 18-24 months) may be achieved.[110] However, even in the presence of stabilizing disaccharides, lyophilization may result in protein structural perturbations and protein aggregation.[115,156–158] These degradation processes are commonly attributed to freezing- or dehydration-related stresses imparted during lyophilization.[159] The formation of nanobubbles upon reconstitution and their subsequent promotion of protein aggregation may provide an alternative explanation for protein destabilization in lyophilized formulations, and thus it may be beneficial to minimize the number of nanobubbles formed during reconstitution of lyophilized protein formulations.

The goal of this work is to identify strategies for minimizing nanobubble formation upon reconstitution of lyophilized formulations. The development of formulation or processing strategies for reducing nanobubble generation in lyophilized samples requires first an understanding of the mechanism(s) by which nanobubbles are generated. We hypothesize that nanobubbles arise from nano-sized voids within glassy lyophilized matrices that become nanobubbles of similar dimensions when the matrix dissolves away during reconstitution. A similar mechanism has been used to explain the larger, micron-sized and visible bubbles observed in protein formulations after lyophilization and reconstitution.[160]

The formation of nano-sized voids during lyophilization of protein formulations likely depends on the physical properties of their components. To date, published studies of nanobubbles in reconstituted lyophilized formulations have relied on the disaccharide trehalose as the major formulation component.[116,152] Because lyophilization of trehalose solutions generates amorphous solids, we hypothesized that such glassy solids might be necessary for the formation and stability of nano-sized voids, and that structural changes in the solids induced by the addition of a crystallizing excipient or by annealing at temperatures above the glass transition temperature could have significant impact on nano-void formation and consequent nanobubble generation. Thus, we first compared nanobubble concentrations observed after reconstitution of lyophilized sucrose and trehalose, two excipients expected to form amorphous solids when lyophilized. Next, we added progressively higher concentrations of mannitol, a crystallizing excipient, to trehalose and sucrose formulations to determine how nanobubble generation was influenced by cake crystallinity. In addition, we evaluated the effect of co-lyophilizing a protein, IL-1ra, on the formation of nanobubbles and monitored protein particle formation following reconstitution.

4.3 Materials and Methods

4.3.1 Materials

Recombinant human interleukin-1 receptor antagonist (IL-1ra), at a concentration of 100 mg/mL, was donated by Amgen (Thousand Oaks, CA). D -(+)- trehalose dihydrate (Pfanstiehl, Waukegan, Illinois), sucrose (Avantor, Radnor, Pennsylvania), D-mannitol (Sigma-Aldrich, St. Louis, Missouri), sodium citrate (Avantor) and sodium chloride (Fisher Scientific, Hampton, New Hampshire) were of pharmaceutical grade or higher.

4.3.2 Sample preparation

Solutions (10% w/v) of each mannitol, sucrose and trehalose were prepared by dissolving in ultrapure water and filtered (0.02 μm, Whatman Anotop 25 sterile syringe filter, Maidstone, UK). These solutions were then mixed to obtain the desired molar fraction of mannitol in each solution while maintaining a total excipient concentration of 10% w/v. After filtering, 3 mL of solution was aliquoted into 20 mL Fiolax vials (Schott, Mainz, Germany) and capped with two-legged high purity stoppers (Wheaton, Millville, New Jersey).

For experiments with IL-1ra, a stock solution of IL-1ra was prepared by dialysis into 10 mM sodium citrate buffer using a 10 kilodalton dialysis cassette (Slide-A-Lyzer, ThermoFisher Scientific, Waltham, Massachusetts) and filtered (0.22 μm, Millex GV PVDF, Millipore Sigma, Burlington, Massachusetts). Subsequently, IL-1ra concentration was verified using UV adsorption at 280 nm. Stock solutions (15% w/v) of mannitol and trehalose were prepared by dissolving each excipient in 10 mM sodium citrate buffer (pH 6.6). These two solutions were mixed to obtain a stock mixture containing 0.43 mole fraction mannitol at a total solute concentration of 15% w/v. Finally, IL-1ra stock solution, excipient stock solutions, and 10 mM sodium citrate buffer (pH 6.6) were combined in appropriate ratios to obtain a final excipient concentration of 10% w/v and IL-1ra concentrations ranging from 0.1 to 10 mg/mL.

4.3.3 Lyophilization protocol

Sample vials were loaded directly into a lyophilizer (FTS Systems Lyostar 1, Warminster, PA) at room temperature. Lyophilizer shelves were cooled from room temperature to -40 °C at 1 °C/min and held at -40 °C for 300 minutes to completely freeze vial contents. Primary drying was initiated by raising the shelf temperature to -20 °C while maintaining a chamber pressure of 70 mTorr. The samples were dried for 1700 minutes before initiating secondary drying by increasing the shelf temperature to 33 °C at 0.1 °C/min. After drying for 240 minutes at 33 °C, the chamber was backfilled with dry nitrogen and the vials were sealed prior to their removal from the chamber.

Some samples were lyophilized according to a protocol that included an annealing step prior to the initiation of primary drying. These samples were frozen as described above for the standard lyophilization cycle. After holding the shelf at -40 °C for 300 min, the temperature was increased to -5 °C over 25 minutes and held for 6 hours. Following the annealing step, the samples were re-cooled to -40 °C and held for another 5 hours. Following these freezing and annealing steps, primary and secondary drying were conducted using the same protocol described previously for the standard lyophilization cycle.

4.3.4 Powder X-ray Diffractometry

Data were collected with a diffractometer (D8 ADVANCE, Bruker AXS, Madison, WI) using Cu Kα radiation (40 kV × 40 mA) over an angular range of 5−35° 2θ with a step size of 0.0196° and a dwell time of 0.5 s at each step. Data were compared with the standard patterns of α-mannitol (# 00-022-1793), β-mannitol (# 00-022-1797), δ-mannitol (# 00-022-1794) and mannitol hemihydrate (# 02-086-22-93) in the Powder Diffraction Files.[161]

The percent crystallinity of the samples were calculated using the relation:[162]

Crystallinity (%) = (Area under the crystalline peaks/ Total diffracted intensity) × 100

4.3.5 Particle Characterization Methods

NanoSight nanoparticle tracking analysis (NTA) (Malvern Panalytical, Westborough, MA) was utilized to measure the concentration and size distribution of nanoparticles with dimensions between 50 and 1000 nm. Samples were injected using a 1 mL silicone oil-free syringe while taking care to minimize bubble formation. Once the samples were loaded, camera settings were optimized based on the particle concentrations and properties of particles in each sample. Following optimization of the camera settings, 60 second videos were recorded in triplicate. Nanoparticle concentrations and diameters were then calculated using the NanoSight 3.0 analysis software.

A resonant mass measurement instrument (Archimedes, Malvern Panalytical, Westborough, MA) was employed to differentiate between particle types based upon their densities relative to that of the bulk fluid. This instrument utilizes the principle of resonant mass measurement to classify particles as either positively or negatively buoyant relative to the bulk fluid density. Samples were measured without any prior filtration or dilution. They were loaded to a Hi-Q micro sensor chip for 20 seconds before acquiring data for 5 minutes. Between samples, the sensor was rinsed with ultrapure water for 90 seconds.

The concentration and size distribution of particles of size greater than 1 micron generated after incubating nanobubbles with IL-1ra were monitored using flow imaging microscopy (FlowCAM VS1; Fluid Imaging Technology Inc., Scarborough, ME). The instrument was operated with a FC100 flow cell as well as a 10x objective and collimator. Analyses were conducted at a flow rate of 0.080 mL/min and a sample volume of 0.2 mL was analyzed for each sample. All measurements were conducted in triplicate.

4.3.6 Secondary Drying of Trehalose Dihydrate

Samples of crystalline trehalose dihydrate (3 g) were placed into 20 mL glass vials (Schott, Mainz, Germany). The vials were placed on the shelf of the lyophilizer and the temperature was rapidly increased to 33 °C. Once the desired temperature was reached, the chamber pressure was reduced to 70 mTorr. The samples were dried for 12 hours before backfilling the chamber with dry nitrogen and stoppered prior to removal from the lyophilizer.

Dried samples were reconstituted with 3 mL of ultrapure water, allowed sufficient time for complete trehalose dissolution, prior to particle characterization with NTA. Particle content in these samples were compared to 3 g samples of trehalose dihydrate dissolved in 3 mL of ultrapure water.

To probe the density of nanoparticles formed upon dissolution of dehydrated trehalose dihydrate, the concentration of nanoparticles in the bottom and top fraction of samples were measured following ultracentrifugation. Samples of dissolved dehydrated trehalose dihydrate (3 mL) were aliquoted into polycarbonate tubes and centrifuged at 208,000 relative centrifugal force (rcf) for 75 minutes using a TLA-100.3 rotor in a benchtop ultracentrifuge (TL-100, Beckman, Indianapolis, Indiana). Aliquots (1 mL) were removed immediately from the bottom and top of the ultracentrifuge tube using an 18-gauge needle and a 1 mL silicone oil-free syringe. Nanoparticle concentrations were then measured with NTA using the procedure described above.

4.3.7 Differential Scanning Calorimetry (DSC)

A differential scanning calorimeter (model Q2000, TA Instruments) equipped with a refrigerated cooling accessory was used. The instrument was calibrated with indium. About 5 mg of the sample was filled in an aluminum pan and heated under nitrogen purge (50 mL/min). The specific pan configuration and the heating rate are given in the figure legend. The DSC data were analyzed using the Universal Analysis software.

4.3.8 Size Exclusion High Performance Liquid Chromatography

Loss of monomeric IL-1ra from solution was monitored at 280 nm using a high-performance liquid chromatograph (Agilent 1100, Santa Clara, California) equipped with a variable wavelength detector. Insoluble IL-1ra was separated from any soluble oligomers using a size exclusion column (Tosoh TSKgel G3000SWxl, Tokyo, Japan) combined with a guard column (Tosoh TSKgel, Tokyo, Japan). The system was operated at 0.6 ml/min with a mobile phase consisting of 10 mM sodium citrate buffer with 140 mM NaCl (pH 6.6). Loss of monomeric protein from the solution was calculated using the area under the monomer peak and compared to areas measured for unstressed controls.

4.4 Results

4.4.1 Effect of Excipient Physical Form on Nanobubble Formation in Lyophilized Cakes

Lyophilized cakes of different compositions were reconstituted with ultrapure water. After allowing sufficient time for complete dissolution of the solid, the generated nanobubbles were characterized using NTA. As described previously and illustrated in Figure 4-1, reconstitution of lyophilized formulations of glassy sugars resulted in the formation of nano-sized air bubbles that were approximately 100 nm in diameter.[116] In mannitol/disaccharide mixtures, as the mole fraction of mannitol increased (and the disaccharide concentration simultaneously decreased), the concentration of nanobubbles decreased until a minimum nanobubble concentration was reached at a mannitol mole fraction of ca. 0.43. At higher mannitol mole fractions, nanobubble concentrations progressively increased, reaching a maximum of 1.5×10^{10} nanobubbles/mL in samples containing pure mannitol.

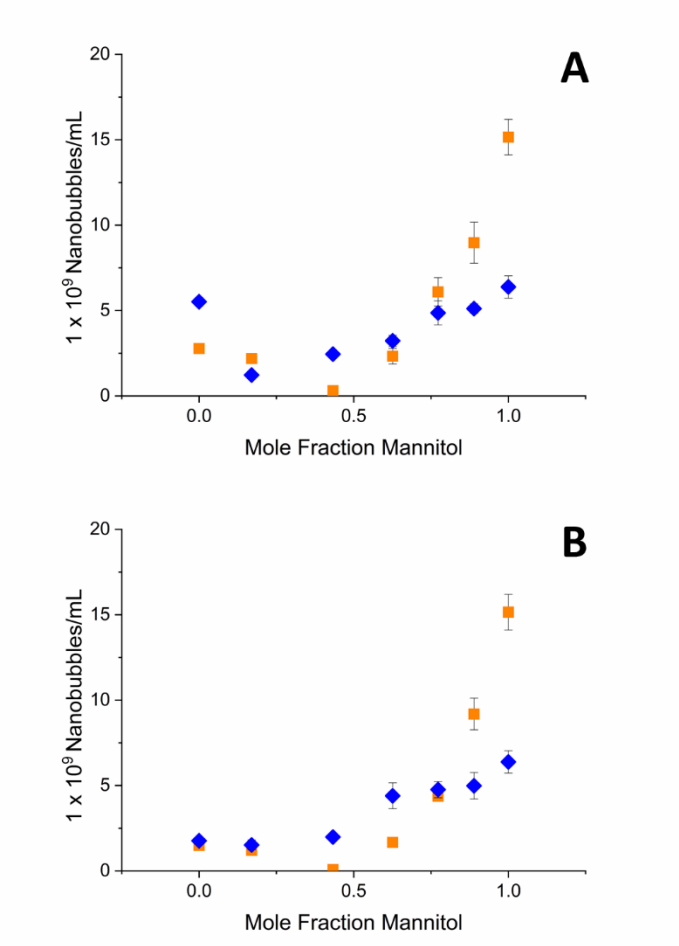

Figure 4-1. Nanobubble concentration as a function of mannitol mole fraction following reconstitution of lyophilized formulations of (A) mannitol and trehalose, and (B) mannitol and sucrose. Samples were lyophilized using the standard lyophilization protocol (orange squares) or with the addition of an annealing step at -5 °C prior to primary drying (blue diamonds). Mean ± SD (n=3).

We were interested in investigating whether excipient crystallization and relaxation processes in frozen solids occurring prior to primary drying affected the concentration of nanobubbles that could be observed after reconstitution. Therefore, a pre-drying annealing step at -5 °C for 6 hours was added to the standard lyophilization protocol. Nanobubble concentrations were profoundly influenced by the annealing step (Figure 4-1). Annealing of frozen trehalose solutions increased nanobubble concentrations from (2.8 ± 0.2) x 10^9 to (5.5 ± 0.3) x 10^9 mL^{-1}. Likewise, increases in nanobubble concentrations were observed after annealing both sucrose and trehalose formulations containing 0.43 and 0.63 molar fraction mannitol. In contrast, at mannitol

mole fractions above 0.77, annealing resulted in a pronounced reduction in nanobubble concentrations (Figure 4-1).

Powder X-ray diffractometry (PXRD) was used to quantify mannitol crystallization in the formulations lyophilized with or without an annealing step. As shown in Figure 4-2, the extent of crystallization was dependent on the ratio of trehalose to mannitol in the lyophilized cake. Following the standard lyophilization protocol, up to a mannitol mole fraction of 0.43, there was no evidence of crystallization of either mannitol or trehalose. As the mannitol concentration was further increased, the extent of crystallization increased, reaching a maximum of 77% crystalline content for pure mannitol. At moderate mannitol mole fractions (0.43 – 0.77), the addition of an annealing step resulted in an appreciable increase in the cake crystallinity. However, when the mannitol mole fraction exceeded 0.75, annealing did not increase the extent of crystallization in lyophilized formulations.

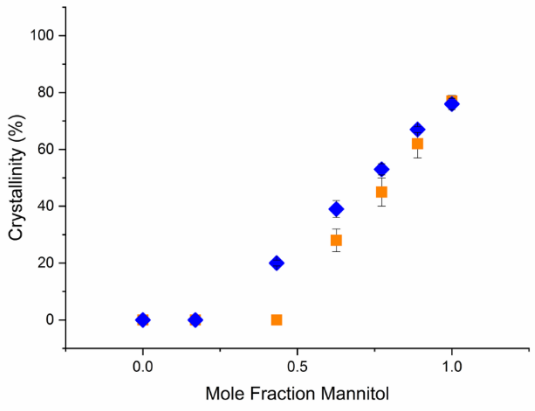

Figure 4-2. The percent crystallinity of lyophiles (determined by powder X-ray diffractometry) as a function of mannitol concentration. The lyophiles were prepared from solutions of mannitol and trehalose with different compositions. Samples were lyophilized using the standard lyophilization protocol (orange squares) or with an additional annealing step at -5 °C prior to primary drying (blue diamonds). Mean ± SD (n=3).

4.4.2 Nanobubble Formation Following Dissolution of Dehydrated Trehalose Dihydrate

During the freezing and primary drying stages of lyophilization, trehalose has been reported to form crystalline trehalose dihydrate.[163,164] During secondary drying, these crystals may dehydrate and revert to an amorphous anhydrate.[163] The baseline thermal behavior of trehalose dihydrate, evaluated by heating in a hermetically sealed pan in a DSC, was in excellent agreement with literature.[165] A sharp endotherm was observed at ~ 99 °C, immediately followed by an exotherm (data not shown). The endotherm is attributable to dehydration of trehalose dihydrate yielding a partially crystalline anhydrate. Since a sealed pan was used, there will be resistance to vaporization of the released water. The exotherm is ascribed to further crystallization of the anhydrate.

We observed that the crystalline trehalose dihydrate became amorphous when dried for 12 hours at 33 °C and a chamber pressure of 70 mTorr. DSC of the dried material revealed a glass transition at ~ 118 °C (Figure 4-3), in agreement earlier literature.[166] The ΔC_p at T_g, 0.5 $J \cdot g^{-1} \cdot °C^{-1}$, was also in excellent agreement with the reported value. The T_g was followed, first by a crystallization exotherm, and then by an endotherm attributed to melting of the crystalline phase. The enthalpy of crystallization (53.9 $J \cdot g^{-1}$) and the enthalpy of fusion (58.0 $J \cdot g^{-1}$) values were similar, suggesting that, under these dehydration conditions, a substantially amorphous trehalose phase was obtained.

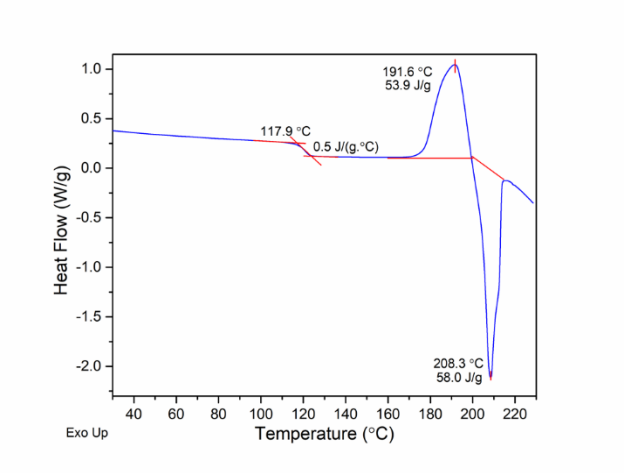

Figure 4-3. DSC heating curve of amorphous trehalose in a non-hermetically crimped pan. The sample was prepared by drying crystalline trehalose dihydrate for 12 hours at 33 ˚C at a chamber pressure of 70 mTorr. After loading in the DSC cell, additional drying was conducted by holding at 60 °C for 5 hours. The glass transition was accompanied by pronounced enthalpic recovery.24 Therefore, the sample was heated to 150 °C and then cooled down to 20 °C. Finally, the sample was heated from RT to 240 C at 10 °C/min (only this scan is shown).

Amorphous trehalose, formed by drying crystalline trehalose dihydrate at 33 °C and 70 mTorr for 12 hours, was dissolved in ultrapure water and subsequently characterized using NTA. A similar analysis was conducted using trehalose dihydrate crystals that were not subjected to drying. As can be observed in Figure 4-4, nanoparticle concentrations after reconstitution of the amorphous trehalose were approximately two orders of magnitude higher, 1.4×10^{10} vs. 2.8×10^{8} mL^{-1}, than those observed in samples formed by dissolving trehalose dihydrate crystals. The nanoparticles formed after reconstituting the amorphous trehalose were monodisperse, with a mean diameter of 73 nm. To confirm the identity of these particles as nanobubbles, ultracentrifugation was employed. Samples of the dehydrated, amorphous trehalose were dissolved in ultrapure water and centrifuged for 75 minutes at 208,000 rcf. Following ultracentrifugation, the bottom and top fraction of the samples were carefully removed using a syringe and needle and particle concentrations were re-measured using NTA. Enrichment of nanoparticle concentrations in the top fraction (data not shown) showed that the nanoparticles were positively buoyant, consistent with their being nanobubbles.

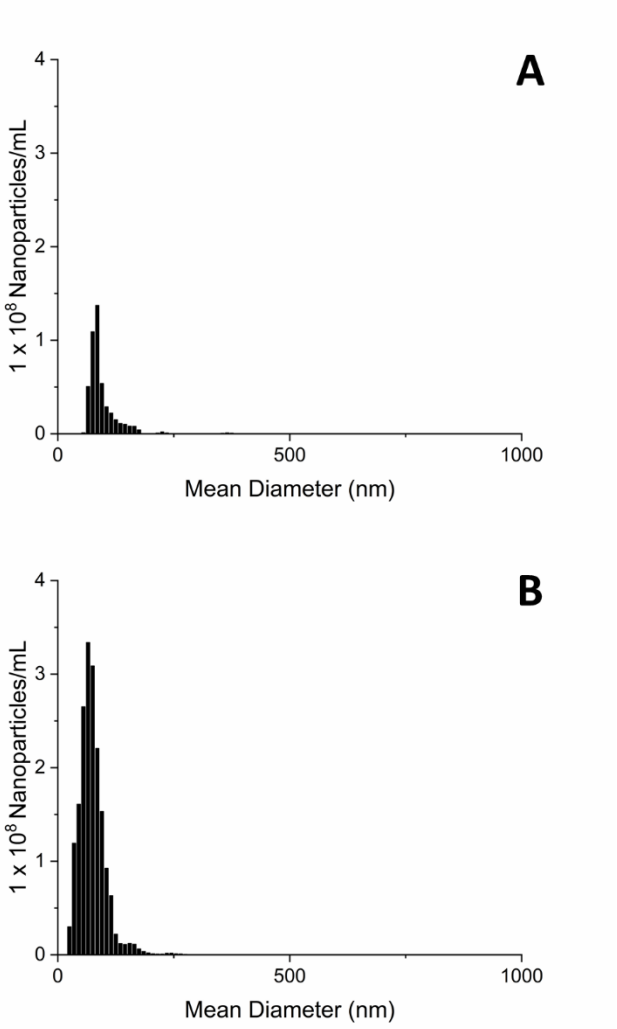

Figure 4-4. Size distribution of nanoparticles generated upon dissolution of either crystalline trehalose (A) or amorphous trehalose (B). Dissolution of trehalose dihydrate generated (2.82 ± 0.22) x 10^8 nanoparticle per mL while dissolution of amorphous trehalose dihydrate formed (1.36 ± 0.14) x 10^{10} nanoparticles per mL.

4.4.3 Effect of IL-1ra on Nanobubble Generation

The presence of proteins within lyophilized formulation may alter phase behavior of excipients.[167,168] To investigate how protein and buffer might alter nanobubble formation, we lyophilized 10% w/v formulations of trehalose that contained 10 mM sodium citrate buffer and IL-1ra at concentrations between 0.1 and 10 mg/mL. After lyophilization, samples were reconstituted with ultrapure water and nanobubble concentrations were measured with NTA. Addition of IL-1ra resulted in significant reduction in nanobubble concentration, as illustrated in Figure 4-5A. The addition of just 0.1 mg/mL IL-1ra in the lyophilized samples resulted in a

decrease in nanobubble concentration from 6.5 x 10^9 particles/mL in samples without protein to 6.2 x 10^8 particles/mL in samples with added protein. Further increases in IL-1ra concentrations up to 10 mg/mL did not induce any significant additional changes in the number of nanobubbles generated.

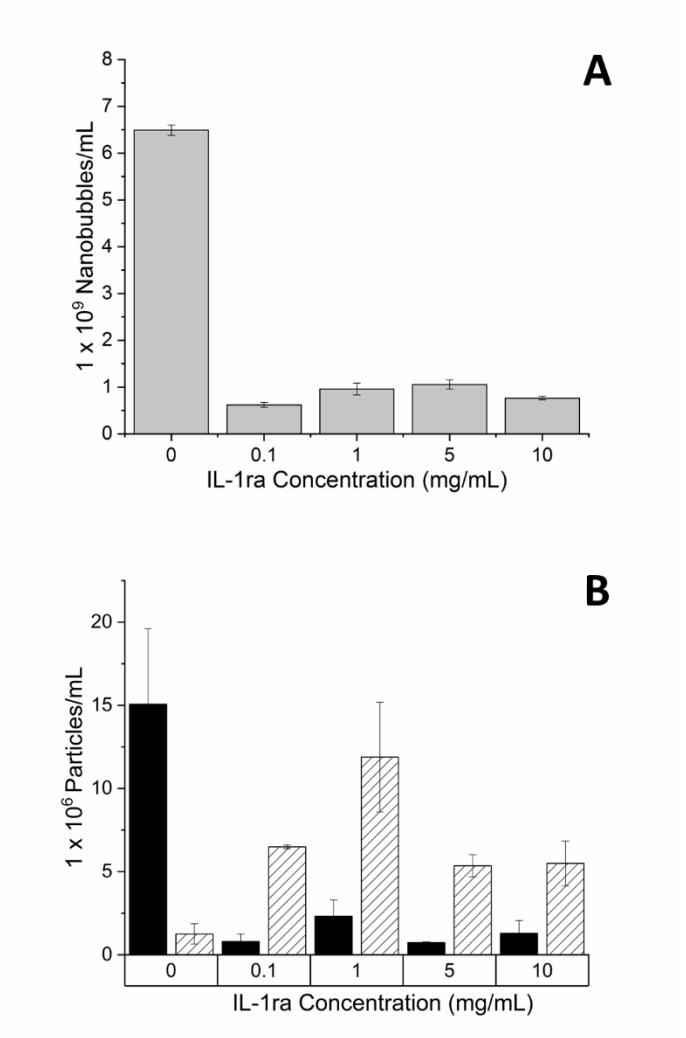

Figure 4-5. A. Number of nanobubbles generated (per mL) following reconstitution of formulations with different concentrations of IL-1ra. B. Number of positively buoyant (black bars) and negatively buoyant particles (cross hatched bars) formed (per mL) following reconstitution of lyophilized formulation with different concentrations of IL-1ra.

Nanoparticles formed following reconstitution of lyophilized IL1-ra formulations could plausibly have been composed of either gas bubbles or protein. To differentiate between these two possible particle types, resonant mass measurement (RMM) analysis of the reconstituted samples

was conducted. The samples showed significant increases in the concentrations of negatively buoyant (denser than the bulk liquid) particles, which can be attributed to the presence of insoluble protein aggregates as shown in Figure 4-5B. Similar to the results obtained from nanoparticle tracking analysis, all reconstituted formulations containing IL-1ra exhibited a decrease in the number of positively buoyant particles compared to equivalent protein-free samples.

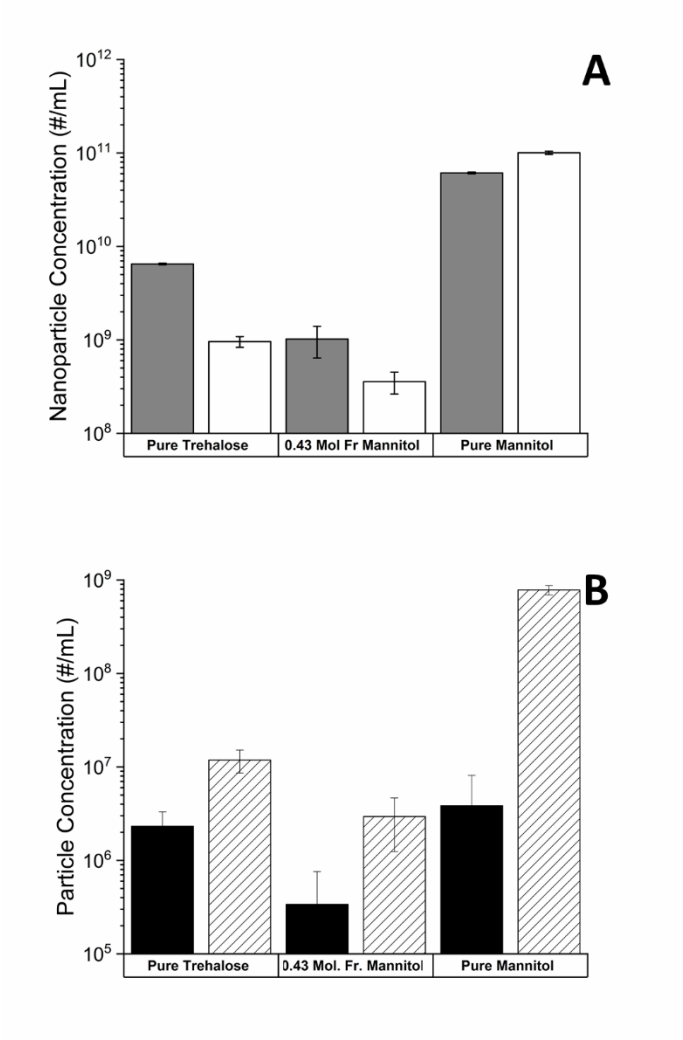

Figure 4-6 A. Nanobubble concentration in formulations with (white bars) and without (dark gray bars) IL-1ra (1 mg/mL). B. Concentration of positively (black bars) and negatively (cross hatched bars) buoyant particles generated after reconstitution of formulations containing IL-1ra. Formulations containing mannitol and/or trehalose without and with IL-1ra (1 mg/mL) were freeze dried using our standard lyophilization procedure. Samples were subsequently reconstituted with water and particle formation was characterized using NTA and RMM.

The effects of IL-1ra on particle concentrations in reconstituted formulations that contained either mannitol alone or mannitol-trehalose mixtures (0.43 mole fraction mannitol) were also studied. As described earlier, nanoparticle concentrations in reconstituted mannitol/trehalose solutions were much lower than in comparable samples of mannitol or trehalose alone. Addition of 1 mg/mL IL-1ra further reduced the number of nanobubbles detected, from 1.0×10^9 nanobubbles/mL to 3.6×10^8 nanobubbles/mL, as shown in Figure 4-6A. In contrast, samples containing 1 mg/mL IL-1ra lyophilized from solutions containing mannitol alone showed higher nanoparticle concentrations than comparable samples without IL-1ra (1.0×10^{11} particles/mL and 6.1×10^{10} particles/mL, respectively). This increase in nanoparticle content in pure mannitol formulations was due to the formation of negatively buoyant particles, as shown in Figure 4-6B. Characterization of the pure mannitol formulations as well as the mannitol/trehalose mixture with RMM showed that both negatively and positively buoyant particles were generated in all reconstituted formulations. However, the concentration of both negatively and positively buoyant particles was significantly lower in mannitol/trehalose formulations compared to those containing pure mannitol or trehalose.

The final component of this study investigated the stability of IL-1ra following reconstitution of lyophilized formulations. Il-1ra was lyophilized using our standard lyophilization protocol in a formulation containing either pure mannitol or trehalose as well as in a 0.43 mole fraction mannitol/trehalose mixture. Following reconstitution of these formulations and incubation for 10 days, formation of micron-sized particles was measured using flow imaging microscopy while IL-1ra monomer loss was monitored with SE-HPLC. Particle concentrations measured with flow imaging microscopy following 10 days of incubation showed that all lyophilized and reconstituted formulations contained more particles than control samples which had not been

lyophilized (Figure 4-7A). After reconstitution, formulations lyophilized with mannitol as the only excipient contained the highest number of particles, with 110,000 particles/mL. Lyophilizing with trehalose as the excipient reduced the total number of particles generated to 5,000 particles/mL, but the fewest particles were observed in the lyophilized mannitol/trehalose mixture with 2,400 particles/mL. Size exclusion chromatography showed that the formulation with mannitol induced the most pronounced destabilization of IL-1ra, with 10% monomer loss observed immediately following reconstitution (Figure 4-7B). Monomer loss in mannitol formulations appeared to be reversible and dropped to 5% after 10 days. The other two lyophilized formulations did not show a significant difference in monomer content over the 10-day period.

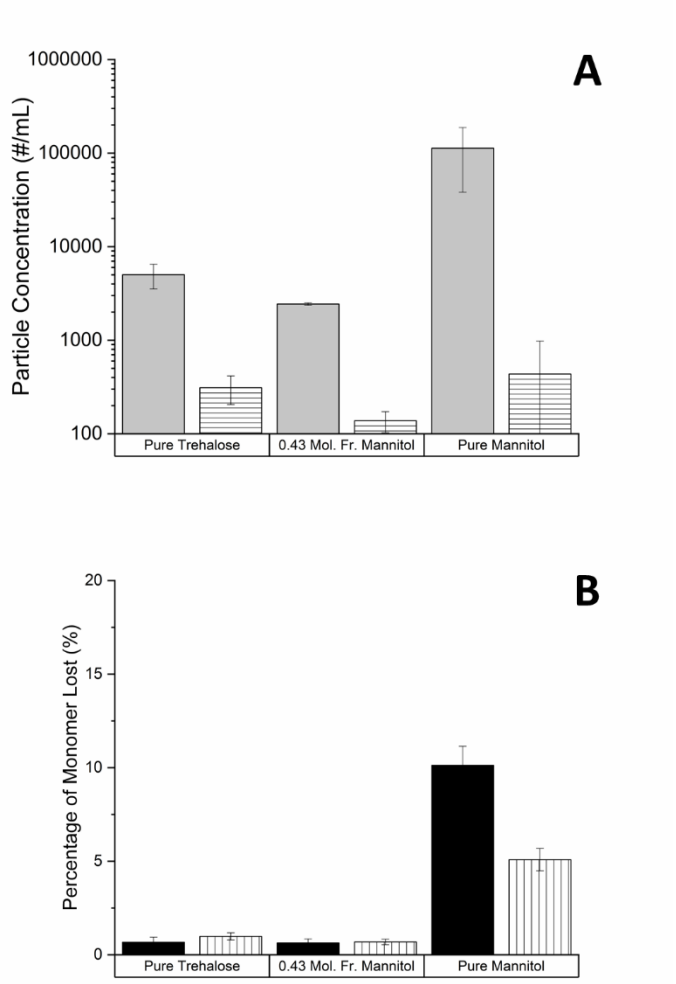

Figure 4-7. The effect of lyophilization (formulations containing mannitol and/or trehalose) on the stability of reconstituted IL-1ra was monitored with flow imaging microscopy and SE-HPLC. A.) The concentrations of particles greater than 2 µm in size were measured after incubating samples for 10 days at 40 °C using flow imaging microscopy. Particle formation after incubation was compared between lyophilized formulations reconstituted at the beginning of the incubation period (light gray bars) to the same aqueous formulations containing IL-1ra which were not lyophilized (horizontal lined bars). B.) Loss of soluble IL-1ra monomer in reconstituted lyophilized formulations was measured using size exclusion chromatography. Monomer loss was measured either immediately after reconstitution (black) or after incubation for 10 days at 40 ˚C (vertical lined bars).

4.5 Discussion

During the early stages of the freezing process, crystals nucleate and grow rapidly. But ice crystals that nucleate within viscous, freeze-concentrated excipient phases may have little opportunity to grow, leaving nanocrystals of ice entrapped within the glassy freeze-concentrate. Sublimation of these ice nanocrystals during primary and secondary drying leaves behind nano-sized voids; we propose that these voids are converted to nanobubbles during reconstitution.

We had initially expected that crystallization of mannitol during lyophilization would greatly reduce the numbers of nanobubbles observed after reconstitution, but in fact, the opposite was observed, with nanobubble concentrations *increasing* as a function of mannitol crystallinity. As shown in Figures 4-1 and 4-2, nanobubble concentrations measured following reconstitution correlated with crystalline content of mannitol/trehalose formulations at mannitol mole fractions greater than 0.5. We explain this somewhat surprising result by suggesting that crystallization of mannitol encourages the nucleation of additional ice nanocrystals. At higher mole fractions, mannitol begins to crystallize and is known to exist in four physical forms. Three of these are anhydrous, and the fourth is a hemihydrate.[169,170] When mannitol crystallizes to form anhydrous polymorphs, water that previously had been associated with amorphous mannitol is excluded from the growing crystals, resulting in local regions of higher water content within the freeze concentrated liquid. The combination of high local concentrations of water and local reductions in viscosity due to water's plasticizing effect promotes additional nucleation of nano-sized ice crystals within these regions.[171] In turn, these nanocrystals become nano-voids when the ice sublimes during primary drying, eventually resulting in the formation of nanobubbles during reconstitution. It is important note that the maximum crystallinity achieved in these studies was 77% for pure mannitol formulations. Therefore, in all formulations a significant fraction of the freeze concentrated liquid remained amorphous. We postulate that this amorphous phase is required for nucleation of nano-sized ice crystals and subsequent nano-void formation in lyophilized formulations.

Because of their small radii of curvature, nano-sized ice crystals are highly susceptible to Ostwald ripening phenomena and coarsening.[172,173] The rate of Ostwald ripening is inversely proportional to viscosity, which decreases rapidly as temperature is increased above the glass

transition temperature.[107,174,175] Therefore, any time that the frozen concentrate spends at temperatures near or above the glass transition temperature of the freeze-concentrated liquid results in a shift in the ice crystal size distribution towards fewer, larger crystals. Maximally freeze-concentrated mixtures of trehalose and mannitol have glass transition temperatures which are lower than those of the pure components.[176] The glass transition temperature of these mixtures decreases as mannitol is added to trehalose. We observed in Figure 4-1 that for amorphous mixtures with mannitol mole fractions less than 0.5, nanobubble concentrations observed after reconstitution were greatly reduced as the concentration of mannitol was increased, correlating with the decreased glass transition temperatures in these mixtures, which lead to increased Ostwald ripening and therefore loss of nano-sized ice crystals.

Reductions in nanobubble generation attributed to Ostwald ripening suggests that promoting coarsening phenomena by annealing could be an effective strategy for reducing nanobubble generation. Therefore, we studied samples annealed at -5 ˚C, well above the glass transition temperature of maximally freeze-concentrated solutions of both disaccharides. Heating above the glass transition of an amorphous sugar solution results in a pronounced reduction in viscosity, significantly increasing Ostwald ripening rates.[107,174,175] Although higher rates of Ostwald ripening increase the average size of crystals and reduce their total number, the decrease in viscosity might also increase the nucleation rate of new crystals. This suggests that annealing could promote competing processes that both inhibit and promote nanobubble formation upon reconstitution.

Our studies of nanobubble generation from annealed formulations show that the effect of annealing is dependent on the solute composition of the lyophilized formulations. To help explain this dependence we have provided illustrations in Figure 4-8 depicting our understanding of the

effect of annealing on the morphology of the freeze concentrate at three mannitol concentrations. We begin by considering the freeze concentrates of formulations at the lowest mannitol concentrations (Figure 4-8A). Under these conditions, mannitol and trehalose mutually inhibit each other's crystallization, resulting in an amorphous continuous phase surrounding ice crystals of various sizes. During annealing of these samples, Ostwald ripening of ice crystals is the primary process that occurs, increasing the size of larger ice crystals and reducing the number of nano-sized ice crystals. Sublimation of the crystals during primary drying converts the nano-sized ice crystals to voids that become nanobubbles following reconstitution, but the decrease in the number of nanocrystals after annealing leads to reduced nanobubble concentrations (Figure 4-1). As the concentration of mannitol is increased to moderate values, trehalose no longer completely inhibits mannitol crystallization, and annealing begins to induce crystallization of previously amorphous mannitol (Figure 4-2). As illustrated in Figure 4-8B, mannitol crystallization releases water molecules into the surrounding glassy matrix, where they may nucleate to form additional nano-sized ice crystals, eventually leading to more nanobubbles during reconstitution.

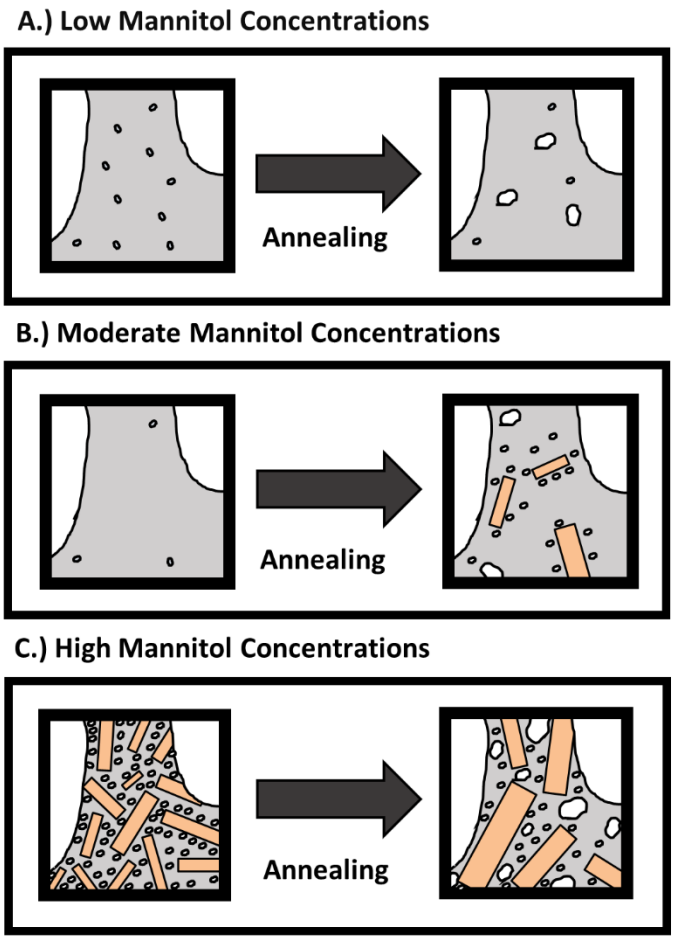

Figure 4-8. Schematic illustration summarizing the effects of mannitol concentration and annealing on the concentration and size distribution of ice crystals within the freeze concentrate. In the above images amorphous domains are represented by the gray regions while ice crystals are shown in white. In addition, mannitol crystals are represented by orange rectangles.

As the concentration of mannitol is increased further in lyophilized formulations, large reductions in the total number of nanobubbles formed following reconstitution are observed in annealed samples (Figure 4-1). PXRD data provided in Figure 4-2 shows that, at the higher mannitol concentrations, annealing has little effect on the crystallinity of mannitol in these formulations, suggesting that disappearance of ice nanocrystals by Ostwald ripening is the primary process occurring during annealing. However, ripening appears to induce larger reductions in nanobubble formation at higher mannitol concentrations compared to low mannitol concentrations. This increased rate of ripening can be attributed to the higher density of ice crystals

present within the amorphous phase in highly crystalline formulations. It is well established that the rate of Ostwald ripening increases with the volume fraction of the dispersed phase.[177–180] As shown in Figure 4-8C at high mannitol crystallinities, nano-sized ice crystals are concentrated within the remaining amorphous phase. Ostwald ripening is a diffusion limited process, therefore shorter distances between ice crystals results in the faster transfer of water molecules between crystals leading to higher dissolution rates of nano-sized crystals and increased growth rates of larger crystals. The culmination of this effect is that annealing of freeze concentrates containing highly crystalline mannitol results in rapid coarsening of nano-sized ice crystals that concentrated within the amorphous domain, thereby reducing nanobubble generation upon reconstitution.

Unexpectedly, lyophilized samples of pure trehalose generated more nanobubbles upon reconstitution if the samples were annealed at -5 °C prior to drying. Although trehalose is commonly found to be amorphous after lyophilization, Sundaramurthi et al. have shown that during freezing, trehalose may crystallize as a dihydrate.[163] During secondary drying, crystalline trehalose dihydrate is unstable and dehydrates back to an amorphous phase.[163,164] We speculate that the annealing–dependent increase in nanobubble generation that we observe in pure trehalose samples can be attributed to the formation of crystalline trehalose dihydrate during the annealing step, and its subsequent dehydration back to an amorphous form during secondary drying. We note that nanobubbles were created when amorphous trehalose formed by dehydrating trehalose dihydrate crystals was reconstituted (Figure 4-4).

There have been reports of mannitol hemihydrate formation during freezing and annealing and its subsequent dehydration back to an anhydrous polymorph during secondary drying.[181,182] Similar to the results obtained following dehydration of trehalose dihydrate, conversion of hemihydrate to an anhydrous polymorph could potentially create nanometer sized voids. Based on

PXRD, there was no evidence of existence of mannitol hemihydrate in the final lyophilized solid. However, because secondary drying can convert hemihydrate to an anhydrous polymorph, it is possible that the hemihydrate was formed during freezing or annealing but it dehydrated during drying. To test this alternate explanation, lyophilization would need to be conducted in the chamber of a variable temperature X-ray powder diffractometer to detect hemihydrate prior to dehydration. However, experiments conducted in such an XRD instrument might not accurately reflect conditions in a laboratory or industrial lyophilizer, where differences in geometry and sample mass could significantly alter cooling rates and ice nucleation temperatures.

After gaining an improved understanding of the mechanism of nanobubble generation in lyophilized formulations, we next evaluated how the presence of a protein (IL-1ra) might impact nanobubble formation. As shown in Figure 4-5, the addition of even 0.1 mg/mL IL-1ra resulted in a large decrease in the number of nanobubbles detected with either NTA or RMM. After this initial drop at low protein concentration, the nanobubble concentration did not change significantly even as the protein concentration was increased by two orders of magnitude. The addition of protein to lyophilized formulations could impact the glass transition temperature of the amorphous phase or inhibit excipient crystallization. Previous studies conducted by Liao et al. [168] found that high concentrations of protein (at least 20 mg/mL) were required to significantly alter the physical properties of lyophilized formulations. Interestingly, the effect of protein addition to the lyophilized trehalose formulations on nanobubble generation appeared to "saturate" by 0.1 mg/mL, a concentration much lower than that reported by Liao et al. [168]

When evaluating this result, we must also consider the limitations of the particle sizing and counting methods employed. With a mean diameter of approximately 100 nm, the full distribution of nanobubbles cannot be obtained with either RMM or NTA. Therefore, any change in the

nanobubble size distribution would alter the total number of nanobubbles detected. Furthermore, changes in nanobubble properties induced by protein adsorption, such as changes in refractive indices or density, alter the sensitivity of RMM or NTA respectively. Therefore, we cannot conclude whether lyophilization with protein reduces the total number of nanobubble generated upon reconstitution or whether size distributions and/or optical properties of the nanobubbles are altered.

The lack of protein concentration dependence on the nanobubble concentration suggests that the effect of IL-1ra is likely dependent on the nanobubble surface area. Despite billions of nanobubbles per milliliter being generated following reconstitution, the total surface area of nanobubbles in these suspensions is small. If monolayer adsorption is assumed, the nanobubble surface could be saturated at IL-1ra concentrations well below 0.1 mg/mL. Once the nanobubble surface becomes completely saturated, further addition of protein would be expected to have a minimal effect on the surface properties of nanobubbles. Furthermore, following reconstitution of lyophilized IL-1ra formulations, large numbers of negatively buoyant particles attributed to protein aggregates are generated. The concentration of IL-1ra aggregates formed was independent of protein concentration. We suggest that following reconstitution, IL-1ra may adsorb to the surface of nanobubbles, where perturbation in protein structure and aggregation may occur. This adsorption may destabilize the nanobubbles, resulting in nanobubble collapse and release of aggregate particles into the bulk suspension.

The final component of this study investigated a potential strategy for reducing nanobubble-induced protein aggregation and particle formation in reconstituted lyophilized formulations. Our results showed that lyophilized mannitol-trehalose mixtures containing 0.43 mole fraction mannitol showed smaller numbers of nanobubbles upon reconstitution and also

smaller amounts of aggregated protein compared to pure mannitol or trehalose formulations. Further, after storing reconstituted suspensions for 10 days, fewer micron-sized particles were detected in the 0.43 mole fraction mannitol formulation. These results clearly showed lyophilized protein formulations can be formulated to reduce nanobubble formation upon reconstitution and thereby reduce aggregation and particle formation.

4.6 Conclusions

Our results suggest that nanobubbles observed after reconstitution of lyophilized formulations depends on the formation of nano-sized ice crystals within the freeze concentrated liquid which leave behind nano-sized voids following primary and secondary drying. Crystallization of excipients such as mannitol release water into the freeze concentrate, promoting additional ice crystallization and therefore increase nanobubble concentrations following reconstitution. Nano-sized ice crystals are susceptible to Oswald ripening phenomena at temperatures near or above the glass transition temperature of the freeze concentrate. Annealing samples above the glass transition temperature promotes coarsening of ice crystals and reduction in nanobubble generation. However, depending on the formulation composition, annealing may promote excipient crystallization facilitating the formation of additional nano-sized ice crystals. In addition, if the formulation is designed to reduce nanobubble generation, there is also reduced protein aggregation, both upon reconstitution of the lyophilized protein formulations and after longer incubation periods. The results included in this work suggest a potential strategy for minimizing nanobubble formation upon reconstitution of lyophilized protein formulations and thereby reducing nanobubble-induced protein aggregation and particle formation.

4.7 Acknowledgements

The authors gratefully acknowledge support from the National Institute of Health, grant REB026006A (TR). The work was partially supported by the William and Mildred Peters Endowment fund (RS).

Chapter 5 DEHP Nanodroplets Leached from Polyvinyl Chloride IV Bags Promote Aggregation of IVIG and Activate Complement

This chapter will be submitted to the Journal of Pharmaceutical Sciences as; Snell, JR., Monticello, CR., Her, C., Ross, EL., Frazer-Abel, AA., Carpenter, JF., & Randolph, TW. DEHP Nanodroplets Leached from Polyvinyl Chloride IV Bags Promote Aggregation of IVIG and Activate Complement.

5.1 Abstract

Concerns regarding the impact of sub-visible particulate contaminants on the safety and efficacy of therapeutic protein products have led manufacturers to implement strategies to minimize protein aggregation and particle formation during manufacturing, storage and shipping. However, once these products are released, manufacturers have limited control over a number of product handling factors that might impact product quality. In this work we investigated the effect of bis (2-ethylhexyl) phthalate (DEHP) nanodroplets generated in polyvinyl chloride (PVC) bags of intravenous (IV) saline on the stability and immunogenicity of intravenous immunoglobulin (IVIG) formulations. We first showed that PVC IV bags containing saline can release DEHP droplets into the solution when agitated or when transported using a pneumatic tube transportation system in a clinical setting. We next evaluated the effects of emulsified DEHP nanodroplets on IVIG stability and immunogenicity. IVIG adsorbed strongly to DEHP nanodroplets, forming a monolayer. Aggregation of IVIG that occurred during agitation was accelerated in mixtures containing DEHP nanodroplets. The immunogenicity of DEHP nanodroplets and IVIG aggregates generated in these formulations were evaluated using an in-vitro assay of complement activation in human serum. Complement was activated by the alternative pathway by IVIG formulations that containing DEHP nanodroplets. The results suggest DEHP nanodroplets shed from PVC IV bags

could reduce protein stability and induce activation of the complement system, potentially contributing to adverse immune responses during the administration of therapeutic proteins.

5.2 Introduction

Therapeutic proteins comprise a rapidly growing segment of the pharmaceutical industry, providing highly specific and targeted therapies.[1] However, one of the challenges associated with the development of therapeutic proteins is the potential for adverse immune responses, which can have consequences ranging from reductions in therapeutic efficacy to severe hypersensitivity reactions.[2,3] Even trace amounts of particulates within formulations of therapeutic proteins are potential contributors to adverse immune responses.[4] Kotarek et al.[5] and Barnard et al.[6] have shown correlations between sub-visible particle contaminants and increased rates of immune responses in patients to marketed therapeutic protein products. Studies such as these have highlighted the importance of identifying and controlling sub-visible particulate matter to ensure the safety and efficacy of therapeutic protein products.[7,8] Furthermore, the increased immunogenicity of protein formulations containing silicone oil droplets, as well as the common use of nano- and micro- particles as adjuvants in vaccines highlight the immunogenic potential of subvisible particulate matter in protein formulations.[9–11]

Therapeutic protein manufacturers devote significant effort to minimizing subvisible particulate matter that may be formed during the manufacturing, storage and transportation of therapeutic protein products.[12] Less focus has been placed on subvisible particle formation during the preparation and administration of therapeutic proteins in clinical settings.[13,14] Recent studies have reported the presence of subvisible particles in solutions in intravenous (IV) bags used for IV infusion of therapeutic protein products.[15,16] These studies suggest that IV solutions and bags used

for the dilution and administration of therapeutic proteins could contribute to subvisible particle contents, potentially impacting the safety and efficacy of these products.

Polyvinyl chloride (PVC) is a common component of medical devices, with desirable properties that include chemical resistance, durability, ease of use and low cost.[17–19] However, PVC is not inherently flexible, and plasticizers may be added to PVC at concentrations as high as 30-40% (wt/wt) to achieve desired material properties.[19,20] These plasticizers are not covalently bound to the PVC matrix, and thus can readily leach into the surrounding solutions.[21] Leaching and extraction of bis (2-ethylhexyl) phthalate (DEHP) from PVC bags have been reported frequently, with the highest levels of DEHP found in bags used to store and deliver blood, enteral and parenteral nutrition admixtures or lipophilic drugs.[22–24]

Concerns regarding DEHP leached from plasticized PVC materials have resulted in many studies focused on potential biological impacts and calls for regulations on the use of PVC in medical devices.[25] DEHP exhibits relatively low acute toxicity, with LD 50 values of 1 – 30 g/kg of bodyweight, and the risk of toxicity in adult patients during infusion of aqueous solutions using PVC medical devices is considered to be minimal .[22,26,27] The greatest risks associated with the use of DEHP-plasticized PVC medical devices are thought to be related to applications involving chronic exposure (e.g., for hemophilia or dialysis patients), and exposure during critical points in childhood development.[20] DEHP has been identified as a reproductive toxicant that affects the development of the male reproductive system, and therefore PVC medical devices are not recommended for use with pregnant women or peripubertal males.[28–30]

Although PVC medical devices are used in a variety of medical applications, there are still potential concerns regarding the safety of DEHP related to its potential incompatibility with therapeutic proteins. Migration from PVC bags into aqueous solutions often results in DEHP

concentrations that exceed its solubility limit in water of 3 µg/mL.[31–33] These findings suggest that DEHP may be present as suspended liquid droplets within PVC bags, consistent with reports of particulate contaminants being detected in solutions administered using PVC IV bags.[15,34,35] One unexplored concern is that DEHP droplets that migrate into protein formulations from PVC bags may negatively impact the stability or immunogenicity of the protein.

The goal of this study was to evaluate leaching of DEHP droplets from IV bags composed of plasticized PVC and to determine the effects of these droplets on the stability and immunogenicity of formulations of intravenous immunoglobulins (IVIG). We began by evaluating the effect of product handling on leaching of DEHP droplets from PVC bags into IV saline solutions. Results were compared to those obtained in polyolefin (PO) IV bags, which do not contain phthalate plasticizers. Particles generated in saline in both bag types were characterized after shaking to mimic shipping-related mechanical stresses. To replicate additional stresses which could occur in clinical settings, we also tested the effects of transporting IV bags using a pneumatic tube system that is commonly used in hospitals. Particles formed in IV bags were characterized using flow imaging microscopy, resonant mass measurement and nanoparticle tracking analysis.

Exposure of proteins to silicone-water interfaces may result in increased protein aggregation and particle formation.[36–40] Because both silicone oil and DEHP present hydrophobic interfaces, we hypothesized that DEHP droplets may behave in a similar fashion as silicone oil droplets.[32,41] We compared the effects of emulsified silicone oil and DEHP nanodroplets on the adsorption behavior and aggregation propensity of IVIG. The formation of intermolecular protein networks at the DEHP-water interface was investigated using interleukin-1 receptor antagonist (IL-1ra) using interfacial shear rheology and compared with corresponding results for silicone oil-

water interfaces obtained from the literature.[42] Finally, as an indicator of the potential immunogenic properties of DEHP suspensions, we evaluated complement activation in human serum by IVIG formulations containing DEHP and silicone oil nanodroplets.

5.3 Materials and Methods

5.3.1 Materials

Intravenous immunoglobulin (IVIG) was purchased from the University of Colorado Boulder Apothecary in a liquid formulation (Gammagard, Baxter, Deerfield, IL). Recombinant human interleukin-1 receptor antagonist (IL-1ra) was donated by Amgen (Thousand Oaks, CA) at a concentration of 100 mg/mL. All buffer salts and excipients including sodium chloride, glycine, (Fisher Chemical, Hampton, NH), sodium citrate (Alfa Aesar, Haverhill, MA), phosphate buffer and MES Buffer (Sigma Aldrich (St. Louis, MO) were of reagent grade or higher. For preparation of emulsions, silicone oil (polydimethylsiloxane, Dow Corning 360, 1000 cSt) was purchased from Nexeo Solutions (Denver, Colorado), and DEHP was acquired from Sigma-Aldrich (St. Louis, MO). The extrinsic fluorescent dye 4,4′-dianilino-1,1′-binaphthyl-5,5′-disulfonic acid dipotassium salt (bis-ANS) was purchased from Thermo Scientific (Waltham, MA).

IV bags containing 100 mL of IV saline, including 100 mL Viaflex bags composed of PVC (NDC 0339-0049-48, Baxter, Deerfield IL) and 100 mL Freeflex bags composed of a multilayer polyolefin (PO) film (NDC 17271-701-03, Becton Dickinson, Franklin Lakes, NJ) were purchased from McKesson Surgical Supply.

5.3.2 Sample Preparation

All saline, mobile phases and buffer solutions were prepared using ultrapure water generated with a PURELAB flex 1 water deionization system (ELGA Labwater, Wycombe, UK). All solutions were filtered using a 0.22 µm filter (MCE membrane filter, Millipore, Burlington, MA) using a vacuum filtration setup. To remove insoluble proteinaceous particles from IVIG or

IL-1ra solutions, solutions were centrifuged at 21,000 xg for 60 minutes using an Eppendorf 5424R centrifuge (Hamburg, Germany). Following centrifugation, the supernatant from each solution was removed and used for subsequent experiments.

5.3.3 Particle Characterization Methods

The concentration and size distributions of particles and droplets with dimensions between 50 and 1000 nm were characterized with NanoSight nanoparticle tracking analysis (NTA) (Malvern Panalytical, Westborough, MA). Samples were loaded in a 1 mL silicone oil-free syringe and injected slowly into the instrument inlet port to minimize bubble formation. Following sample injection, camera settings were optimized based on the particle concentration and properties of particles in each sample. Once the settings were optimized, 5 videos were recorded with a duration of 30 seconds each. Using the NanoSight 3.0 analysis software the particle and droplet concentrations and size distributions were calculated as an average of the results obtained from the 5 videos.

The concentration and size distribution of particles and droplets with dimensions between 200 nm and 5 µm were measured using a resonant mass measurement (RMM) instrument (Archimedes, Malvern Panalytical, Westborough MA). Using RMM, particles were counted and classified as either positively or negatively buoyant based on their density relative to that of the bulk fluid. Samples were loaded to the Hi-Q micro sensor chip for 20 seconds before acquiring data for 10 minutes. The sensor was rinsed for 90 seconds with ultrapure water after each sample.

A SALD7500-nano (Shimadzu, Kyoto, Japan) was employed to measure the concentration and size distribution of DEHP droplets over the range of 100 nm to 60 µm using a quantitative laser diffraction (qLD) based method. This instrument calculates both concentration and size distribution from laser diffraction data using scattering patterns predicted by Mie scattering theory

and the intensity of scattered light.[85] All measurements were conducted using a batch cell with a sample volume of 8 mL and measured in triplicate. Concentrations and size distributions were calculated using a DEHP refractive index of 1.49 and the WingSALD bio-7500 software version 3.3.[216]

The concentration, size distribution and morphology of micron-sized particles were characterized using flow imaging microscopy (Flowcam, Fluid Imaging Technologies, Scarborough, ME). For each sample the instrument was primed with 0.1 mL of sample before 0.2 mL was analyzed at a flowrate of 0.080 mL/min using an FC100 flow cell, combined with a 10X objective and collimator. All measurements were conducted in triplicate.

5.3.4 Measurements of Surface Charge

The zeta potentials of DEHP nanodroplets and IVIG molecules were measured with a Litesizer 500 instrument (Anton Paar, Graz, Austria) using the principle of electrophoretic light scattering. For each measurement, 350 µL of sample was loaded into an Omega cuvette purchased from Anton Paar. All measurements were conducted at 25 °C, and sample concentrations were optimized to provide light intensities between 300 and 800 kcounts/s. All zeta potential measurements were completed in triplicate in 5 mM sodium citrate buffer pH 5.

5.3.5 Chemical Analysis of Contaminants Leached from PVC IV Bags

To determine the chemical identity of contaminants leached from PVC IV bags, samples from a shaken PVC IV bag were extracted into hexane and characterized using gas chromatography coupled with mass spectrometry (GC/MS). GC/MS analysis was conducted using a Thermo ISQ single quadrupole mass spectrometer coupled to a ThermoFisher Scientific TRACE 1310 gas chromatograph. Sample volumes of 1 µL were injected using a Hamilton 701N 10 µL syringe, and separation was performed on a Phenomenex Zebron ZB-HT5 column. Following sample injection, the oven temperature was held at 100 °C for 3 minutes before being ramped to

325 °C at a rate of 40 °C/min and then subsequently held at 325 °C for 2 minutes. GC/MS data were acquired from 3.5 min of the temperature gradient ranging from 50 to 500 amu, with a 0.2 second scan time. Data were analyzed using Chromeleon 7.2 SR4 with embedded library.

5.3.6 Quantification of Soluble IVIG Monomer and Dimer Concentration by SE-HPLC

The loss of soluble IVIG monomer and dimer from solutions with or without DEHP nanodroplets was evaluated using size exclusion high performance liquid chromatography (SE-HPLC). For analysis, all samples were diluted by 50% with deuterium oxide and subsequently centrifuged at 21,000 x *g* for 1 hour at 4 °C. Deuterium oxide was added to increase the difference in density between the bulk fluid and the DEHP nanodroplets, significantly improving separation. The samples were injected into an Agilent 1100 HPLC (Santa Clara, California), and IVIG elution was monitored at 280 nm. This system was operated at 0.6 mL/min with a mobile phase composed of 200 mM phosphate buffer pH 7 with 400 mM NaCl. Separation was achieved using a Tosoh TSKgel G3000SWxl size exclusion column coupled with a Tosoh TSKgel guard column (Tokyo, Japan). The extent of IVIG loss was quantified by comparing the areas under the monomer and dimer peaks of stressed samples to those for unstressed controls.

5.3.7 Particle Formation from Shaken PVC IV Bags

PVC and PO IV bags (100 mL nominal volume) containing 100 mL of intravenous (IV) saline were stressed to evaluate particle formation in bags exposed to stresses typical of those encountered during shipping and handling. Bags were placed in an I26 incubator shaker (New Brunswick Scientific, Edison, NJ) for 3 days at 40 ˚C with a constant rotation speed of 350 rpm. Following incubation, bags were left at room temperature for 1 hour to allow bubbles to dissipate before characterizing particle concentration using flow imaging microscopy, NTA and quantitative laser diffraction.

5.3.8 Pneumatic Tube System Studies

A pneumatic tube system (Swisslog, Buchs, Switzerland) at the Children's Hospital Colorado was used to transport IV bags containing 100 mL of saline between the central pharmacy located in the hospital basement to a 4th floor nursing station. To evaluate particle formation caused by transportation in this system, bags were transported either once or multiple times. Bags were transported both from the central pharmacy to the 4th floor nursing station as well as from the 4th floor nursing station back to the central pharmacy. Each time that bags were transported either up or down was counted as a single pass. Particle concentrations in the IV bags were measured using flow imaging microscopy, NTA and RMM immediately after transporting the bags

5.3.9 Preparation and Characterization of DEHP and Silicone Oil Emulsions

Silicone oil emulsions were prepared in water using a combination of mechanical mixing proceeded by high pressure homogenization following the procedure developed by Ludwig et al.[217] DEHP-in-water emulsions were prepared using a modified version of the protocol for generation of silicone oil emulsions. Using a Gilson Microman 1 mL positive displacement pipette, 3 mL of DEHP was combined with 97 mL of ultrapure water in a stainless-steel cylinder. This suspension was mixed under high shear using a Virtishear mechanical homogenizer (The Virtis Company, Gardiner, New York) for 15 minutes at 30,000 rpm. Immediately after the completion of mechanical homogenization, the suspensions were emulsified using a high-pressure Emulsiflex C5 homogenizer. The suspension was first emulsified for 7 passes at a pressure which oscillated between 5,000 to 10,000 psi; followed by an additional 5 passes at a 10,000 – 15,000 psi. The final emulsions were collected and stored at 4 °C in 50 mL polypropylene tubes.

The concentration of silicone oil and DEHP emulsions was evaluated using a procedure developed by Ludwig et al. utilizing infrared spectroscopy[217] Silicone oil and DEHP emulsions were extracted into hexane and subsequently analyzed using attenuated total reflectance Fourier-

transform infrared spectroscopy (Thermo Nicolet 6700 FTIR, Waltham, MA). The mass of DEHP or silicone oil in each emulsion was determined by comparing the area under the peak for each sample to a standard curve prepared for both DEHP and silicone oil. The region of the spectrum integrated was dependent on the chemical structure of each molecule. For silicone oil emulsions, absorbance by Si-CH_3 groups between 1280 and 1240 cm^{-1} was used, whereas absorbance by carbonyl groups between 1680 and 1760 cm^{-1} was utilized for quantitation of DEHP emulsions.[218]

The size distribution of nanodroplets in both emulsions were measured using a Beckman Coulter LS230 (Fullerton, CA). Size distributions were calculated from laser diffraction data using refractive indices of 1.4046 and 1.4853 for silicone oil and DEHP, respectively.[216,219] Using a combination of the emulsion concentration and droplet size distribution, the total surface area of DEHP droplets in each emulsion was calculated.

5.3.10 Evaluation of Protein Surface Coverage

IVIG adsorption to DEHP nanodroplets was quantified using a solution depletion method similar to that described previously by Gerhardt et al.[34] Adsorption studies were conducted with DEHP emulsions containing 5 mM sodium citrate buffer pH 5 with 154 mM NaCl. In addition, to aid in separation of DEHP nanodroplets each formulation contained 25% deuterium oxide by volume. Following sample preparation, samples were incubated quiescently at room temperature for 1 hour. After incubation, samples were centrifuged at 21,000 x *g* for 1 hour to separate the aqueous phase from the DEHP nanodroplets. Centrifugation resulted in a creamed layer of DEHP at the surface of each sample, but no pellet formation was observed. Following centrifugation, to avoid disruption of the creamed DEHP layer the middle fraction of each sample was removed carefully for analysis with a 1 mL silicone oil-free syringe and needle. The concentration of protein remaining following separation of the DEHP nanodroplets was measured with a Pierce 660 nm

protein assay (Thermo Fisher Scientific, Waltham MA) in a microplate format using an Infinite M Plex plate reader (Tecan, Mannedorf Switzerland). Protein surface coverage was calculated using the concentration of adsorbed protein and the surface area of DEHP nanodroplets added.

Adsorption data were fit to a Langmuir isotherm:

$$\Gamma = \frac{\Gamma_{max} K C}{1 + KC}$$

where K is a binding constant, Γ is the surface coverage and Γ_{max} is the maximum surface coverage.[220,221]

5.3.11 Extrinsic Fluorescence Measurements with bis-ANS

Bis-ANS is a fluorescent dye that is sensitive to hydrophobic protein regions and is frequently used for characterization of structural changes in proteins.[222] Formulations were prepared that contained 5 mM sodium citrate buffer pH 5, 154 mM NaCl, 0.1 mg/mL IVIG and various concentrations of emulsified DEHP and silicone oil droplets. DEHP and silicone oil emulsions contained sufficient nanodroplet surface area to essentially completely adsorb all added IVIG molecules. Samples were incubated quiescently at room temperature for 2 hours prior to addition of bis-ANS and fluorescence analysis (see below). To minimize nanodroplet coalescence and associated reductions in surface area of emulsions, fluorescence intensities in IVIG-free DEHP and silicone oil emulsion controls were measured immediately following sample preparation.

Stock bis-ANS at a concentration of 32 µm was prepared in ultrapure water and protected from light. For each measurement, 100 µL of 32 µm bis-ANS solution was added to 3 mL of sample and incubated for 3 minutes before fluorescence intensities were measured in a front-face orientation using a SLM Aminco Fluorimeter (SLM Instruments, Urbana, IL). Samples were

excited at 390 nm, and emission spectra were recorded from 450 to 600 nm. All samples were prepared and analyzed in triplicate.

5.3.12 Interfacial Shear Rheometry

Formation of interfacial gel layers at DEHP-water interfaces was investigated using a custom-built interfacial shear rheometer[28,29,223]. Experiments were designed for direct comparison to previous studies[223] of IL-1ra gelation at the silicone oil-water interface. Gelation experiments were conducted with 1 mg/mL IL-1ra in 10 mM MES buffer pH 6.5 containing 150 mM NaCl. Sufficient volumes of DEHP were added to completely cover the buffer surface. Rheological measurement experiments were conducted by monitoring motion in the presence of an oscillating magnetic field of a magnetized rod (diameter x length = 0.06 x 2.60 cm^2) suspended by surface tension forces at the DEHP-water interface for up to 14 hours. All additional experimental conditions were identical to those described by Sorret et al.[223]

5.3.13 IVIG Aggregation in Emulsified DEHP and Silicone Oil

Studies of the effect of DEHP and silicone oil nanodroplets on IVIG stability were conducted with emulsified DEHP and silicone oil. Concentrated buffer solutions and IVIG were added to both emulsions to obtain solutions containing 5 mM sodium citrate buffer pH 5 with 154 mM sodium chloride and 0.5 mg/mL IVIG. In droplet-free control samples, sodium chloride and IVIG were diluted in ultrapure water to obtain the same excipient and IVIG concentrations. Samples were incubated at room temperature in 1.7 mL polypropylene test tubes either quiescently or rotated at 8 rpm using a Barnstead Labquake Rotator (Barnstead, Dubuque, IA). For all samples, tubes were filled with 1 mL of liquid, providing a headspace air bubble of 0.7 mL. At each time point, samples from three test tubes from each condition were analyzed for monomer and dimer loss by SE-HPLC.

5.3.14 Complement Activation by IVIG in the Presence of DEHP and Silicone Oil Nanodroplets

Complement activation was measured in mixtures of donated human serum and samples from formulations that contained DEHP or silicone oil nanodroplets and 0.5 mg/mL IVIG in 5 mM sodium citrate buffer pH 5 with 154 mM NaCl. IVIG formulations were prepared that contained 0, 0.01, 0.1 and 1 mg/mL of either silicone oil or DEHP nanodroplets. The formulations were aliquoted into 1.7 mL polypropylene centrifuge tubes and stored at room temperature either quiescently or rotated end-over-end at 8 rpm for 24 hours. The samples were then submitted to Exsera Biolabs (Denver, CO) for complement activation testing. Samples were also characterized for monomer and dimer loss using SE-HPLC and for particle concentration using flow imaging microscopy.

Complement activation was measured in normal human serum pooled from three individual donors previously screened for normal complement function. Test samples were mixed with the pooled human serum at a ratio of one part of sample to nine parts of serum. Immediately following mixing, samples were incubated at 37 ˚C for 30 minutes and then aliquoted and stored at -80 ˚C until further testing was conducted. The extent of complement activation was determined by measuring the levels of four activation fragments that mark activation across the multiple pathways of the complement cascade. Specifically C4a was measured as a marker of activation of the classical or lectin pathway, Bb as a marker of the alternative pathway, C3a as the central point of complement activation and C5a as a marker of terminal pathway activation.[224] The concentrations of each of the markers of complement activation were measured individually using an enzyme linked immunosorbent assay (ELISA) purchased from Quidel Corporation (San Diego, CA). The concentration of each complement protein was measured in quadruplicate for each

sample. The average of these four measurements were plotted as a fold increase compared to concentrations measured in control samples consisting of 1:9 mixtures of saline and human serum.

5.4 Results

5.4.1 Formation of DEHP Droplets in PVC Bags

Table 5-1: Characterization of particles in PVC and PO IV bags using Flowcam, NTA and SALD-7500nano. Particle concentrations in PO and PVC IV bags were measured before and after shaking IV bags at 350 rpm for 3 days at 40 °C.

Particle Characterization Method	IV Bag Material	Particle Concentration Before Shaking (#/mL)	Particle Concentration After Shaking (#/mL)
Flowcam	PVC	2,300 ± 440	96,000 ± 28,000
	PO	720 ± 450	640 ± 110
Nanoparticle Tracking Analysis	PVC	$(3.9 \pm 2.6) \times 10^7$	$(2.5 \pm 0.8) \times 10^8$
	PO	$(8.0 \pm 1.4) \times 10^6$	$(4.5 \pm 1.1) \times 10^7$
SALD-7500nano	PVC	LOD	$(3.0 \pm 0.2) \times 10^7$
	PO	LOD	LOD

LOD – Limit of Detection

The concentrations of micro- and nanoparticulate contaminants in IV bags containing saline were characterized both before and after bags were agitated, which was used to mimic shipping- or handling-related stresses. As shown in Table 5-1, before application of shaking stress, saline solutions in IV bags composed of PVC contained significantly more micro-particles compared to solutions in PO bags and the differences in particle content between the two bag types was exacerbated by stress. Agitation at 350 rpm for 3 days greatly increased micro-particle concentrations in saline in PVC bags, whereas no significant increase in micro-particle content was observed for saline in PO bags. Agitation caused an increase in nanoparticle concentrations for both bag materials (Table 5-1). However, significantly more nanoparticles were detected in saline in PVC bags than in PO bags (Table 5-1). Essentially all micro-particles generated in PVC IV bags appeared to be spherical, consistent with the morphology expected for DEHP droplets (Figure 5-1).

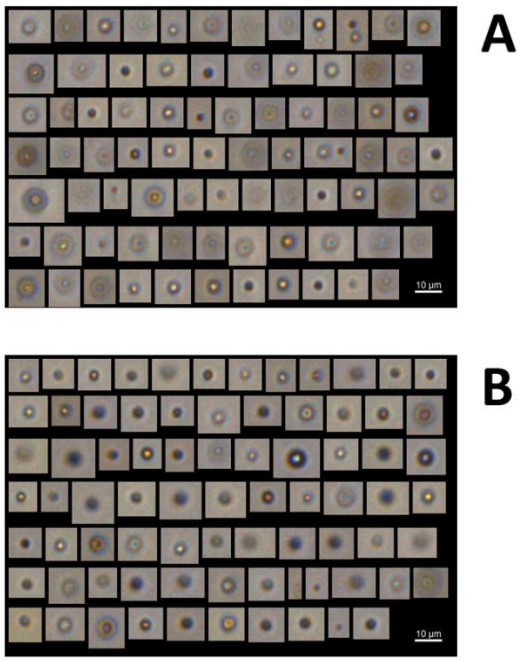

Figure 5-1: Flow microscopy images of particles generated in a PVC IV bag after shaking for three days at 350 rpm (A) or after being transported using a pneumatic tube system (B). A total of 80 particle images was selected randomly from 10,558 images from a shaken bag and 5,146 images from a tubed IV bag.

To investigate the chemical composition of leachates from PVC IV bags, saline solutions from agitated bags were characterized by GC/MS. The results confirmed that the solutions contained the plasticizer DEHP as well as a second, similar plasticizer identified as dioctyl sebacate (data not shown). Because any suspended air bubbles would also exhibit spherical morphologies and might be mistaken for DEHP droplets, we differentiated between these two types of suspended particles using their rising velocities. In aqueous media, the rising velocity of spherical particles composed of either DEHP or air can be easily estimated using the difference in density between the particle and that of the bulk solution. A 2 µm particle composed of air would rise at a rate of 21 cm/day, whereas a DEHP droplet of the same size would rise at a much slower rate of only 0.3 cm/day. Laser diffraction was employed to monitor the change in size distribution of droplet suspensions generated in a saline from an agitated PVC IV bag while the suspensions were stored quiescently at room temperature. Nanoparticles generated in IV bags appeared to

coalesce, because size distributions rapidly shifted towards larger particle sizes (Figure 5-2B). Flow imaging microscopy of samples measured immediately after agitation showed micro-particle counts of 62,000 particles/mL. As DEHP nanodroplets coalesced during 4 days of quiescent incubation, larger microdroplets formed that could be detected by flow imaging microscopy and counts increased to a maximum of 210,000 particles/mL (Figure 5-2C). After reaching a maximum, the concentration of micro-particles decreased slowly as coalescence proceeded over longer storage periods. The rate of loss of micron-sized particles was consistent with the lower rising velocity calculated for DEHP droplets.

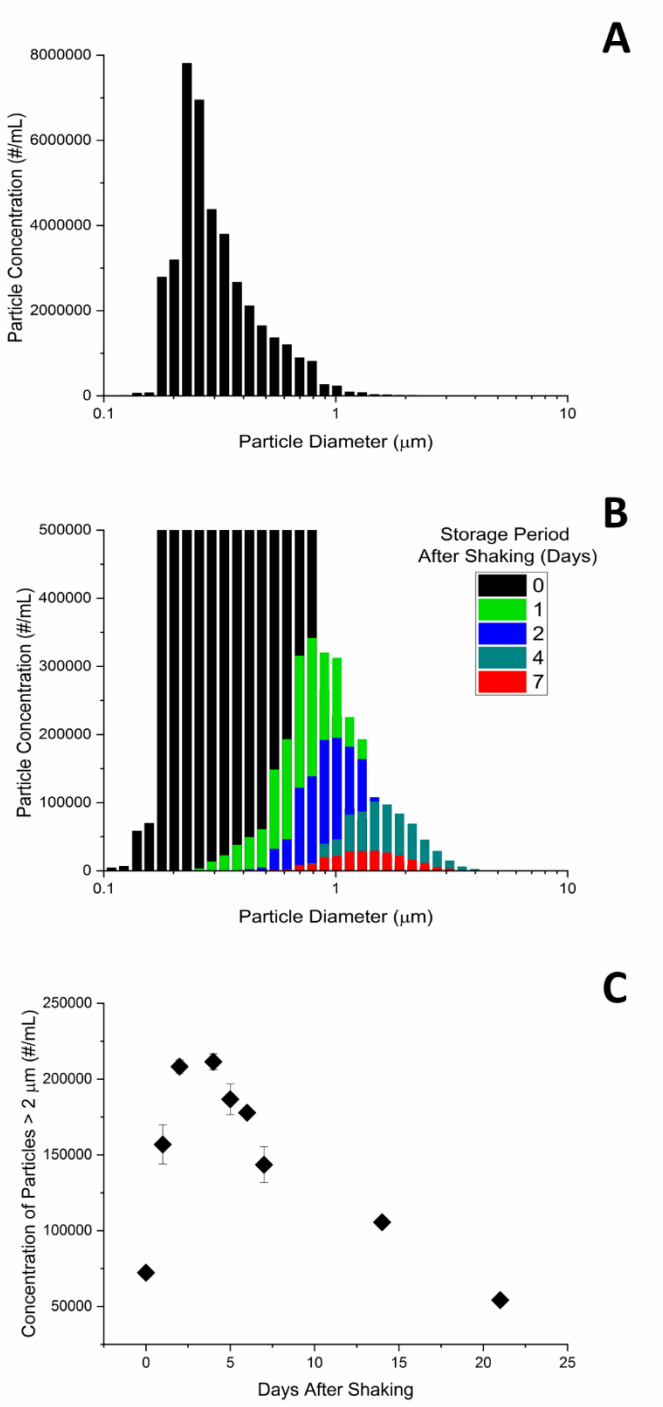

Figure 5-2: Stability of particles generated in shaken PVC IV bags during quiescent incubation at room temperature. A.) Size distribution of DEHP droplets measured with the SALD7500-nano immediately after shaking a PVC IV bag at 350 rpm. B.) Change in size distribution of particles generated by shaking during quiescent storage at room temperature over a 1-week storage period measured with SALD7500-nano C.) Concentration of droplets greater than 2 μm measured with Flowcam over a 3-week incubation period following shaking.

As an example of mechanical stress that can be encountered in clinical settings, we investigated particle formation in IV bags containing IV saline that were transported using a pneumatic tube system used at the Children's Hospital Colorado. Micro- and nanoparticles in either PVC or PO IV bags were plotted as a function of number of passes through the pneumatic tube system. For both PVC and PO bags, transportation in the pneumatic tube system resulted in increases in particle content as measured with flow imaging microscopy and RMM. For PVC IV bags, a single pass increased the micro-particle content by 18,200 ± 2,400 particles per mL, whereas no significant change in particle concentration was observed in PO bags (Figure 5-3A). In addition, after twelve passes, 79,400 ± 13,900 microparticles/mL were detected in PVC IV bags, whereas only 4,500 ± 2,500 microparticles/mL were measured in PO bags (Figure 5-3A). As shown in Figure 5-1B, particles generated in PVC IV bags all had a spherical morphology consistent with droplets of DEHP.

To differentiate between particles based on their densities relative to the bulk fluid, particles generated in saline in IV bags during transportation using the pneumatic tube system also were characterized with RMM. In saline from PVC bags, only negatively buoyant particles were detected, suggesting that particles composed of PVC (ρ = 1.38 g/cm^3) could be shed as the bags are transported within the pneumatic tube system (Figure 3C). The lack of positively buoyant particles detected by RMM (Figure 5-3C) does not rule out the presence of DEHP droplets, because the minimal difference in density between water (ρ = 1.01 g/cm^3) and DEHP (ρ = 0.99 g/cm^3) makes RMM analysis insensitive to small DEHP droplets. Finally, only positively buoyant particles were detected in PO bags following transportation with a pneumatic tube system (Figure 5-3D). The morphologies of the small number of particles generated in PO bags monitored with flow imaging microscopy were inconsistent with the detected positively buoyant particles being

air bubbles. Rather, because PO bags are composed of a multilayer polyolefin film with an inner polypropylene layer, positively buoyant particles detected by RMM may be composed of polypropylene ($\rho = 0.90$ g/cm^3) shed from the bags during transportation with the pneumatic tube system.

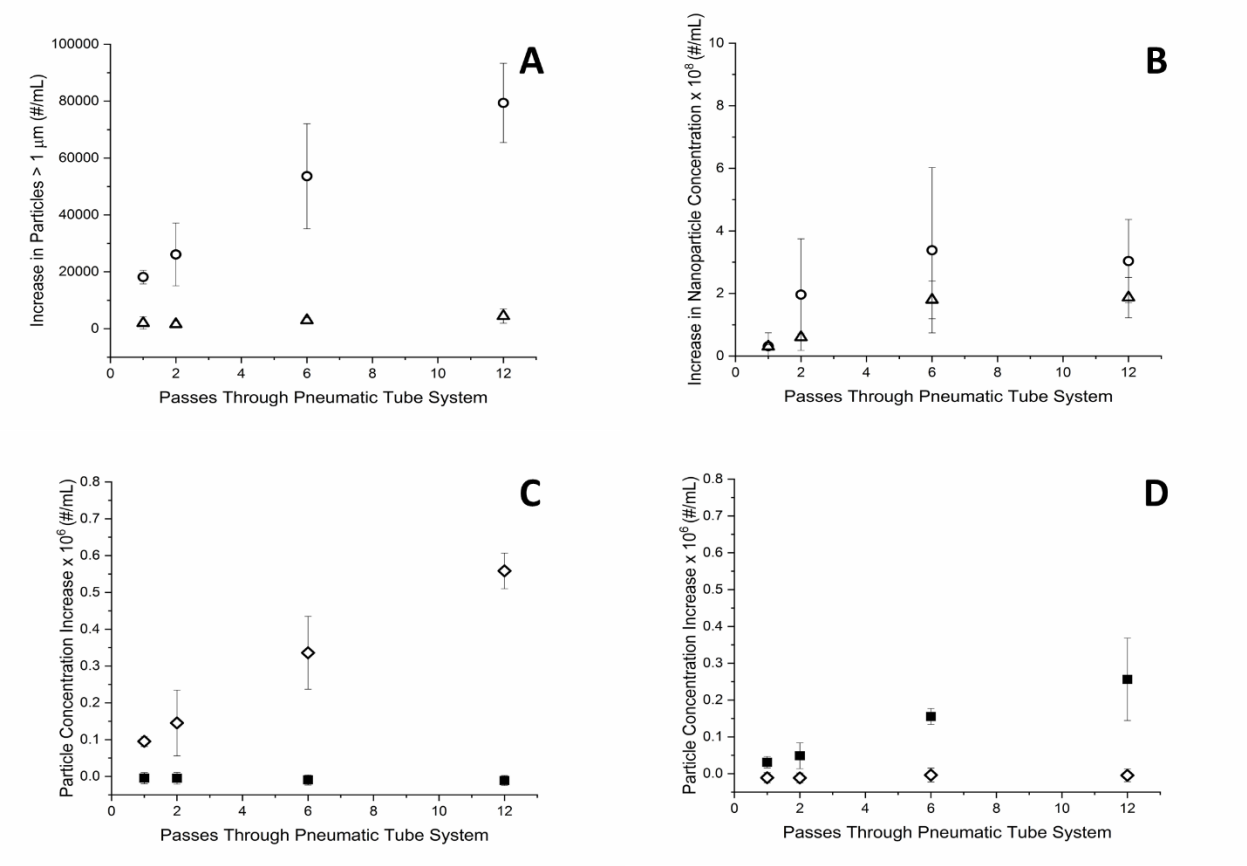

Figure 5-3: Formation of particulate contaminants in PVC (white circles) or PO bags (grey triangles) containing IV saline as a function of passes through a pneumatic tube system were measured with flow imaging microscopy (A) and nanoparticle tracking analysis (B). Using RMM, particles generated after passing bags through the pneumatic tube system were classified as either negatively buoyant (white diamonds) or positively buoyant (black squares) based on their density relative to the bulk fluid for particles generated in PVC (C) and PO (D) IV bags.

5.4.2 Interactions between DEHP Emulsions and IVIG

We next investigated adsorption of the polyclonal antibody molecules in the IVIG product to the surface of emulsified DEHP droplets. Emulsions contained DEHP nanodroplets with a mean diameter of approximately 300 nm. Adsorption of IVIG to DEHP nanodroplets was measured using a solution depletion method in which reductions in IVIG concentrations were determined

after incubation with DEHP droplets and subsequent removal of the droplets by centrifugation.[34] As shown in Figure 5-4, IVIG exhibited a relatively strong binding affinity for DEHP droplets as displayed by the sharp initial slope of the adsorption isotherm. IVIG surface coverage saturated at 2.65 ± 0.50 mg of IVIG adsorbed per m^2 of DEHP surface area. This surface coverage is consistent with monolayer adsorption of polyclonal IgG molecules, assuming hexagonal closest packing of disks and a hydrodynamic radius of 6.3 nm.[225] This surface coverage is similar to previously reported values for adsorption of a monoclonal antibodies and IL-1ra to the silicone oil-water interface.[212,223]

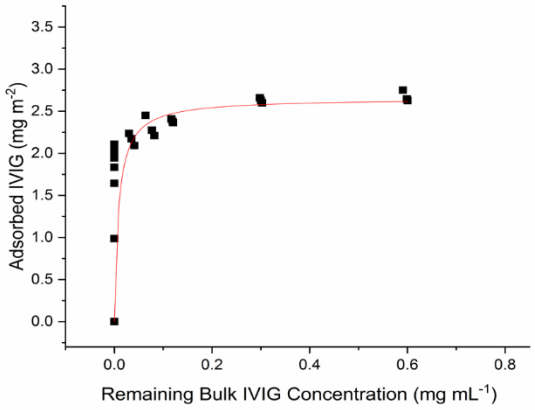

Figure 5-4: Mass of IVIG adsorbed per m^2 of DEHP nanodroplet surface area plotted as a function of the remaining concentration of IVIG in the bulk solution. The surface coverage of IVIG on DEHP droplets was measured in 5 mM sodium citrate buffer pH 5 containing 154 mM sodium chloride. IVIG surface coverage saturated at 2.65 ± 0.50 mg/m^2. Adsorption data were fitted to a Langmuir isotherm (red line) to determine the surface coverage.

The potential impact of adsorption of IVIG and the surface DEHP nanodroplets on protein conformation was evaluated using the extrinsic fluorescent dye bis-ANS. Binding and fluorescence of bis-ANS depends on a combination of hydrophobic and electrostatic interactions, making it sensitive to perturbations in protein structure that alter exposure of previously buried protein regions.[226] IVIG (0.1 mg/mL) was added to a DEHP emulsion containing sufficient droplet surface area to completely adsorb all added antibody molecules in the sample. Samples were

incubated for 2 hours prior to addition of bis-ANS and measurement of fluorescence intensity. As shown in Figure 5-5, adsorption of IVIG to DEHP nanodroplets greatly increased the fluorescence intensity maxima of bis-ANS at 490 nm. In comparison, the fluorescence intensity maxima in samples containing IVIG adsorbed to silicone oil droplets were lower than those for IVIG adsorbed to DEHP droplets (Figure 5-5). In formulations containing silicone oil or DEHP droplets without IVIG, fluorescence intensities were much lower (Figure 5-5). The increased fluorescence intensity of IVIG formulations containing DEHP and silicone oil nanodroplets indicates that IVIG adsorption to these interfaces promotes bis-ANS binding.

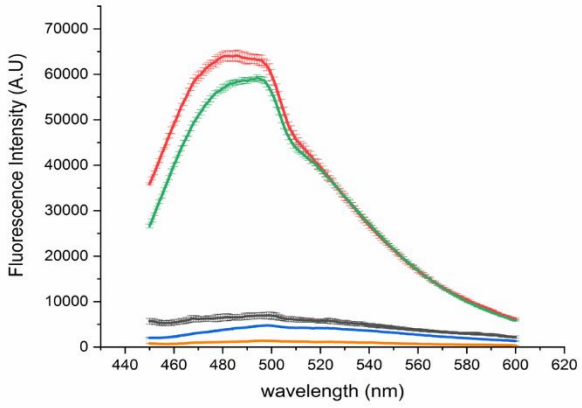

Figure 5-5: Fluorescence intensity of the extrinsic fluorescent probe bis-ANS plotted as function of wavelength. Sufficient surface area of DEHP (red line) or silicone oil (green line) nanodroplets were added to formulations containing 0.5 mg/mL IVIG in 5 mM sodium citrate buffer pH 5 with 154 mM NaCl for complete adsorption of IVIG. Samples were incubated for 2 hours before the addition of 1 µm bis-ANS and measurement of fluorescence intensity. Fluorescence intensity of bis-ANS was also measured in droplet-free 0.5 mg/mL IVIG formulations (orange line) as well as DEHP (gray line) and silicone oil (blue line) emulsions without IVIG. The average of three independent samples is plotted and error bars represent the standard deviation from the mean.

5.4.3 Loss of Soluble IVIG Monomer and Dimer in DEHP and Silicone oil Emulsions

The effects of DEHP on the stability of IVIG were evaluated by monitoring the loss of soluble IVIG monomers and dimers by SEC during a 24-hour incubation period at room temperature (Figure 5-6). Formulations containing 0.5 mg/mL IVIG were either rotated end-over-end or stored quiescently at room temperature for the duration of the incubation period. At DEHP concentrations up to 0.1 mg/mL, no significant decreases in soluble IVIG concentrations

(compared to droplet-free controls) were observed in either rotated or quiescent samples. However, at a DEHP concentration of 1 mg/mL, DEHP emulsions reduced the IVIG concentration to 0.47 ± 0.01 mg/mL after 6 hours of rotation, which was reduced further to 0.40 ± 0.02 mg/mL after 24 hours of agitation. At the highest concentration of DEHP studied (2 mg/mL), after just 3 hours of rotation IVIG concentrations were decreased to 0.40 ± 0.1 mg/mL, and only 0.25 ± 0.03 mg/mL remained after 24 hours. IVIG aggregation in DEHP emulsions was dependent on agitation, as insignificant losses of IVIG due to aggregation were observed in quiescently incubated samples. The initial reduction in IVIG concentration in samples containing 2 mg/mL emulsified DEHP to 0.45 ± 0.1mg/mL can be attributed to IVIG adsorption to DEHP nanodroplets, and is consistent with monolayer adsorption.

Loss of soluble IVIG was also monitored for formulations containing silicone oil emulsions under otherwise identical conditions (Figure 5-6). For formulations stored quiescently, no significant loss of soluble IVIG was detected for any silicone oil emulsion concentration beyond that attributed to monolayer protein adsorption at the silicone oil-water interface. A combination of both agitation and silicone oil emulsions concentrations greater than 0.1 mg/mL was required to induce significant loss of soluble IVIG relative to droplet-free control samples. Agitating IVIG formulations containing 1 mg/mL silicone oil droplets reduced IVIG concentrations to 0.40 ± 0.02 mg/mL after 24 hours. Increasing the silicone oil emulsion concentration to 2 mg/mL resulted in reductions in soluble IVIG concentrations to 0.37 ± 0.02 mg/mL after 3 hours of agitation and complete loss of soluble IVIG after 24 hours.

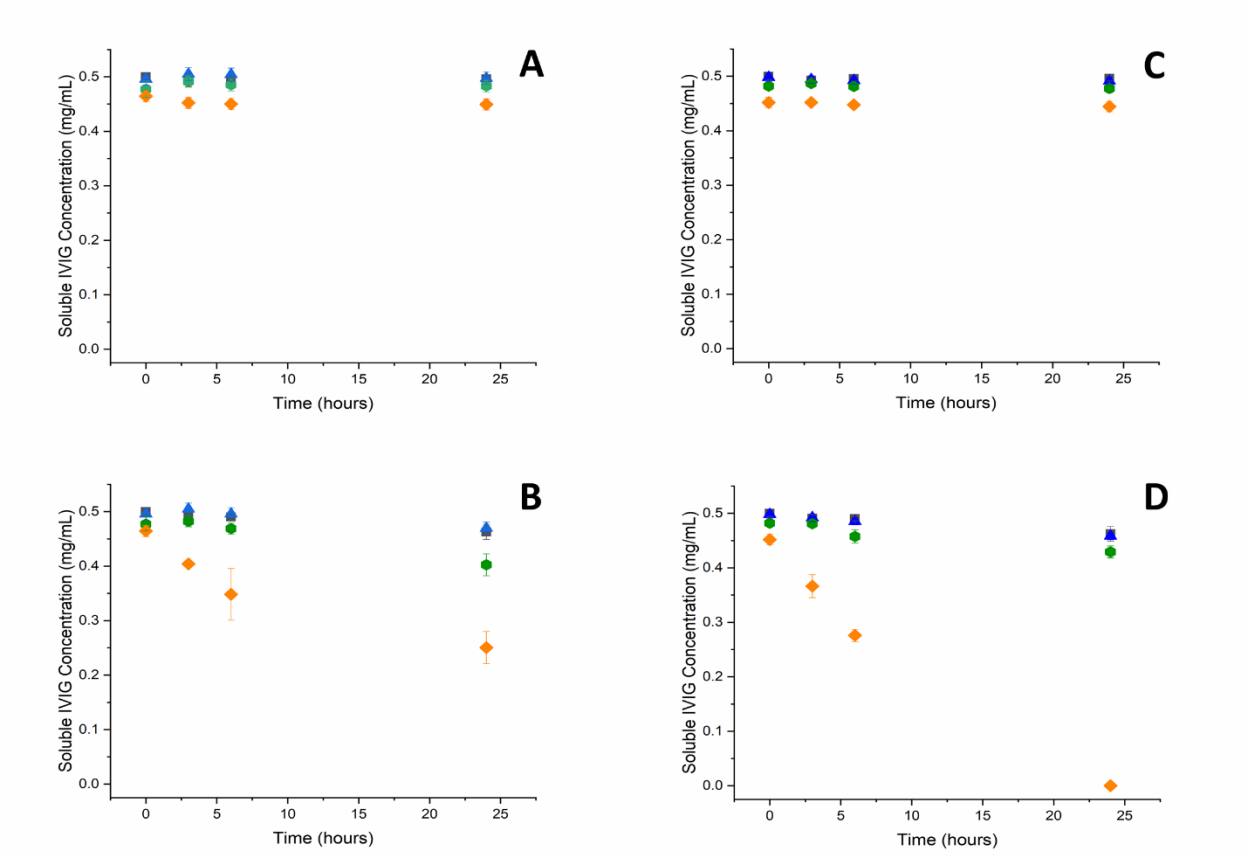

Figure 5-6: Soluble IVIG concentrations measured with SE-HPLC during incubation at room temperature in formulations containing DEHP (A, B) or silicone oil emulsions (C, D). Concentrations of soluble IVIG were monitored over a 24-hour incubation period in which samples were either stored quiescently (A, C) or rotated end-over-end at 8 rpm (B, D). Formulations consisted of 0.5 mg/mL IVIG in 5 mM sodium citrate buffer with 154 NaCl and contained emulsions concentrations of either 0 (gray squares), 0.1 (blue triangles), 1 (green hexagons) or 2 mg/mL (orange diamonds). Each point represents the average of three replicates with error bars indicating the standard deviation from the mean. Some error bars are smaller than the data point size.

5.4.4 Formation of Interfacial Protein Gels at the DEHP-Water Interface

Protein gelation was measured using an interfacial shear rheometer to investigate intermolecular protein interactions resulting in the formation of viscoelastic gels at the DEHP-water interface. Gelation studies were conducted with IL-1ra as a model therapeutic protein to allow for direct comparisons with studies of IL-1ra at the silicone oil-water interface conducted by Sorret et al.[223]

As shown in Figure 5-7, the elastic and viscous moduli of the interfacial layer are plotted as a function of aging time following the addition of IL-1ra. Initially the elastic modulus was lower

than the viscous modulus, indicating that the interface maintained a predominantly viscous character. After sufficient aging time, the elastic modulus increased, exceeding the value of the viscous modulus. The point at which the elastic modulus exceeds the viscous modulus is considered the gel transition point, as the interfacial layer adopts a more elastic character. The formation of viscoelastic gels at the DEHP-water interface occurred after 8.7 ± 1.4 hours, requiring significantly longer aging times than previously reported for IL-1ra at the silicone oil-water interface (5.3 ± 1.2 hours).[223] The strength of gels formed at the DEHP-water interface was variable, as evident from the variations in the magnitude of elastic modulus following gelation.

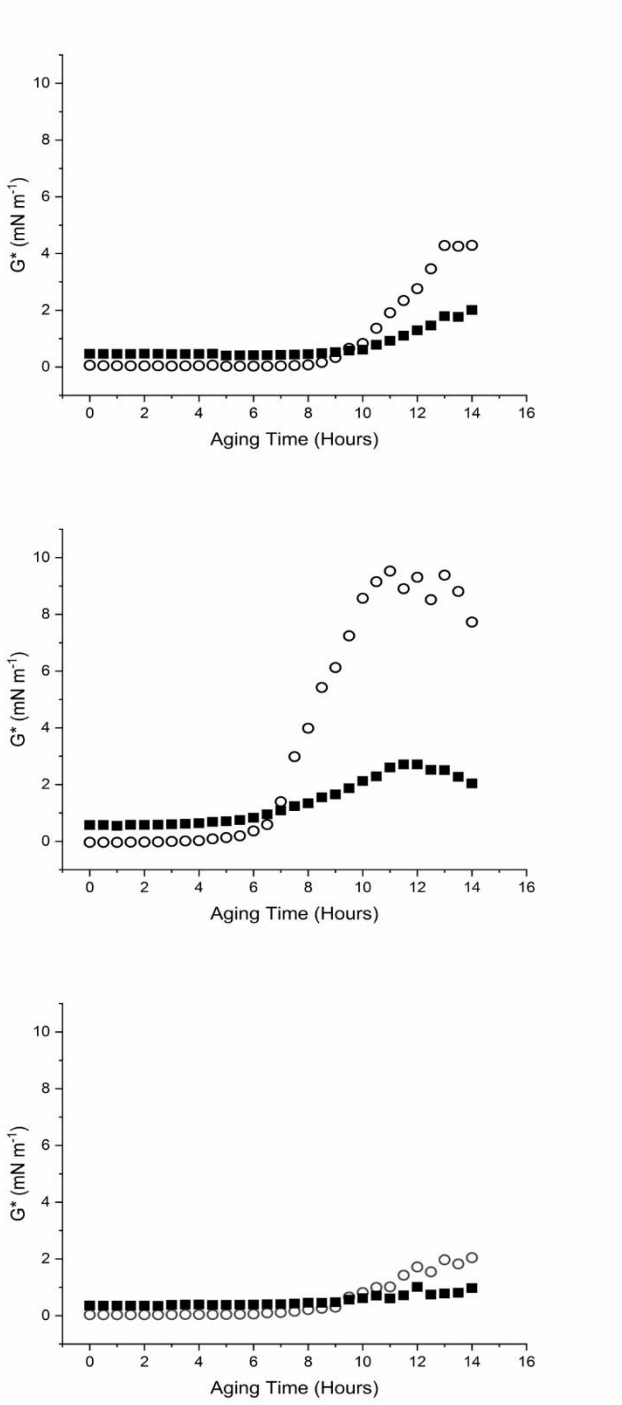

Figure 5-7: Figure 7. Dynamic interfacial shear moduli plotted as a function of aging time for three independent measurements of interfacial rheology as a function of time. The dynamic interfacial moduli at the DEHP-water interface was measured in 1 mg/ml IL-1ra formulations containing 10 mM MES buffer pH 6.5 and 150 mM NaCl. Both the elastic storage moduli (G') (black squares) and viscous loss moduli (G") (white circles) are plotted for the duration of a 14-hour aging period. Gelation was considered to have occurred once G' exceeded G". Gelation was observed in all samples and occurred after 8.3 ± 1.6 hours. Following gelation, the strength of gels formed in each sample varied significantly as shown in the above plots.

5.4.5 Complement Activation by IVIG in the Presence of DEHP and Silicone Oil Nanodroplets

In Figure 5-8, the fold increases in concentrations of the C5a, C3a and Bb proteins involved in the complement cascade are plotted as a function of droplet concentration in solutions containing 0.5 mg/mL IVIG (all droplet concentration are reported as prior to ten-fold dilution in serum for the complement activation assay). Fold increases are relative to that for complement activation measured for saline formulations without IVIG. Increases in the concentrations of C4a protein, which would be indicative of the classical or lectin pathway of complement activation, were not observed for any IVIG formulations containing silicone oil or DEHP nanodroplets. Therefore, DEHP and silicone oil nanodroplets in IVIG formulations appeared promote activation of the complement system through the alternative pathway for activation significant enough to reach the terminal pathway.[227]

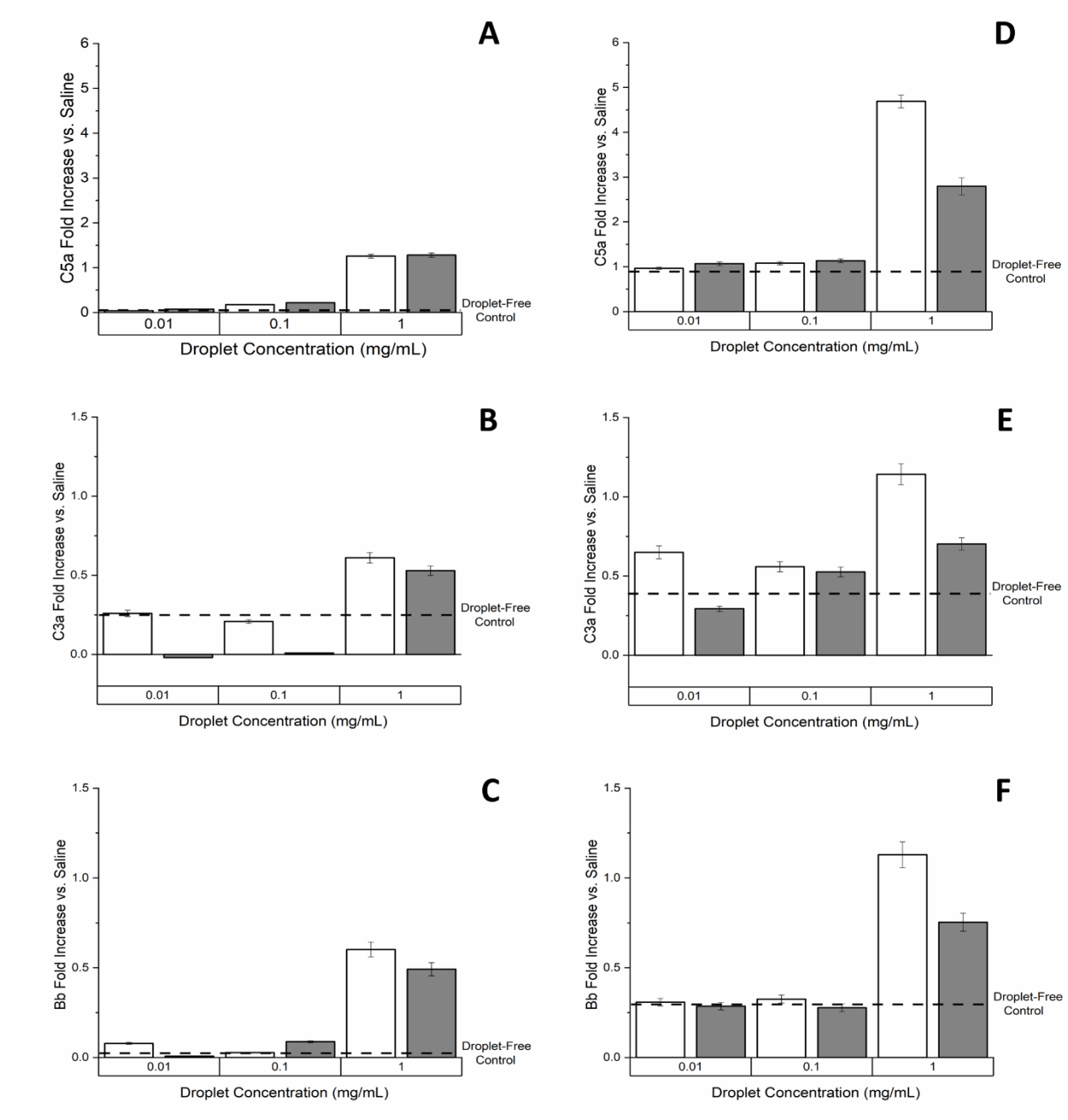

Figure 5-8: Activation of the complement system by IVIG formulations containing DEHP nanodroplets (white bars) or silicone oil nanodroplets (gray bars). All samples contained 0.5 mg/mL IVIG and were incubated at room temperature for 24 hours in 5 mM sodium citrate buffer pH 5 with 154 mM NaCl either quiescently (A-C) or rotated end-over-end at 8 rpm (D-F). Following incubation for 24 hours, samples were exposed to pooled human serum and concentrations of the Bb, C3a, C5a and C4a complement proteins were measured using standard ELISA techniques. In each plot complement activation induced by IVIG formulations containing emulsified droplets is compared to activation in response to controls that contained 0.5 mg/mL IVIG, but no silicone oil or DEHP droplets (dashed lines). Results for C4a are not shown as no significant increases in C4a serum levels were detected in any samples.

The alternative pathway is primarily activated by binding of C3b proteins to foreign surfaces, which leads to further amplification steps that result in complement activation. But this

pathway is also important as an amplification loop for activation starting in the classical or lectin pathway, as well as a baseline level of tick-over activation.[227] Previous studies of complement activation by nanoparticles have shown that activation depends on particle surface properties including surface charge and hydrophobicity.[228–230] Negatively charged nanoparticles activate complement predominantly through the classical pathway, resulting from interactions with a positively charged region of the C1q protein.[231] In contrast, positively charged nanoparticles have been associated with activation through the alternative pathway.[232] Silicone oil droplets are negatively charged, but become positively charged upon adsorption of positively charged antibodies.[233] In our current study, DEHP droplets in the absence of adsorbed protein had a negative surface charge of -6.8 ± 0.6 mV. However, adsorption of positively charged IVIG at pH 5 (zeta potential of IVIG monomers is 3.9 ± 1.1 mV) increased the surface charge to 6.0 ± 0.1 mV. The observed complement activation through the alternative pathway was therefore consistent with the positive charge of DEHP and silicone oil droplets in IVIG formulations.

Because IVIG adsorbs strongly to DEHP droplets and forms a complete monolayer, binding of complement proteins such as C3b is likely driven by interactions with adsorbed IVIG rather than by direct interactions with DEHP or silicone oil water interfaces. IVIG formulations containing DEHP or silicone oil droplets that were incubated without agitation had nearly undetectable amounts of aggregated protein, and both formulations activated complement to essentially the same degree. In the absence of aggregates produced by agitation stresses, high concentrations (e.g., 1 mg/mL) of both DEHP and silicone oil droplets in IVIG formulations were required to induce large increases in complement activation relative to droplet-free controls. For IVIG formulations containing droplet concentrations of 1 mg/mL, both droplet types induced similar activation, with fold increases vs. saline controls for the anaphylatoxin C5a of 1.26 ± 0.04

and 1.28 ± 0.05 in IVIG formulations containing silicone oil and DEHP droplets, respectively. At droplet concentrations of 100 μg/mL, small but significant increases in complement activation were observed in IVIG formulations compared to droplet-free controls with 0.18 ± 0.01 and 0.22 ± 0.01 fold increases in concentrations of the C5a anaphylatoxin for formulations containing either DEHP or silicone oil emulsions.

Similar to nanoparticles, proteinaceous aggregates can activate the alternative pathway of the complement system.[67,234,235] IVIG aggregates formed during agitation of droplet-free controls resulted in increased complement activation relative to quiescent control samples. In IVIG formulations without nanodroplets, fold increases of the C5a anaphylatoxin rose from 0.05 ± 0.01 to 0.89 ± 0.03 when samples were rotated to induce the formation of IVIG aggregates. As shown previously, DEHP and silicone oil droplet concentrations of 1 mg/mL or greater were required to induce detectable IVIG monomer and dimer loss compared to droplet-free controls. In agitated IVIG formulations containing 1 mg/mL DEHP or silicone oil nanodroplets, increased IVIG aggregation promoted greater complement activation relative to quiescent samples, resulting in fold increases of the C5a anaphylatoxin of 4.69 ± 0.14 and 2.79 ± 0.19 in DEHP and silicone oil emulsion respectively (Figure 5-8D). Interestingly, at a concentration of 1 mg/mL, DEHP nanodroplets in agitated IVIG formulations promoted greater complement activation than IVIG formulations containing the same concentration of silicone oil droplets despite similar levels of IVIG aggregation in formulations containing either silicone oil or DEHP droplets. In figures 5-8E and 5-8F greater fold increases in the concentrations of the C3a and Bb proteins were measured in IVIG formulations containing 1 mg/mL DEHP (1.14 ± 0.07 and 1.13 ± 0.07) when compared directly to formulations containing silicone oil emulsions (0.70 ± 0.04 and 0.75 ± 0.05) at the same droplet concentrations.

5.5 Discussion

5.5.1 DEHP Droplet Formation in PVC IV Bags

When PVC IV bags containing saline are either shaken to replicate shipping- and handling-related stresses or transported using a pneumatic tube system, higher concentrations of subvisible particles are generated relative to PO IV bags of the same volume. Subvisible particles generated in PVC IV bags had morphologies and densities consistent with the particles being composed of DEHP. Increased particle formation in PVC IV bags likely results from migration of DEHP within PVC matrices, resulting in the accumulation of DEHP as the surface of plasticized PVC materials.[194,236,237] Shear at the PVC-liquid interface caused by agitation or severe mechanical stress induced during transportation using a pneumatic tubing system may cause DEHP droplets to be shed into liquid formulations.

5.5.2 Effect of DEHP and Silicone Oil Nanodroplets on IVIG Stability

Similar to our observations with PVC IV bags, agitation of silicone oil-lubricated prefilled syringes has been associated with shedding of silicone oil droplets into protein formulations.[238,239] Biophysical characterization methods such as intrinsic fluorescence quenching and circular dichroism have shown that perturbations in protein structure may occur following protein adsorption to silicone oil-water interfaces presented by these droplets.[212,215,233] Due to interference caused by the aromatic and chiral nature of DEHP, we could not use these same biophysical characterization methods to probe possible structural perturbations in proteins at the DEHP-water interface. Instead, we showed that IVIG adsorbed strongly to DEHP nanodroplets, resulting in surface coverages similar to those previously reported for monoclonal antibodies at the silicone oil–water interface.[212] Further, similar increases in fluorescence intensity of bis-ANS in IVIG formulations containing either silicone oil or DEHP droplets indicate that protein adsorption to both interfaces creates an environment favorable for bis-ANS binding. Although we cannot

conclude whether the increased fluorescence results from perturbations in IVIG structure or from bis-ANS binding to a combination of native IVIG and the DEHP-water interface, it provides evidence of similar behavior of IVIG at both interfaces. This may suggest that similar to results previously observed at silicone-oil water interfaces, protein adsorption to DEHP-water interfaces may promote perturbations in both protein secondary and tertiary structure.

A combination of agitation induced by end-over-end rotation and relatively high DEHP droplet concentrations were required to induce easily detected IVIG monomer loss over the 24-hour incubation period studied. This result suggested the combination of the DEHP-water interface presented by nanodroplets combined with movement of the air-water interface during agitation synergistically promoted protein aggregation. This mechanism of aggregation is consistent with that previously reported and observed in this study for aggregation of protein formulations containing silicone oil.[34,209] One mechanism used to explain protein aggregation and particle formation at interfaces is the formation and subsequent disruption of gelled protein layers.[28,44,240,241] Proteins gel readily at silicone oil-water interfaces, and correlations have been identified between gel strength and the extent of protein monomer loss during agitation.[28,223] In our studies of IL-1ra at the DEHP-water interface we found that IL-1ra formed interfacial gels, but the time period required for gel formation was significantly longer than that required for gel formation at silicone oil-water interfaces. Further, IL-1ra gels at DEHP-water interfaces exhibited more variability in strength compared with those at the silicone-oil interface.[215,223] A slower rate of gelation combined with weaker gels could explain reduced rates of IVIG aggregation in formulations containing DEHP nanodroplets compared to rates in formulations containing silicone oil nanodroplets.

Comparison between protein adsorption, gelation and aggregation at silicone oil-water and DEHP-water interfaces shows that both interfaces appeared to induce aggregation through an agitation-dependent mechanism. The similarities between the effect of silicone oil-water and DEHP-water interfaces are not surprising as both present hydrophobic, negatively charged interfaces to which positively charged, amphiphilic proteins such as antibodies would be expected to adsorb. Once adsorbed, structural perturbations may occur as previously buried hydrophobic regions become reoriented toward hydrophobic interfaces.[242] A major difference between these two interfaces appears to be the rate at which gelation and aggregation occurs at the interface, with faster rates observed at the silicone-oil water interface. More rapid gelation and aggregation at the silicone oil-water interface may result from the greater surface tension of the silicone oil-water interface (40 mN/m) compared to that of the DEHP-water interface (30 mN/m).[243,244] Adsorbed protein molecules tend to unfold until increases in protein surface area are created that are sufficient to equalize the internal tension of the protein with the surface tension of the interface.[245] Therefore, the higher surface tension of the silicone oil water interface may induce greater and more rapid changes in protein structure, resulting in faster gelation at the silicone oil-water interface and increased aggregation rates.

5.5.3 Immunogenicity of IVIG Formulations Containing DEHP and Silicone Oil Nanodroplets

Severe reactions during IV infusions are often associated with activation of the complement system.[246] Complement activation can promote hypersensitivity reactions, with effects varying from mild patient discomfort to severe anaphylaxis and fatalities.[247,248] The development of nanomedicines which utilize nanoparticles for diagnostic and therapeutic applications has placed significant focus on the complement-activating capacity of nanoparticles.[247,249,250] These studies have shown that certain types of nanoparticles can induce

complement activation, where the extents and mechanisms of activation are dependent on a variety of factors including nanoparticle size, surface characteristics and morphology.[248] This complement-activating capacity of nanoparticles raises questions as to whether subvisible particulate contaminants in formulations of therapeutic proteins might stimulate similar activation, contributing to the hypersensitivity reactions frequently observed during infusion of therapeutic proteins.

Our studies of complement activation documented that both quiescent and agitated IVIG formulations containing nanodroplets of either DEHP or silicone oil can increase complement activation relative to droplet-free controls. Activation proceeds by the alternative pathway, indicating that complement proteins identified IVIG adsorbed to both DEHP and silicone oil nanodroplets as foreign surfaces, resulting in increased binding of C3b.[227,251] C3b binding was likely promoted by positively charged IVIG adsorbed to the surface of silicone oil and DEHP droplets as well as by insoluble IVIG aggregates generated in agitated samples. When mixed with human serum, both silicone oil and DEHP nanodroplets promoted formation of the potent anaphylatoxins C3a and C5a, which can induce clinically relevant symptoms including inflammatory reactions and cardiopulmonary distress.[247,252]

Formulations containing DEHP can destabilize IVIG, activate the complement system and provoke generation of potent anaphylatoxins, but the potential clinical relevance of this finding is unclear. In general, *in vivo-in vitro* correlations of complement activation are challenging, as both genetic and acquired factors contribute to the extent of complement activation in any given patient,[247,252–254] and direct correlations often cannot be assumed between *in vitro* complement testing and complement activation in patients.[250,255] Furthermore, it seems likely that the sensitivity of complement activation to proteins adsorbed on DEHP droplets will depend in part on the

identity of proteins. Thus, from our current in vitro study using IVIG, determination of the minimum concentration of DEHP droplets that might be required to provoke a clinically relevant *in vivo* response for a given therapeutic protein is not possible.

While evaluating the effect of DEHP nanodroplets on protein stability and complement activation in this study, we sought to consider conditions which would have relevance in clinical settings. Therapeutic proteins are typically diluted into saline solution within PVC IV bags immediately prior to their infusion into patients, a process that may require multiple hours.[256,257] Therefore, therapeutic protein typically will not be exposed to DEHP droplets for periods longer than 6-8 hours. But our results show that protein adsorption to DEHP droplets, formation of intermolecular protein networks and monomer loss can occur even over this relatively short timescale.

We observed that IVIG aggregation rates depended on DEHP droplet concentrations. In clinical settings, the extent of DEHP leaching from PVC IV bags is anticipated to be highly dependent on agitation-related stresses incurred shipping and handling. In our own studies, we estimate the concentration of DEHP droplets shed from agitated bags to be on the order of 5 µg/mL. This droplet concentration is well below that required to generate detectable monomer loss over 6-hour timescales. However, the presence of as little as 10 µg/mL DEHP droplets in pooled human serum caused release of C5a anaphylatoxin. The production of C5a is particularly important as this activation fragment is a strong anaphylatoxin capable of inducing a number of proinflammatory and immunogenic effects including acting as an adjuvant. Thus, it seems plausible that clinically relevant levels of DEHP droplets shed from PVC IV bags could promote complement activation, resulting in subsequent inflammatory and immune consequences in vivo.

5.6 Conclusions

Considerations of the potential impact of DEHP droplets shed from PVC IV bags on the safety and efficacy of therapeutic protein products administered using PVC IV bags is a matter of evaluating and mitigating potential risk. The issue of risk associated with the presence of subvisible particulate contaminants has been a recent source of controversy in the biopharmaceutical industry.[70,78] For considerations of the risks associated with subvisible particles, FDA regulators have highlighted the importance of applying the precautionary principle when considering factors which may adversely impact product safety.[91] The precautionary principal establishes the importance of proving a certain substance is safe rather than placing the burden of proof on proving a substance is dangerous.[258] Decades of use of PVC IV bags for administration of therapeutic products without reports of adverse effects directly attributed to these plasticized materials may provide evidence for many of the safety of this material. However, the variety of variables which may contribute to an adverse immune response following administration of therapeutic protein product makes it challenging to isolate a single factor when an adverse response is observed. We believe the impact of DEHP droplets on IVIG stability and complement activation shown in this work indicate a potential risk associated with the administration of therapeutic protein products using PVC IV bags. Therefore, especially given the wide availability of DEHP-free alternatives such as the PO bags tested here, it would be prudent to avoid the use of PVC IV bags for dilution and administration of therapeutic protein products.

5.7 Acknowledgments

Funding for this work was provided by NIH grant RO1 EB006006.

Chapter 6 Conclusions and Recommendations

6.1 Conclusions

Subvisible particulate contaminants and their associated interfaces may have significant impacts on the stability of therapeutic proteins. Furthermore, the impact of subvisible particles on protein stability could have serious clinical consequences for both the safety and efficacy therapeutic protein products upon administration. There are growing concerns from both regulatory agencies and academia focusing on the impacts of particulate contaminant, especially in the sub-visible particle size range. Currently, regulations provided by the United States Pharmacopeia provide regulations down to 10 µm. However, multiple studies have shown an association between particles smaller than 10 µm and the immunogenicity of market therapeutic products. In this work we characterized nanobubbles and DEHP nanodroplets which may be commonly present in therapeutic protein formulation to investigate their effect on protein stability and immunogenicity.

Our results showed clear evidence of interactions between IL-1ra and nanobubbles. Reconstitution of lyophilized formulations composed of 10% w/v trehalose resulted in approximately 3 x 10^9 nanoparticles/mL with a mean diameter of 100 nm as measured with nanoparticle tracking analysis (NTA). The identity of these nanoparticles as nanobubbles was confirmed using resonant mass measurement (RMM). Characterization of reconstituted trehalose formulations with RMM resulted in the detection of only positively buoyant particles, consistent with the gaseous composition of nanobubbles. When the same lyophilized formulations of trehalose were reconstituted with a solution containing 1 mg/mL IL-1ra a significant decrease in nanobubble formation was observed with both NTA and RMM. In addition to reductions in nanoparticle concentrations, RMM detected the presence of negatively buoyant particles following reconstitution with IL-1ra which was attributed to formation of protein aggregates. These initial

results suggested that protein may adsorb readily to nanobubbles, resulting in nanobubble destabilization and collapse which subsequently induced formation of insoluble proteinaceous particles.

The effect of IL-1ra on the concentration of nanobubbles formed following reconstitution of lyophilized protein formulations appeared to result from protein adsorption at the nanobubble air-water interface. Resulting from the small quantity of surface area generated in nanobubbles suspension, protein adsorption could not be quantified using standard methods such as solution depletion. Instead, we evaluated change in nanobubble surface charge upon addition of IL-1ra under various buffer conditions. In formulations containing nanobubbles and IL-1ra, measured zeta potentials were dependent on the zeta-potential of IL-1ra. These results showed that IL-1ra adsorbed readily to nanobubbles resulting in significant changes in the nanobubble surface charge.

An investigation of the effect of nanobubbles on the long-term stability of IL-1ra showed a clear correlation between nanobubble concentrations and IL-1ra aggregation following incubation. Following just 24 hours of incubation in nanobubble suspensions up to 2.5% of the IL-1ra added to these suspensions aggregated. This result indicated that nanobubbles can induce significant aggregation in protein formulations. Interestingly, the extent of aggregation in nanobubble suspensions far exceeded the total quantity of protein that could adsorb to the nanobubble surface by a factor of approximately 300. A direct mechanism by which IL-1ra molecules adsorb at the nanobubble air-water interface, therefore, would not be sufficient to explain the aggregation observed in these suspensions. Further, addition of the metal chelator EDTA was capable of inhibiting aggregation in these suspensions. This result suggested that interactions between nanobubbles and cations such as those leached from borosilicate glass vials

could catalyze perturbations in IL-1ra structure and potentially promote further aggregation in the bulk solution.

The extent of aggregation observed in nanobubble suspensions suggested that nanobubbles formed upon reconstitution of lyophilized therapeutic protein products could induce protein aggregation potentially compromising the safety and efficacy of therapeutic protein products. We, therefore, focused on better understanding the mechanism of nanobubble formation in lyophilized formulations and leveraging this knowledge to reduce nanobubble formation and associated protein aggregation. Our earlier studies had shown that nanobubble generation occurred upon reconstitution of lyophilized formulations consisting of either trehalose or sucrose. These disaccharides commonly used in lyophilized formulations are expected to remain amorphous throughout the freezing and drying process. We hypothesized that nanobubble formation was dependent on the formation of nano-sized ice crystals within the freeze concentrated liquid which sublimated during drying leaving behind voids. Upon dissolution of the surrounding matrix, these voids could result in nanobubble formation.

Addition of mannitol, a crystallizing excipient, to lyophilized formulations of either trehalose or sucrose resulted in a significant increase in nanobubble formation following reconstitution. The concentration of nanobubbles generated following reconstitution of lyophilize mixtures of trehalose and mannitol correlated with the extent of crystallization in the final freeze-dried solid measured using powder X-ray diffractometry. Analysis of polymorphs present in these lyophilized solids showed that mannitol formed only amorphous polymorphs and that the hemihydrate form was not present. The dependence of nanobubble formation on excipient crystallinity was attributed to the formation of anhydrous crystals. As anhydrous mannitol crystals form, water previously associated with amorphous mannitol would be excluded from the growing

mannitol crystal. This would result in local regions of higher water content within the freeze concentrated liquid in the region immediately surrounding growing mannitol crystals. The increased concentration of water within these regions combined with local reductions in viscosity could promote nucleation of additional nano-sized ice crystals.

While crystallization of mannitol appeared to promote nanobubble generation, the addition of low concentrations of mannitol to trehalose formulations reduced nanobubble generation compared to pure trehalose formulations. This reduction of nanobubble generation in lyophilized formulations of trehalose containing low mannitol concentrations suggested a possible strategy for reducing nanobubble generation following reconstitution of lyophilized protein formulations. Lyophilization of IL-1ra formulations containing trehalose and low mannitol concentrations resulted in significant reductions in the concentration of insoluble proteinaceous particles following reconstitution as well as lower nanobubble formation compared to IL-1ra lyophilized in formulations containing only mannitol or trehalose. Furthermore, after incubation for ten days at 40 °C following reconstitution, IL-1ra formulations containing mannitol and trehalose again had lower microparticle concentrations compared to pure mannitol formulations. These results showed that lyophilized formulations can be optimized to reduce nanobubble formation following reconstitutions as well as the formation of insoluble protein aggregates.

The final component of this research focused on the formation of insoluble DEHP droplets in PVC IV bags containing saline used for the dilution and administration of therapeutic proteins. We showed that PVC IV bags could shed DEHP droplets when stressed by either shaking to replicate shipping and handling related stresses or when bags were transported within a hospital using a pneumatic tube system. Particles generated in PVC IV bags exhibited spherical morphologies consist with expected geometry of DEHP droplets. Applying the same stress to

DEHP-free PO bags did not induce the formation of droplets further suggesting that the observed particle formation was dependent on the presence of plasticized PVC.

DEHP droplets in therapeutic protein formulations could have similar destabilizing effects on proteins as previously observed from silicone oil droplets. Using the model protein, IVIG, we showed that protein adsorbed rapidly to the DEHP-water interface completely saturating the surface. The extent of adsorption was consistent with complete monolayer surface coverage. Adsorption of IVIG to DEHP droplets improved the colloidal stability of droplets inhibiting droplet coalescence.

Similar to the silicone oil-water interface, IL-1ra formed interfacial gels when exposed to DEHP-water interfaces. Gelation at the DEHP-water interface required significantly longer aging times compared to silicone oil interfaces and formed weaker gels. These long gelation times at the DEHP-water interface may explain differences in aggregation between IVIG formulations containing either DEHP or silicone oil emulsion. With both droplet types agitation was required to induce significant loss of soluble IVIG compared to a DEHP-free control. Furthermore, high concentrations of both droplets were required to induce significant aggregation when rotated. However, the results showed that a combination of the DEHP-water interface and interfacial shear induced by end-over-end rotation could synergistically promote IVIG aggregation. Interestingly at the highest droplet concentration of 2 mg/mL significantly greater aggregation was observed in formulation containing silicone oil. This suggest that the faster rate of gel formation combined with the formation of stronger gels could significantly increase aggregation rates in agitated samples.

Finally, we showed that DEHP droplets may be capable of promoting immune responses through activation of the complement system. DEHP droplets activated the complement system

through the alternative pathway indicating that complement proteins present in human serum identified DEHP droplets as foreign surfaces. Significant complement increases in complement were observed whether samples were rotated or stored quiescently. However, to induce significant increases in complement activation relative to droplet free controls, droplet concentration of at least 1 mg/mL were required. This concentration was significantly greater than that observed in PVC IV bags. Despite this discrepancy, DEHP droplets may still pose a significant risk for the safety and efficacy of therapeutic protein products diluted and administered using PVC IV bags. Complement activation and related infusion reactions in patients will be dependent on a variety of mitigating factors including; particle content within the bag, product handling and protein sensitivity to the DEHP-water interface. Therefore, we cannot determine the probability that DEHP droplets will induce adverse reactions but rather the results we have presented indicate that DEHP may pose an uncontrolled risk to patient safety. Therefore, we recommend that based on the wide availability of PVC-free alternatives that PVC bags should be avoided for the dilution and administration of therapeutic proteins.

6.2 Recommendations

The work described in this thesis has illustrated the impacts of sub-visible particulate contaminants and their associated interfaces on the stability and immunogenicity of therapeutic protein formulations and has highlighted the importance of characterizing all contaminants present in therapeutic protein products. Ensuring the safety and efficacy of therapeutic protein products requires a detailed understanding of the sub-visible content of therapeutic protein formulations as well as where sub-visible particles may originate. From this information, action can be taken to minimize the effect of particulate through formulation or process-based strategies. In addition, a complete analysis of particle throughout the subvisible size range would allow deviations from

standard operating conditions resulting in increased particle formation to be quickly and easily identified and mediated.

Throughout this work we have employed a variety of particle characterization method to quantify particles throughout the sub-visible size range. Particle characterization methods such as RMM, NTA and flow imaging microscopy provide powerful tools for characterizing therapeutic protein formulations. Using these methods, minute quantities of protein aggregates as well as other foreign particles can be easily detected and quantified. This allows problems resulting in reduced proteins stability to detected and troubleshooted long before large reduction in monomer or visible particles are observed. Furthermore, particle characterization methods such as flow imagining microscopy provide detailed images of particles which can be used to identify particle types and can be even used to identify how protein aggregates were generated.

As the regulatory landscape related to therapeutic protein continues to evolve, regulators will begin to expect more information from manufactures regarding particle characterization throughout the sub-visible size range. Therefore, manufactures of proteins should begin to explore particle characterization methods beyond the standard light obscuration methods described in USP 788. These studies will likely uncover a range of different particle contaminants which may be commonly in therapeutic protein products. Care should be applied to the characterization of these particle types to determine if they could impact the stability or immunogenicity of therapeutic proteins.

Complete particle characterization of therapeutic protein throughout the sub-visible size range is currently limited by instrumentation. Detection and characterization of proteinaceous particles can be challenging based on their refractive indices and irregular morphologies. Applying particle characterization method developed for other applications can therefore be challenging

based upon the lack of proper particle standards for instrument calibration and method validation. Furthermore, significant focus is being placed on characterizing the full subvisible particle ranges which spans from 100 μm to 10s of nms. However, no one instrument can characterize this complete range so multiple instruments must be utilized for complete characterization. This highlight the necessity for the development of new characterization instruments that can completely characterize the full subvisible size range in a high throughput manner.

Significant effort is placed into ensuring that long-term stability of therapeutic protein products in the final product container, but less focus has been placed on what occurs when these products reach the end user. While the challenges associated with protein stability and the necessary handling and storage procedures for maintaining product quality are well known among biological manufacturers, practitioners in a clinical setting may not be fully aware of the labile nature of therapeutic proteins. Furthermore, as we have shown in this work, medical devices such as PVC IV bags are handled or stored could contribute to the concentration of subvisible particle concentrations in therapeutic protein products. Therefore, it is important to consider the complete life cycle of a therapeutic protein product from manufacturing until administration when considering factors which may influence the stability and consequently the safety and efficacy of therapeutic protein products.

Bibliography

1. Carter PJ. Introduction to current and future protein therapeutics: A protein engineering perspective. *Exp Cell Res*. 2011;317(9):1261-1269. doi:10.1016/j.yexcr.2011.02.013
2. Schellekens H. Immunogenicity of therapeutic proteins: Clinical implications and future prospects. *Clin Ther*. 2002;24(11):1720-1740. doi:10.1016/S0149-2918(02)80075-3
3. Walsh G. Biopharmaceuticals: recent approvals and likely directions. *Trends Biotechnol*. 2005;23(11):553-558. doi:10.1016/j.tibtech.2005.07.005
4. Leader B, Baca QJ, Golan DE. Protein therapeutics: a summary and pharmacological classification. *Nat Rev Drug Discov*. 2008;7(1):21-39. doi:10.1038/nrd2399
5. Pace CN. Conformational stability of globular proteins. *Trends Biochem Sci*. 1990;15(1):14-17. doi:10.1016/0968-0004(90)90124-T
6. Wang W. Instability, stabilization, and formulation of liquid protein pharmaceuticals. *Int J Pharm*. 1999;185(2):129-188. http://www.ncbi.nlm.nih.gov/pubmed/10460913. Accessed October 26, 2018.
7. Rathore N, Rajan RS. Current perspectives on stability of protein drug products during formulation, fill and finish operations. *Biotechnol Prog*. 24(3):504-514. doi:10.1021/bp070462h
8. Pace CN, Shirley BA, McNutt M, Gajiwala K. Forces contributing to the conformational stability of proteins. *FASEB J*. 1996;10(1):75-83. doi:10.1096/FASEBJ.10.1.8566551
9. Kueltzo LA, Wang W e. i., Randolph TW, Carpenter JF. Effects of Solution Conditions, Processing Parameters, and Container Materials on Aggregation of a Monoclonal Antibody during Freeze-Thawing. *J Pharm Sci*. 2008;97(5):1801-1812. doi:10.1002/JPS.21110
10. Zheng K, Middaugh CR, Siahaan TJ. Evaluation of the physical stability of the EC5 domain of E-cadherin: Effects of pH, temperature, ionic strength, and disulfide bonds. *J Pharm Sci*. 2009;98(1):63-73. doi:10.1002/JPS.21418
11. Randolph TW, Carpenter JF. Engineering challenges of protein formulations. *AIChE J*. 2007;53(8):1902-1907. doi:10.1002/aic.11252
12. Ratner RE, Phillips TM, Steiner M. Persistent cutaneous insulin allergy resulting from high-molecular-weight insulin aggregates. *Diabetes*. 1990;39(6):728-733. http://www.ncbi.nlm.nih.gov/pubmed/2189764. Accessed March 2, 2019.
13. Thornton CA. Safety of Intravenous Immunoglobulin. *Arch Neurol*. 1993;50(2):135-136. doi:10.1001/archneur.1993.00540020013009
14. Carpenter JF, Kendrick BS, Chang BS, Manning MC, Randolph TW. Inhibition of stress-induced aggregation of protein therapeutics. *Methods Enzymol*. 1999;309:236-255. doi:10.1016/S0076-6879(99)09018-7
15. Randolph TW, Chang BS, Chi EY, Kendrick BS, Carpenter JF, Krishnan S. Roles of conformational stability and colloidal stability in the aggregation of recombinant human

granulocyte colony-stimulating factor. *Protein Sci*. 2003;12(5):903-913. doi:10.1110/ps.0235703

16. Wang W, Singh S, Zeng DL, King K, Nema S. Antibody Structure, Instability, and Formulation. *J Pharm Sci*. 2007;96(1):1-26. doi:10.1002/JPS.20727

17. Tanford C. Protein Denaturation. *Adv Protein Chem*. 1968;23:121-282. doi:10.1016/S0065-3233(08)60401-5

18. Koseki T, Kitabatake N, Doi E. Irreversible thermal denaturation and formation of linear aggregates of ovalbumin. *Food Hydrocoll*. 1989;3(2):123-134. doi:10.1016/S0268-005X(89)80022-0

19. Wang W, Nema S, Teagarden D. Protein aggregation--pathways and influencing factors. *Int J Pharm*. 2010;390(2):89-99. doi:10.1016/j.ijpharm.2010.02.025

20. Krishnamurthy R, Manning M. The Stability Factor: Importance in Formulation Development. *Curr Pharm Biotechnol*. 2002;3(4):361-371. doi:10.2174/1389201023378229

21. Clarkson J., Cui Z., Darton R. Effect of solution conditions on protein damage in foam. *Biochem Eng J*. 2000;4(2):107-114. doi:10.1016/S1369-703X(99)00038-8

22. Maa YF, Hsu CC. Protein denaturation by combined effect of shear and air-liquid interface. *Biotechnol Bioeng*. 1997;54(6):503-512. doi:10.1002/(SICI)1097-0290(19970620)54:6<503::AID-BIT1>3.0.CO;2-N

23. Bee JS, Schwartz DK, Trabelsi S, et al. Production of particles of therapeutic proteins at the air–water interface during compression/dilation cycles. *Soft Matter*. 2012;8(40):10329-10335. doi:10.1039/c2sm26184g

24. Yano YF. Kinetics of protein unfolding at interfaces. *J Phys Condens Matter*. 2012;24(50):503101. doi:10.1088/0953-8984/24/50/503101

25. Kondo A, Oku S, Higashitani K. Adsorption of γ-globulin, a model protein for antibody, on colloidal particles. *Biotechnol Bioeng*. 1991;37(6):537-543. doi:10.1002/bit.260370607

26. Baszkin A, Boissonnade MM, Kamyshny A, Magdassi S. Native and Hydrophobically Modified Human Immunoglobulin G at the Air/Water Interface. *J Colloid Interface Sci*. 2002;239(1):1-9. doi:10.1006/jcis.2001.7521

27. Kim HJ, Decker EA, McClements DJ. Impact of protein surface denaturation on droplet flocculation in hexadecane oil-in-water emulsions stabilized by β-lactoglobulin. *J Agric Food Chem*. 2002;50(24):7131-7137. doi:10.1021/jf020366q

28. Mehta SB, Lewus R, Bee JS, Randolph TW, Carpenter JF. Gelation of a monoclonal antibody at the silicone oil–water interface and subsequent rupture of the interfacial gel results in aggregation and particle formation. *J Pharm Sci*. 2015;104(4):1282-1290. doi:10.1002/JPS.24358

29. Bantchev GB, Schwartz DK. Surface shear rheology of β-casein layers at the air/solution interface: Formation of a two-dimensional physical gel. *Langmuir*. 2003;19(7):2673-2682.

doi:10.1021/la0262349

30. Rühs PA, Scheuble N, Windhab EJ, Mezzenga R, Fischer P. Simultaneous Control of pH and Ionic Strength during Interfacial Rheology of β-Lactoglobulin Fibrils Adsorbed at Liquid/Liquid Interfaces. *Langmuir*. 2012;28(34):12536-12543. doi:10.1021/la3026705

31. Ziegler GR, Foegeding EA. The gelation of proteins. *Adv Food Nutr Res*. 1990;34(C):203-298. doi:10.1016/S1043-4526(08)60008-X

32. Graham D., Phillips M. Proteins at liquid interfaces. *J Colloid Interface Sci*. 1979;70(3):403-414. doi:10.1016/0021-9797(79)90048-1

33. Mehta SB, Carpenter JF, Randolph TW. Colloidal Instability Fosters Agglomeration of Subvisible Particles Created by Rupture of Gels of a Monoclonal Antibody Formed at Silicone Oil-Water Interfaces. *J Pharm Sci*. 2016;105(8):2338-2348. http://linkinghub.elsevier.com/retrieve/pii/S0022354916415054. Accessed November 13, 2017.

34. Gerhardt A, Mcgraw NR, Schwartz DK, Bee JS, Carpenter JF, Randolph TW. Protein aggregation and particle formation in prefilled glass syringes. *J Pharm Sci*. 2014;103(6):1601-1612. doi:10.1002/jps.23973

35. Cleland JL, Powell MF, Shire SJ. The development of stable protein formulations: a close look at protein aggregation, deamidation, and oxidation. *Crit Rev Ther Drug Carrier Syst*. 1993;10(4):307-377. http://www.ncbi.nlm.nih.gov/pubmed/8124728. Accessed March 7, 2019.

36. Pikal-Cleland KA, Rodríguez-Hornedo N, Amidon GL, Carpenter JF. Protein denaturation during freezing and thawing in phosphate buffer systems: Monomeric and tetrameric β-galactosidase. *Arch Biochem Biophys*. 2000;384(2):398-406. doi:10.1006/abbi.2000.2088

37. Chang BS, Kendrick BS, Carpenter JF. Surface-Induced Denaturation of Proteins during Freezing and its Inhibition by Surfactants. *J Pharm Sci*. 1996;85(12):1325-1330. doi:10.1021/JS960080Y

38. Suslick KS, Flannigan DJ. Inside a Collapsing Bubble: Sonoluminescence and the Conditions During Cavitation. *Annu Rev Phys Chem*. 2008;59(1):659-683. doi:10.1146/annurev.physchem.59.032607.093739

39. Riesz P, Kondo T. Free radical formation induced by ultrasound and its biological implications. *Free Radic Biol Med*. 1992;13(3):247-270. doi:10.1016/0891-5849(92)90021-8

40. Juretic H, Montalbo-Lomboy M, van Leeuwen JH, Cooper WJ, Grewell D. Hydroxyl radical formation in batch and continuous flow ultrasonic systems. *Ultrason Sonochem*. 2015;22:600-606. doi:10.1016/j.ultsonch.2014.07.003

41. Randolph TW, Schiltz E, Sederstrom D, et al. Do Not Drop: Mechanical Shock in Vials Causes Cavitation, Protein Aggregation, and Particle Formation. *J Pharm Sci*. 2015;104(2):602-611. doi:10.1002/JPS.24259

42. Nejadnik MR, Randolph TW, Volkin DB, et al. Postproduction handling and

administration of protein pharmaceuticals and potential instability issues. *J Pharm Sci*. 2018;107(8):2013-2019. doi:10.1016/J.XPHS.2018.04.005

43. Chi EY, Krishnan S, Randolph TW, Carpenter JF. Physical stability of proteins in aqueous solution: mechanism and driving forces in nonnative protein aggregation. *Pharm Res*. 2003;20(9):1325-1336. doi:10.1023/A:1025771421906

44. Liu L, Qi W, Schwartz DK, Randolph TW, Carpenter JF. The effects of excipients on protein aggregation during agitation: an interfacial shear rheology study. *J Pharm Sci*. 2013;102(8):2460-2470. doi:10.1002/jps.23622

45. Arakawa T, Timasheff SN. Stabilization of protein structure by sugars. *Biochemistry*. 1982;21(25):6536-6544. http://www.ncbi.nlm.nih.gov/pubmed/7150574. Accessed March 16, 2015.

46. Timasheff SN. Protein-solvent preferential interactions, protein hydration, and the modulation of biochemical reactions by solvent components. *Proc Natl Acad Sci*. 2002;99(15):9721-9726. doi:10.1073/pnas.122225399

47. Sauerborn M, Brinks V, Jiskoot W, Schellekens H. Immunological mechanism underlying the immune response to recombinant human protein therapeutics. *Trends Pharmacol Sci*. 2010;31(2):53-59. doi:10.1016/j.tips.2009.11.001

48. De Groot AS, Scott DW. Immunogenicity of protein therapeutics. *Trends Immunol*. 2007;28(11):482-490. doi:10.1016/j.it.2007.07.011

49. Moussa EM, Panchal JP, Moorthy BS, et al. Immunogenicity of Therapeutic Protein Aggregates. *J Pharm Sci*. 2016;105(2):417-430. doi:10.1016/j.xphs.2015.11.002

50. Fda, Cder, pritzlaffo. *Guidance for Industry Immunogenicity Assessment for Therapeutic Protein Products*.; 2014. http://www.fda.gov/Drugs/GuidanceComplianceRegulatoryInformation/Guidances/default.htmand/orhttp://www.fda.gov/BiologicsBloodVaccines/GuidanceComplianceRegulatoryInformation/Guidances/default.htm. Accessed March 7, 2019.

51. Hermeling S, Crommelin DJA, Schellekens H, Jiskoot W. Structure-Immunogenicity Relationships of Therapeutic Proteins. *Pharm Res*. 2004;21(6):897-903. doi:10.1023/B:PHAM.0000029275.41323.a6

52. Braun A, Kwee L, Labow MA, Alsenz J. Protein aggregates seem to play a key role among the parameters influencing the antigenicity of interferon alpha (IFN-α) in normal and transgenic mice. *Pharm Res*. 1997;14(10):1472-1478. doi:10.1023/A:1012193326789

53. Tamilvanan S, Raja NL, Sa B, Basu SK. Clinical concerns of immunogenicity produced at cellular levels by biopharmaceuticals following their parenteral administration into human body. *J Drug Target*. 2010;18(7):489-498. doi:10.3109/10611861003649746

54. Rosenberg AS, Sauna ZE. Immunogenicity assessment during the development of protein therapeutics. *J Pharm Pharmacol*. 2018;70(5):584-594. doi:10.1111/jphp.12810

55. Schellekens H. Bioequivalence and the immunogenicity of biopharmaceuticals. *Nat Rev Drug Discov*. 2002;1(6):457-462. doi:10.1038/nrd818

56. Rosenberg AS. Effects of protein aggregates: an immunologic perspective. *AAPS J*. 2006;8(3):E501-7. doi:10.1208/aapsj080359

57. Chirino AJ, Ary ML, Marshall SA. Minimizing the immunogenicity of protein therapeutics. *Drug Discov Today*. 2004;9(2):82-90. doi:10.1016/S1359-6446(03)02953-2

58. Koren E, Zuckerman L, Mire-Sluis A. Immune Responses to Therapeutic Proteins in Humans - Clinical Significance, Assessment and Prediction. *Curr Pharm Biotechnol*. 2002;3(4):349-360. doi:10.2174/1389201023378175

59. Hermeling S, Aranha L, Damen JMA, et al. Structural Characterization and Immunogenicity in Wild-Type and Immune Tolerant Mice of Degraded Recombinant Human Interferon Alpha2b. *Pharm Res*. 2005;22(12):1997-2006. doi:10.1007/s11095-005-8177-9

60. Gamble CN. The Role of Soluble Aggregates in the Primary Immune Response of Mice to Human Gamma Globulin. *Int Arch Allergy Immunol*. 1966;30(5):446-455. doi:10.1159/000229829

61. Brinks V, Jiskoot W, Schellekens H. Immunogenicity of Therapeutic Proteins: The Use of Animal Models. *Pharm Res*. 2011;28(10):2379-2385. doi:10.1007/s11095-011-0523-5

62. Valdés I, Bernardo L, Gil L, et al. A novel fusion protein domain III-capsid from dengue-2, in a highly aggregated form, induces a functional immune response and protection in mice. *Virology*. 2009;394(2):249-258. doi:10.1016/j.virol.2009.08.029

63. Bessa J, Boeckle S, Beck H, et al. The Immunogenicity of Antibody Aggregates in a Novel Transgenic Mouse Model. *Pharm Res*. 2015;32(7):2344-2359. doi:10.1007/s11095-015-1627-0

64. Boll B, Bessa J, Folzer E, et al. Extensive Chemical Modifications in the Primary Protein Structure of IgG1 Subvisible Particles Are Necessary for Breaking Immune Tolerance. *Mol Pharm*. 2017;14(4):1292-1299. doi:10.1021/acs.molpharmaceut.6b00816

65. Hochuli E. Interferon immunogenicity: technical evaluation of interferon-alpha 2a. *J Interferon Cytokine Res*. 1997;17 Suppl 1:S15-21. http://www.ncbi.nlm.nih.gov/pubmed/9241611. Accessed March 7, 2019.

66. Wayne M, Leppert P. Role of aggregate human growth hormone (hGH) in development of antibodies to hGH. *J Clin Endocrinol Metab*. 190AD;51(4):691-697. https://academic.oup.com/jcem/article-abstract/51/4/691/2678060. Accessed March 2, 2019.

67. Ring J, Stephan W, Brendel W. Anaphylactoid reactions to infusions of plasma protein and human serum albumin Role of aggregated proteins and of stabilizers added during production. *Clin Exp Allergy*. 1979;9(1):89-97. doi:10.1111/j.1365-2222.1979.tb01527.x

68. Telikepalli S, Shinogle HE, Thapa PS, et al. Physical Characterization and In Vitro Biological Impact of Highly Aggregated Antibodies Separated into Size-Enriched Populations by Fluorescence-Activated Cell Sorting. *J Pharm Sci*. 2015;104(5):1575-1591. doi:10.1002/JPS.24379

69. Bachmann MF, Zinkernagel RM. Neutralizing Antiviral B Cell Responses. *Annu Rev Immunol*. 2002;15(1):235-270. doi:10.1146/annurev.immunol.15.1.235

70. Carpenter JF, Randolph TW, Jiskoot W, et al. Overlooking subvisible particles in therapeutic protein products: gaps that may compromise product quality. *J Pharm Sci*. 2009;98(4):1201-1205. doi:10.1002/jps.21530

71. Scherer TM, Leung S, Owyang L, Shire SJ. Issues and challenges of subvisible and submicron particulate analysis in protein solutions. *AAPS J*. 2012;14(2):236-243. doi:10.1208/s12248-012-9335-8

72. Bee JS, Goletz TJ, Ragheb JA. The future of protein particle characterization and understanding its potential to diminish the immunogenicity of biopharmaceuticals: a shared perspective. *J Pharm Sci*. 2012;101(10):3580-3585. doi:10.1002/jps.23247

73. Barnard JG, Babcock K, Carpenter JF. Characterization and quantitation of aggregates and particles in interferon-β products: potential links between product quality attributes and immunogenicity. *J Pharm Sci*. 2013;102(3):915-928. doi:10.1002/jps.23415

74. Kotarek J, Stuart C, De Paoli SH, et al. Subvisible particle content, formulation, and dose of an erythropoietin peptide mimetic product are associated with severe adverse postmarketing events. *J Pharm Sci*. 2016;105(3):1023-1027. doi:10.1016/S0022-3549(15)00180-X

75. Hermeling S, Schellekens H, Maas C, Gebbink MFBG, Crommelin DJA, Jiskoot W. Antibody Response to Aggregated Human Interferon Alpha2b in Wild-type and Transgenic Immune Tolerant Mice Depends on Type and Level of Aggregation. *J Pharm Sci*. 2006;95(5):1084-1096. https://linkinghub.elsevier.com/retrieve/pii/S0022354916320068. Accessed March 2, 2019.

76. Fradkin AH, Carpenter JF, Randolph TW. Immunogenicity of aggregates of recombinant human growth hormone in mouse models. *J Pharm Sci*. 2009;98(9):3247-3264. doi:10.1002/jps.21834

77. Dumetz AC, Chockla AM, Kaler EW, Lenhoff AM. Effects of pH on protein-protein interactions and implications for protein phase behavior. *Biochim Biophys Acta*. 2008;1784(4):600-610. doi:10.1016/j.bbapap.2007.12.016

78. Singh SK, Afonina N, Awwad M, et al. An industry perspective on the monitoring of subvisible particles as a quality attribute for protein therapeutics. *J Pharm Sci*. 2010;99(8):3302-3321. doi:10.1002/jps.22097

79. Philo J, Arakawa T. Mechanisms of Protein Aggregation. *Curr Pharm Biotechnol*. 2009;10(4):348-351. doi:10.2174/138920109788488932

80. Narhi LO, Corvari V, Ripple DC, et al. Subvisible (2-100 μm) Particle Analysis During Biotherapeutic Drug Product Development: Part 1, Considerations and Strategy. *J Pharm Sci*. 2015;104(6):1899-1908. doi:10.1002/jps.24437

81. Bee JS, Chiu D, Sawicki S, et al. Monoclonal antibody interactions with micro- and nanoparticles: adsorption, aggregation, and accelerated stress studies. *J Pharm Sci*.

2009;98(9):3218-3238. doi:10.1002/jps.21768

82. Chi EY, Weickmann J, Carpenter JF, Manning MC, Randolph TW. Heterogeneous nucleation-controlled particulate formation of recombinant human platelet-activating factor acetylhydrolase in pharmaceutical formulation. *J Pharm Sci*. 2005;94(2):256-274. doi:10.1002/jps.20237

83. Barber TA, Lannis MD, Williams JG, Ryan JF. Application of improved standardization methods and instrumentation in the USP particulate test for SVI. *J Parenter Sci Technol*. 1990;44(4):185-203. http://www.ncbi.nlm.nih.gov/pubmed/2213427. Accessed March 7, 2019.

84. Narhi LO, Jiang Y, Cao S, Benedek K, Shnek D. A critical review of analytical methods for subvisible and visible particles. *Curr Pharm Biotechnol*. 2009;10(4):373-381. http://www.ncbi.nlm.nih.gov/pubmed/19519412. Accessed April 14, 2018.

85. Totoki S, Yamamoto G, Tsumoto K, Uchiyama S, Fukui K. Quantitative laser diffraction method for the assessment of protein subvisible particles. *J Pharm Sci*. 2015;104(2):618-626. doi:10.1002/jps.24288

86. Kiyoshi M, Shibata H, Harazono A, et al. Collaborative Study for Analysis of Subvisible Particles Using Flow Imaging and Light Obscuration: Experiences in Japanese Biopharmaceutical Consortium. *J Pharm Sci*. 2019;108(2):832-841. doi:10.1016/J.XPHS.2018.08.006

87. Strehl R, Rombach-Riegraf V, Diez M, et al. Discrimination Between Silicone Oil Droplets and Protein Aggregates in Biopharmaceuticals: A Novel Multiparametric Image Filter for Sub-visible Particles in Microflow Imaging Analysis. *Pharm Res*. 2012;29(2):594-602. doi:10.1007/s11095-011-0590-7

88. Zhou C, Krueger AB, Barnard JG, Qi W, Carpenter JF. Characterization of Nanoparticle Tracking Analysis for Quantification and Sizing of Submicron Particles of Therapeutic Proteins. *J Pharm Sci*. 2015;104(8):2441-2450. doi:10.1002/JPS.24510

89. Weinbuch D, Zölls S, Wiggenhorn M, et al. Micro-flow imaging and resonant mass measurement (Archimedes)--complementary methods to quantitatively differentiate protein particles and silicone oil droplets. *J Pharm Sci*. 2013;102(7):2152-2165. doi:10.1002/jps.23552

90. Capelle MAH, Gurny R, Arvinte T. High throughput screening of protein formulation stability: Practical considerations. *Eur J Pharm Biopharm*. 2007;65(2):131-148. doi:10.1016/J.EJPB.2006.09.009

91. Rosenberg AS, Verthelyi D, Cherney BW. Managing uncertainty: a perspective on risk pertaining to product quality attributes as they bear on immunogenicity of therapeutic proteins. *J Pharm Sci*. 2012;101(10):3560-3567. doi:10.1002/jps.23244

92. Carpenter JF, Pikal MJ, Chang BS, Randolph TW. Rational design of stable lyophilized protein formulations: some practical advice. *Pharm Res*. 14(8):969-975. doi:10.1023/A:1012180707283

93. Izutsu K, Kojima S. Excipient crystallinity and its protein-structure-stabilizing effect

during freeze-drying. *J Pharm Pharmacol*. 2002;54(8):1033-1039. doi:10.1211/002235702320266172

94. Wang W. Lyophilization and development of solid protein pharmaceuticals. *Int J Pharm*. 2000;203(1-2):1-60. doi:10.1016/S0378-5173(00)00423-3

95. Arakawa T, Prestrelski SJ, Kenney WC, Carpenter JF. Factors affecting short-term and long-term stabilities of proteins. *Adv Drug Deliv Rev*. 1993;10:1-28. https://ac.els-cdn.com/0169409X9390003M/1-s2.0-0169409X9390003M-main.pdf?_tid=83cdd409-c9f9-40f8-b127-b4218e169958&acdnat=1533661391_d09109c2320a3df0859c3ee1b9b3f77c. Accessed August 7, 2018.

96. Pikal MJ. Mechanisms of Protein Stabilization During Freeze-Drying and Storage: The Relative Importance of Thermodynamic Stabilization and Glassy State Relaxation Dynamics. In: *Freeze-Drying/Lyophilization of Pharmaceutical and Biological Products*. Marcel Dekker, Inc.; 2004:63-108. https://ci.nii.ac.jp/naid/10029415794/. Accessed March 3, 2019.

97. Franks F. Freeze-drying of bioproducts: putting principles into practice. *Eur J Pharm Biopharm*. 1998;45(3):221-229. doi:10.1016/S0939-6411(98)00004-6

98. Manning MC, Patel K, Borchardt RT. Review - Stability of Protein Pharmaceuticals. *Pharm res*. 1989;6(11):903-918. doi:10.1023/A:1015929109894

99. Lam XM, Costantino HR, Overcashier DE, Nguyen TH, Hsu CC. Replacing succinate with glycolate buffer improves the stability of lyophilized interferon-γ. *Int J Pharm*. 1996;142(1):85-95. doi:10.1016/0378-5173(96)04656-X

100. Franks F. Solid aqueous solutions. *Pure Appl Chem*. 2007;65(12):2527-2537. doi:10.1351/pac199365122527

101. Franks F. Freeze-drying: from empiricism to predictability. *Cryo-Lett*. 1990;11:93-110. https://ci.nii.ac.jp/naid/10015095748/. Accessed December 11, 2018.

102. Anchordoquy TJ, Carpenter JF. Polymers protect lactate fehydrogenase during freeze-drying by inhibiting dissociation in the frozen state. *Arch Biochem Biophys*. 1996;332(2):231-238. doi:10.1006/ABBI.1996.0337

103. Strambini GB, Gabellieri E. Proteins in frozen solutions: evidence of ice-induced partial unfolding. *Biophys J*. 1996;70(2):971-976. doi:10.1016/S0006-3495(96)79640-6

104. Chang BS, Kendrick BS, Carpenter JF. Surface-induced denaturation of proteins during freezing and its inhibition by surfactants. *J Pharm Sci*. 1996;85(12):1325-1330. doi:10.1021/js960080y

105. Devi S, Williams D. Morphological and compressional mechanical properties of freeze-dried mannitol, sucrose, and trehalose cakes. *J Pharm Sci*. 2013;102(12):4246-4255. doi:10.1002/jps.23736

106. Searles JA, Carpenter JF, Randolph TW. The ice nucleation temperature determines the primary drying rate of lyophilization for samples frozen on a temperature-controlled shelf.

J Pharm Sci. 2001;90(7):860-871. http://www.ncbi.nlm.nih.gov/pubmed/11458335. Accessed January 18, 2015.

107. Searles JA, Carpenter JF, Randolph TW. Annealing to optimize the primary drying rate, reduce freezing-induced drying rate heterogeneity, and determine Tg' in pharmaceutical lyophilization. *J Pharm Sci*. 2001;90(7):872-887. doi:10.1002/jps.1040

108. Searles J. Freezing and annealing phenomena in lyophilization. In: Rey L, May JC, eds. *Freeze Drying/Lyophilization of Pharmaceutical and Biological Products*. Third Edition. ; 2010:52-81. https://content.taylorfrancis.com/books/e/download?dac=C2009-0-02826-6&isbn=9781439825761&doi=10.3109/9781439825761-3&format=pdf. Accessed March 6, 2019.

109. Nail SL, Jiang S, Chongprasert S, Knopp SA. Fundamentals of Freeze-Drying. In: Springer, Boston, MA; 2002:281-360. doi:10.1007/978-1-4615-0549-5_6

110. Tang X, Pikal MJ. Design of freeze-drying processes for pharmaceuticals: practical advice. *Pharm Res*. 2004;21(2):191-200. doi:10.1023/B:PHAM.0000016234.73023.75

111. Ken-ichi I, Sumie Y, Yasushi T. The effects of additives on the stability of freeze-dried β-galactosidase stored at elevated temperature. *Int J Pharm*. 1991;71(1-2):137-146. doi:10.1016/0378-5173(91)90075-Y

112. Izutsu K, Yoshioka S, Terao T. Decreased protein-stabilizing effects of cryoprotectants due to crystallization. *Pharm Res*. 1993;10(8):1232-1237. doi:10.1023/A:1018988823116

113. Rupley JA, Careri G. Protein Hydration and Function. *Adv Protein Chem*. 1991;41:37-172. doi:10.1016/S0065-3233(08)60197-7

114. Carpenter H. John and, John CF. An infrared spectroscopic study of the interactions of carbohydrates with dried proteins. *Biochemistry*. 1989;28(9):3916−3922. https://pubs.acs.org/sharingguidelines. Accessed March 6, 2019.

115. Prestrelski SJ, Arakawa T, Carpenter JF. Separation of freezing- and drying-induced denaturation of lyophilized proteins using stress-specific stabilization: II. structural studies using infrared spectroscopy. *Arch Biochem Biophys*. 1993;303(2):465-473. doi:10.1006/ABBI.1993.1310

116. Zhou C, Cleland D, Snell J, Qi W, Randolph TW, Carpenter JF. Formation of stable nanobubbles on reconstituting lyophilized formulations containing trehalose. *J Pharm Sci*. 2016;105(7):2249-2253. doi:10.1016/j.xphs.2016.04.035

117. Fujita T, Kashiwa M, Maeda S, Kobayashi H, Nishihara I, Ida K. The effect of dilution on the quantitative measurement of bubbles in high-density ultrafine bubble-filled water using the light scattering method. In: Aya N, Iki N, Shimura T, Shirai T, eds. *International Conference on Optical Particle Characterization (OPC 2014)*. Vol 9232. International Society for Optics and Photonics; 2014:92320V. doi:10.1117/12.2064810

118. Ushikubo FY, Furukawa T, Nakagawa R, et al. Evidence of the existence and the stability of nano-bubbles in water. *Colloids Surfaces A Physicochem Eng Asp*. 2010;361(1-3):31-37. doi:10.1016/j.colsurfa.2010.03.005

119. Ohgaki K, Khanh NQ, Joden Y, Tsuji A, Nakagawa T. Physicochemical approach to nanobubble solutions. *Chem Eng Sci*. 2010;65(3):1296-1300. doi:10.1016/j.ces.2009.10.003

120. Azevedo A, Etchepare R, Calgaroto S, Rubio J. Aqueous dispersions of nanobubbles: Generation, properties and features. *Miner Eng*. 2016;94:29-37. doi:10.1016/j.mineng.2016.05.001

121. Alheshibri M, Qian J, Jehannin M, Craig VSJ. A History of Nanobubbles. *Langmuir*. 2016;32(43):11086-11100. doi:10.1021/acs.langmuir.6b02489

122. Ljunggren S, Eriksson JC. The lifetime of a colloid-sized gas bubble in water and the cause of the hydrophobic attraction. *Colloids Surfaces A Physicochem Eng Asp*. 1997;129-130:151-155. doi:10.1016/S0927-7757(97)00033-2

123. Yasui K, Tuziuti T, Kanematsu W. Mysteries of bulk nanobubbles (ultrafine bubbles); stability and radical formation. *Ultrason Sonochem*. 2018;48:259-266. doi:10.1016/J.ULTSONCH.2018.05.038

124. Epstein PS, Plesset MS. On the Stability of Gas Bubbles in Liquid-Gas Solutions. *J Chem Phys*. 1950;18(11):1505-1509. doi:10.1063/1.1747520

125. Mohamedi G, Azmin M, Pastoriza-Santos I, et al. Effects of Gold Nanoparticles on the Stability of Microbubbles. *Langmuir*. 2012;28(39):13808-13815. doi:10.1021/la302674g

126. Yasui K, Tuziuti T, Kanematsu W, Kato K. Dynamic Equilibrium Model for a Bulk Nanobubble and a Microbubble Partly Covered with Hydrophobic Material. *Langmuir*. 2016;32(43):11101-11110. doi:10.1021/acs.langmuir.5b04703

127. Cho S-H, Kim J-Y, Chun J-H, Kim J-D. Ultrasonic formation of nanobubbles and their zeta-potentials in aqueous electrolyte and surfactant solutions. *Colloids Surfaces A Physicochem Eng Asp*. 2005;269(1-3):28-34. doi:10.1016/j.colsurfa.2005.06.063

128. Takahashi M. Zeta potential of microbubbles in aqueous solutions: electrical properties of the gas-water interface. *J Phys Chem B*. 2005;109(46):21858-21864. doi:10.1021/jp0445270

129. Calgaroto S, Wilberg KQ, Rubio J. On the nanobubbles interfacial properties and future applications in flotation. *Miner Eng*. 2014;60:33-40. doi:10.1016/j.mineng.2014.02.002

130. Bunkin NF, Ninham BW, Ignatiev PS, Kozlov VA, Shkirin A V, Starosvetskij A V. Long-living nanobubbles of dissolved gas in aqueous solutions of salts and erythrocyte suspensions. *J Biophotonics*. 2011;4(3):150-164. doi:10.1002/jbio.201000093

131. Bunkin NF, Bunkin FV. Bubbstons: stable microscopic gas bubbles in very dilute electrolytic solutions. *ZhEkspTeorFiz*. 1992;101:512-527. https://www.researchgate.net/profile/Nikolay_Bunkin/publication/303156878_Bubstons-stable_gaseous_bubbles_in_strongly_dilute_electrolytic_solutions/links/58b81721458515 91c5d7c525/Bubstons-stable-gaseous-bubbles-in-strongly-dilute-electrolytic-solutions.pd. Accessed March 13, 2018.

132. Bunkin NF, Shkirin A V. Nanobubble clusters of dissolved gas in aqueous solutions of

electrolyte. II. Theoretical interpretation. *J Chem Phys*. 2012;137(5):054707. doi:10.1063/1.4739530

133. Zhu J, An H, Alheshibri M, et al. Cleaning with Bulk Nanobubbles. *Langmuir*. 2016;32(43):11203-11211. doi:10.1021/acs.langmuir.6b01004

134. Wu Z, Chen H, Dong Y, et al. Cleaning using nanobubbles: defouling by electrochemical generation of bubbles. *J Colloid Interface Sci*. 2008;328(1):10-14. doi:10.1016/j.jcis.2008.08.064

135. Agarwal A, Ng WJ, Liu Y. Principle and applications of microbubble and nanobubble technology for water treatment. *Chemosphere*. 2011;84(9):1175-1180. doi:10.1016/j.chemosphere.2011.05.054

136. Bunkin NF, Shkirin A V., Babenko VA, Sychev AA, Lomkova AK, Kulikov ES. Laser diagnostics of the Bubston phase in the bulk of aqueous salt solutions. *Phys Wave Phenom*. 2015;23(3):161-175. doi:10.3103/S1541308X15030012

137. Jin F, Ye J, Hong L, Lam H, Wu C. Slow relaxation mode in mixtures of water and organic molecules: supramolecular structures or nanobubbles? *J Phys Chem B*. 2007;111(9):2255-2261. doi:10.1021/jp068665w

138. Attard P. The stability of nanobubbles. *Eur Phys J Spec Top*. April 2013:1-22. doi:10.1140/epjst/e2013-01817-0

139. Bunkin NF, Shkirin A V, Ignatiev PS, Chaikov LL, Burkhanov IS, Starosvetskij A V. Nanobubble clusters of dissolved gas in aqueous solutions of electrolyte. I. Experimental proof. *J Chem Phys*. 2012;137(5):054706. doi:10.1063/1.4739528

140. Seddon JRT, Lohse D, Ducker WA, Craig VSJ. A deliberation on nanobubbles at surfaces and in bulk. *Chemphyschem*. 2012;13(8):2179-2187. doi:10.1002/cphc.201100900

141. Jin F, Li J, Ye X, Wu C. Effects of pH and ionic strength on the stability of nanobubbles in aqueous solutions of alpha-cyclodextrin. *J Phys Chem B*. 2007;111(40):11745-11749. doi:10.1021/jp074260f

142. Liu G, Wu Z, Craig VSJ. Cleaning of protein-coated surfaces using nanobubbles: an investigation using a quartz crystal microbalance. *J Phys Chem C*. 2008;112(43):16748-16753. doi:10.1021/jp805143c

143. Morris VJ, Gunning AP. Microscopy, microstructure and displacement of proteins from interfaces: implications for food quality and digestion. *Soft Matter*. 2008;4(5):943-951. doi:10.1039/b718904d

144. Vessely CR, Carpenter JF, Schwartz DK. Calcium-induced changes to the molecular conformation and aggregate structure of beta-casein at the air-water interface. *Biomacromolecules*. 2005;6(6):3334-3344. doi:10.1021/bm050353w

145. Yano YF, Uruga T, Tanida H, et al. Driving force behind adsorption-induced protein unfolding: a time-resolved x-ray reflectivity study on lysozyme Adsorbed at an Air/Water Interface. *Langmuir*. 2009;25(1):32-35. doi:10.1021/la803235x

146. Song KB, Damodaran S. Influence of electrostatic forces on the adsorption of succinylated .beta.-lactoglobulin at the air-water interface. *Langmuir*. 1991;7(11):2737-2742. doi:10.1021/la00059a055

147. de Jongh HHJ, Kosters HA, Kudryashova E, Meinders MBJ, Trofimova D, Wierenga PA. Protein adsorption at air-water interfaces: a combination of details. *Biopolymers*. 2004;74(1-2):131-135. doi:10.1002/bip.20036

148. Magdassi S. Surface Activity of Proteins: Chemical and Physicochemical Modifications. In: CRC Press; 1996:336. https://books.google.com/books/about/Surface_Activity_of_Proteins.html?id=fqJea2arRfIC&pgis=1. Accessed April 12, 2016.

149. Randolph TW, Jones LS. Rational Design of Stable Protein. In: Manning MC, Carpenter JF, eds. *Rational Design of Stable Protein*. New York; 2002:159-175.

150. Barnard JG, Singh S, Randolph TW, Carpenter JF. Subvisible particle counting provides a sensitive method of detecting and quantifying aggregation of monoclonal antibody caused by freeze-thawing: insights into the roles of particles in the protein aggregation pathway. *J Pharm Sci*. 2011;100(2):492-503. doi:10.1002/jps.22305

151. Carpenter J, Cherney B, Lubinecki A, et al. Meeting report on protein particles and immunogenicity of therapeutic proteins: Filling in the gaps in risk evaluation and mitigation. *Biologicals*. 2010;38(5):602-611. doi:10.1016/j.biologicals.2010.07.002

152. Snell JR, Zhou C, Carpenter JF, Randolph TW. Particle formation and aggregation of a therapeutic protein in nanobubble suspensions. *J Pharm Sci*. 2016;105(10):3057-3063. doi:10.1016/j.xphs.2016.06.020

153. Izutsu K. Stabilization of therapeutic proteins in aqueous solutions and freeze-dried solids: an overview. In: Humana Press, Totowa, NJ; 2014:435-441. doi:10.1007/978-1-62703-977-2_31

154. Raut AS, Kalonia DS. Pharmaceutical perspective on opalescence and liquid-liquid phase separation in protein solutions. *Mol Pharm*. 2016;13(5):1431-1444. doi:10.1021/acs.molpharmaceut.5b00937

155. Roberts CJ. Protein aggregation and its impact on product quality. *Curr Opin Biotechnol*. 2014;30:211-217. doi:10.1016/j.copbio.2014.08.001

156. Carpenter JF, Izutsu K, Randolph TW. Freezing- and drying-induced perturbations of protein structure and mechanism of protein protection by stabilizing additives. In: *Freeze-Drying/Lyophilization of Pharmaceutical and Biological Products*. CRC Press; 2016:167-197. doi:10.3109/9781439825761-7

157. Dong A, Prestrelski SJ, Allison SD, Carpenter JF. Infrared spectroscopic studies of lyophilization- and temperature-induced protein aggregation. *J Pharm Sci*. 1995;84(4):415-424. doi:10.1002/jps.2600840407

158. Andya JD, Hsu CC, Shire SJ. Mechanisms of aggregate formation and carbohydrate excipient stabilization of lyophilized humanized monoclonal antibody formulations. *AAPS PharmSci*. 2003;5(2):21-31. doi:10.1208/ps050210

159. Carpenter JF, Prestrelski SJ, Arakawa T. Separation of Freezing- and Drying-Induced Denaturation of Lyophilized Proteins Using Stress-Specific Stabilization: I. Enzyme Activity and Calorimetric Studies. *Arch Biochem Biophys*. 1993;303(2):456-464. doi:10.1006/ABBI.1993.1309

160. Webb SD, Cleland JL, Carpenter JF, Randolph TW. Effects of annealing lyophilized and spray-lyophilized formulations of recombinant human interferon-gamma. *J Pharm Sci*. 2003;92(4):715-729. doi:10.1002/jps.10334

161. *Powder Diffraction File*.(2004).

162. Nunes C, Suryanarayanan R, Botez CE, Stephens PW. Characterization and Crystal Structure of D-Mannitol Hemihydrate. *J Pharm Sci*. 2004;93(11):2800-2809. doi:10.1002/jps.20185

163. Sundaramurthi P, Suryanarayanan R. Trehalose crystallization during freeze-drying: implications On lyoprotection. *J Phys Chem Lett*. 2010;1(2):510-514. doi:10.1021/jz900338m

164. Ding S-P, Fan J, Green JL, Lu Q, Sanchez E, Angell CA. Vitrification of trehalose by water loss from its crystalline dihydrate. *J Therm Anal*. 1996;47(5):1391-1405. doi:10.1007/BF01992835

165. Taylor LS, York P. Characterization of the Phase Transitions of Trehalose Dihydrate on Heating and Subsequent Dehydration. *J Pharm Sci*. 1998;87(3):347-355. doi:10.1021/js970239m

166. Surana R, Pyne A, Suryanarayanan R. Effect of Preparation Method on Physical Properties of Amorphous Trehalose. *Pharm Res*. 2004;21(7):1167-1176. doi:10.1023/B:PHAM.0000033003.17251.c3

167. Jena S, Horn J, Suryanarayanan R, Friess W, Aksan A. Effects of excipient interactions on the state of the freeze-concentrate and protein stability. *Pharm Res*. 2017;34(2):462-478. doi:10.1007/s11095-016-2078-y

168. Liao X, Krishnamurthy R, Suryanarayanan R. Influence of the active pharmaceutical ingredient concentration on the physical state of mannitol—implications in freeze-drying. *Pharm Res*. 2005;22(11):1978-1985. doi:10.1007/s11095-005-7625-x

169. Yu L, Milton N, Groleau EG, Mishra DS, Vansickle RE. Existence of a mannitol hydrate during freeze-drying and practical implications. *J Pharm Sci*. 1999;88(2):196-198. doi:10.1021/js980323h

170. Campbell Roberts SN, Williams AC, Grimsey IM, Booth SW. Quantitative analysis of mannitol polymorphs. X-ray powder diffractometry—exploring preferred orientation effects. *J Pharm Biomed Anal*. 2002;28(6):1149-1159. doi:10.1016/S0731-7085(02)00053-5

171. Roos Y, Karel M. Phase transitions of mixtures of amorphous polysaccharides and sugars. *Biotechnol Prog*. 1991;7(1):49-53. doi:10.1021/bp00007a008

172. Houk LR, Challa SR, Grayson B, Fanson P, Datye AK. The definition of “Critical

Radius" for a collection of nanoparticles undergoing Ostwald ripening. *Langmuir*. 2009;25(19):11225-11227. doi:10.1021/la902263s

173. Voorhees PW. The theory of Ostwald ripening. *J Stat Phys*. 1985;38(1-2):231-252. doi:10.1007/BF01017860

174. Duddu SP, Dal Monte PR. Effect of glass transition temperature on the stability of lyophilized formulations containing a chimeric therapeutic monoclonal antibody. *Pharm Res*. 1997;14(5):591-595. doi:10.1023/A:1012144810067

175. Ablett S, Clarke CJ, Izzard MJ, Martin DR. Relationship between ice recrystallisation rates and the glass transition in frozen sugar solutions. *J Sci Food Agric*. 2002;82(15):1855-1859. doi:10.1002/jsfa.1263

176. Jena S, Suryanarayanan R, Aksan A. Mutual influence of mannitol and trehalose on crystallization behavior in frozen solutions. *Pharm Res*. 2016;33(6):1413-1425. doi:10.1007/s11095-016-1883-7

177. Brailsford A., Wynblatt P. The dependence of Ostwald ripening kinetics on particle volume fraction. *Acta Metall*. 1979;27(3):489-497. doi:10.1016/0001-6160(79)90041-5

178. Voorhees PW, Glicksman ME. Ostwald ripening during liquid phase sintering—Effect of volume fraction on coarsening kinetics. *Metall Mater Trans A*. 1984;15(6):1081-1088. doi:10.1007/BF02644701

179. Marqusee JA, Ross J. Theory of Ostwald ripening: Competitive growth and its dependence on volume fraction. *J Chem Phys*. 1984;80(1):536-543. doi:10.1063/1.446427

180. Yao JH, Elder KR, Guo H, Grant M. Theory and simulation of Ostwald ripening. *Phys Rev B*. 1993;47(21):14110-14125. doi:10.1103/PhysRevB.47.14110

181. Cao W, Xie Y, Krishnan S, Lin H, Ricci M. Influence of process conditions on the crystallization and transition of metastable mannitol forms in protein formulations during lyophilization. *Pharm Res*. 2013;30(1):131-139. doi:10.1007/s11095-012-0855-9

182. Mehta M, Bhardwaj SP, Suryanarayanan R. Controlling the physical form of mannitol in freeze-dried systems. *Eur J Pharm Biopharm*. 2013;85(2):207-213. doi:10.1016/j.ejpb.2013.04.010

183. Baker MP, Reynolds HM, Lumicisi B, Bryson CJ. Immunogenicity of protein therapeutics: The key causes, consequences and challenges. *Self Nonself*. 2010;1(4):314-322. doi:10.4161/self.1.4.13904

184. Xiang SD, Scholzen A, Minigo G, et al. Pathogen recognition and development of particulate vaccines: Does size matter? *Methods*. 2006;40(1):1-9. doi:10.1016/j.ymeth.2006.05.016

185. Leleux J, Roy K. Micro and nanoparticle-based delivery systems for vaccine immunotherapy: an immunological and materials perspective. *Adv Healthc Mater*. 2013;2(1):72-94. doi:10.1002/adhm.201200268

186. Chisholm CF, Nguyen BH, Soucie KR, Torres RM, Carpenter JF, Randolph TW. In Vivo

Analysis of the Potency of Silicone Oil Microdroplets as Immunological Adjuvants in Protein Formulations. *J Pharm Sci*. 2015;104(11):3681-3690. doi:10.1002/jps.24573

187. Werner BP, Winter G. Expanding Bedside Filtration—A Powerful Tool to Protect Patients From Protein Aggregates. *J Pharm Sci*. 2018;107(11):2775-2788. doi:10.1016/J.XPHS.2018.07.022

188. Pardeshi NN, Qi W, Dahl K, Caplan L, Carpenter JF. Microparticles and nanoparticles delivered in intravenous saline and in an intravenous solution of a therapeutic antibody product. *J Pharm Sci*. 2017;106(2):511-520. doi:10.1016/j.xphs.2016.09.028

189. Kumru OS, Liu J, Ji JA, et al. Compatibility, Physical Stability, and Characterization of an IgG4 Monoclonal Antibody After Dilution into Different Intravenous Administration Bags. *J Pharm Sci*. 2012;101(10):3636-3650. doi:10.1002/jps.23224

190. Al Salloum H, Saunier J, Dazzi A, et al. Characterization of the surface physico-chemistry of plasticized PVC used in blood bag and infusion tubing. *Mater Sci Eng C*. 2017;75:317-334. doi:10.1016/j.msec.2017.02.057

191. Bernard L, Cueff R, Breysse C, Décaudin B, Sautou V, Armed Study Group. Migrability of PVC plasticizers from medical devices into a simulant of infused solutions. *Int J Pharm*. 2015;485(1-2):341-347. doi:10.1016/j.ijpharm.2015.03.030

192. Bernard L, Décaudin B, Lecoeur M, et al. Analytical methods for the determination of DEHP plasticizer alternatives present in medical devices: A review. *Talanta*. 2014;129:39-54. doi:10.1016/J.TALANTA.2014.04.069

193. Tickner JA, Schettler T, Guidotti T, McCally M, Rossi M. Health risks posed by use of di-2-ethylhexyl phthalate (DEHP) in PVC medical devices: A critical review. *Am J Ind Med*. 2001;39(1):100-111. doi:10.1002/1097-0274(200101)39:1<100::AID-AJIM10>3.0.CO;2-Q

194. Navarro R, Perrino MP, Tardajos MG, Reinecke H. Phthalate plasticizers covalently bound to PVC: Plasticization with suppressed migration. *Macromolecules*. 2010;43(5):2377-2381. doi:10.1021/ma902740t

195. Haishima Y, Seshimo F, Higuchi T, et al. Development of a simple method for predicting the levels of di(2-ethylhexyl) phthalate migrated from PVC medical devices into pharmaceutical solutions. *Int J Pharm*. 2005;298(1):126-142. doi:10.1016/J.IJPHARM.2005.04.009

196. Inoue K, Kawaguchi M, Yamanaka R, et al. Evaluation and analysis of exposure levels of di(2-ethylhexyl) phthalate from blood bags. *Clin Chim Acta*. 2005;358(1-2):159-166. doi:10.1016/j.cccn.2005.02.019

197. Loff S, Hannmann T, Subotic U, Reinecke F-M, Wischmann H, Brade J. Extraction of Diethylhexylphthalate by Home Total Parenteral Nutrition From Polyvinyl Chloride Infusion Lines Commonly Used in the Home. *J Pediatr Gastroenterol Nutr*. 2008;47(1):81-86. doi:10.1097/MPG.0b013e318164d933

198. Magdouli S, Daghrir R, Brar SK, Drogui P, Tyagi RD. Di 2-ethylhexylphtalate in the aquatic and terrestrial environment: A critical review. *J Environ Manage*. 2013;127:36-49.

doi:10.1016/j.jenvman.2013.04.013

199. Heudorf U, Mersch-Sundermann V, Angerer J. Phthalates: Toxicology and exposure. *Int J Hyg Environ Health*. 2007;210(5):623-634. doi:10.1016/J.IJHEH.2007.07.011

200. Erythropel HC, Maric M, Nicell JA, Leask RL, Yargeau V. Leaching of the plasticizer di(2-ethylhexyl)phthalate (DEHP) from plastic containers and the question of human exposure. *Appl Microbiol Biotechnol*. 2014;98(24):9967-9981. doi:10.1007/s00253-014-6183-8

201. Andrade AJM, Grande SW, Talsness CE, et al. A dose response study following in utero and lactational exposure to di-(2-ethylhexyl) phthalate (DEHP): Reproductive effects on adult male offspring rats. *Toxicology*. 2006;228(1):85-97. doi:10.1016/j.tox.2006.08.020

202. Testai E, Hartemann P, Rastogi SC, et al. The safety of medical devices containing DEHP plasticized PVC or other plasticizers on neonates and other groups possibly at risk (2015 update). *Regul Toxicol Pharmacol*. 2016;76:209-210. doi:10.1016/j.yrtph.2016.01.013

203. U.S. Food & Drug Administration. *DEHP in Plastic Medical Devices*.; 2017. https://www.fda.gov/MedicalDevices/ResourcesforYou/ucm142643.htm. Accessed October 25, 2018.

204. Jara S, Lysebo C, Greibrokk T, Lundanes E. Determination of phthalates in water samples using polystyrene solid-phase extraction and liquid chromatography quantification. *Anal Chim Acta*. 2000;407(1-2):165-171. doi:10.1016/S0003-2670(99)00829-6

205. Staples CA, Peterson DR, Parkerton TF, Adams WJ. The environmental fate of phthalate esters: A literature review. *Chemosphere*. 1997;35(4):667-749. doi:10.1016/S0045-6535(97)00195-1

206. De Lemos ML, Hamata L, Vu T. Leaching of diethylhexyl phthalate from polyvinyl chloride materials into etoposide intravenous solutions. *J Oncol Pharm Pract*. 2005;11(4):155-157. doi:10.1191/1078155205jp164oa

207. Subramanian P, Ainsworth ÆP, Cassey ÆJ. Lost bits : particle shedding with polyvinyl chloride intravenous administration sets. *Pediatr Surg Int*. 2002;18(8):658-661. doi:10.1007/s00383-002-0753-z

208. Madsen H, Winding O. Release of foreign bodies (particles) by clinical use of intravenous infusion sets. *Biomaterials*. 1996;17(7):663-666. doi:10.1016/0142-9612(96)86735-4

209. Thirumangalathu R, Krishnan S, Ricci MS, Brems DN, Randolph TW, Carpenter JF. Silicone oil- and agitation-induced aggregation of a monoclonal antibody in aqueous solution. *J Pharm Sci*. 2009;98(9):3167-3181. doi:10.1002/jps.21719

210. Majumdar S, Ford BM, Mar KD, Sullivan VJ, Ulrich RG, D'souza AJM. Evaluation of the Effect of Syringe Surfaces on Protein Formulations. *J Pharm Sci*. 2011;100(7):2563-2573. doi:10.1002/jps.22515

211. Basu P, Krishnan S, Thirumangalathu R, Randolph TW, Carpenter JF. IgG1 aggregation and particle formation induced by silicone-water interfaces on siliconized borosilicate glass beads: A model for siliconized primary containers. *J Pharm Sci*. 2013;102(3):852-

865. doi:10.1002/jps.23434

212. Gerhardt A, Bonam K, Bee JS, Carpenter JF, Randolph TW. Ionic strength affects tertiary structure and aggregation propensity of a monoclonal antibody adsorbed to silicone oil-water interfaces. *J Pharm Sci*. 2013;102(2):429-440. doi:10.1002/jps.23408

213. Jones LS, Kaufmann A, Middaugh CR. Silicone oil induced aggregation of proteins. *J Pharm Sci*. 2005;94(4):918-927. doi:10.1002/jps.20321

214. Castellino V, Cheng Y-L, Acosta E. The hydrophobicity of silicone-based oils and surfactants and their use in reactive microemulsions. *J Colloid Interface Sci*. 2011;353(1):196-205. doi:10.1016/j.jcis.2010.09.004

215. Sorret LL, Monticello CR, DeWinter MA, Schwartz DK, Randolph TW. Steric Repulsion Forces Contributed by PEGylation of Interleukin-1 Receptor Antagonist Reduce Gelation and Aggregation at the Silicone Oil-Water Interface. *J Pharm Sci*. 2019;108(1):162-172. doi:10.1016/j.xphs.2018.10.045

216. Haynes WM, ed. *CRC Handbook of Chemistry and Physics*. 95th ed. Boca Raton: FL: CRC Press LLC; 2015.

217. Ludwig DB, Carpenter JF, Hamel J, Randolph TW. Protein adsorption and excipient effects on kinetic stability of silicone oil emulsions. *J Pharm Sci*. 2010;99(4):1721-1733. doi:10.1002/jps.21982

218. Pretsch E, Buhlmann P AC. *Structure Determination of Organic Compounds: Table of Spectral Data*. Berlin: Springer-Verlag; 2000. doi:10.1007/978-3-540-93810-1

219. *Dow Corning 360 Medical Fluid [Product Information]*.; 2009.

220. Rabe M, Verdes D, Seeger S. Understanding protein adsorption phenomena at solid surfaces. *Adv Colloid Interface Sci*. 2011;162(1-2):87-106. doi:10.1016/j.cis.2010.12.007

221. Langmuir I. The adsorption of gases on plane surfaces of glass, mica and platinum. *J Am Chem Soc*. 1918;40(9):1361-1403. doi:10.1021/ja02242a004

222. Hawe A, Sutter M, Jiskoot W. Extrinsic fluorescent dyes as tools for protein characterization. *Pharm Res*. 2008;25(7):1487-1499. doi:10.1007/s11095-007-9516-9

223. Sorret LL, DeWinter MA, Schwartz DK, Randolph TW. Protein–protein interactions controlling interfacial aggregation of rhIL-1ra are not described by simple colloid models. *Protein Sci*. 2018;27(7):1191-1204. doi:10.1002/pro.3382

224. Janeway C, Travers P, Walport M, Shlomchik MJ. *Immunobiology: The Immune System in Health and Disease*. 5th ed. New York: Garland Science; 2001.

225. Burckbuchler V, Mekhloufi G, Giteau AP, Grossiord JL, Huille S, Agnely F. Rheological and syringeability properties of highly concentrated human polyclonal immunoglobulin solutions. *Eur J Pharm Biopharm*. 2010;76(3):351-356. doi:10.1016/J.EJPB.2010.08.002

226. Hawe A, Rispens T, Herron JN, Jiskoot W. Probing bis-ANS Binding Sites of Different Affinity on Aggregated IgG by Steady-State Fluorescence, Time-Resolved Fluorescence and Isothermal Titration Calorimetry. *J Pharm Sci*. 2011;100:1294-1305.

doi:10.1002/jps.22368

227. Muller-Eberhard H. Molecular Organization And Function Of The Complement System. *Annu Rev Biochem*. 2002;57(1):321-347. doi:10.1146/annurev.biochem.57.1.321

228. Arima Y, Toda M, Iwata H. Surface plasmon resonance in monitoring of complement activation on biomaterials. *Adv Drug Deliv Rev*. 2011;63(12):988-999. doi:10.1016/J.ADDR.2011.06.018

229. Andersson J, Ekdahl KN, Lambris JD, Nilsson B. Binding of C3 fragments on top of adsorbed plasma proteins during complement activation on a model biomaterial surface. *Biomaterials*. 2005;26(13):1477-1485. doi:10.1016/J.BIOMATERIALS.2004.05.011

230. Yeong-Shang L, Hlady V, Janatova J. Adsorption of complement proteins on surfaces with a hydrophobicity gradient. *Biomaterials*. 1992;13(8):497-504. doi:10.1016/0142-9612(92)90100-3

231. Sou K, Tsuchida E. Electrostatic interactions and complement activation on the surface of phospholipid vesicle containing acidic lipids: Effect of the structure of acidic groups. *Biochim Biophys Acta - Biomembr*. 2008;1778(4):1035-1041. doi:10.1016/J.BBAMEM.2008.01.006

232. Chonn A, Cullis PR, Devine D V. The role of surface charge in the activation of the classical and alternative pathways of complement by liposomes. *J Immunol*. 1991;146(12):4234-4241. http://www.ncbi.nlm.nih.gov/pubmed/2040798. Accessed October 20, 2018.

233. Britt KA, Schwartz DK, Wurth C, Mahler H-C, Carpenter JF, Randolph TW. Excipient effects on humanized monoclonal antibody interactions with silicone oil emulsions. *J Pharm Sci*. 2012;101(12):4419-4432. doi:10.1002/jps.23318

234. Frank MM, Gaither T, Adkinson F, Terry WD, May JE. Activation of the alternate complement pathway by human immunoglobulins. *J Immunol*. 1976;116(6):1733-1733. http://www.jimmunol.org/content/116/6/1733.1.short. Accessed March 29, 2019.

235. Hiemstra PS, Gorter A, Stuurman ME, Van Es LA, Daha MR. Activation of the alternative pathway of complement by human serum IgA. *Eur J Immunol*. 1987;17(3):321-326. doi:10.1002/eji.1830170304

236. Ekelund M, Azhdar B, Gedde UW. Evaporative loss kinetics of di(2-ethylhexyl)phthalate (DEHP) from pristine DEHP and plasticized PVC. *Polym Degrad Stab*. 2010;95(9):1789-1793. doi:10.1016/j.polymdegradstab.2010.05.007

237. Al Salloum H, Saunier J, Tfayli A, Yagoubi N. Studying DEHP migration in plasticized PVC used for blood bags by coupling Raman confocal microscopy to UV spectroscopy. *Mater Sci Eng C*. 2016;61:56-62. doi:10.1016/J.MSEC.2015.12.008

238. Chantelau EA, Berger M. Pollution of insulin with silicone oil, a hazard of disposable plastic syringes. *Lancet (London, England)*. 1985;1(8443):1459. http://www.ncbi.nlm.nih.gov/pubmed/2861406. Accessed March 24, 2019.

239. Chantelau E, Berger M, Böhlken B. Silicone oil released from disposable insulin syringes.

Diabetes Care. 1986;9(6):672-673. doi:10.2337/DIACARE.9.6.672

240. Wiesbauer J, Prassl R, Nidetzky B. Renewal of the air-water interface as a critical system parameter of protein stability: aggregation of the human growth hormone and its prevention by surface-active compounds. *Langmuir*. 2013;29(49):15240-15250. doi:10.1021/la4028223

241. Rudiuk S, Cohen-Tannoudji L, Huille S, Tribet C. Importance of the dynamics of adsorption and of a transient interfacial stress on the formation of aggregates of IgG antibodies. *Soft Matter*. 2012;8(9):2651. doi:10.1039/c2sm07017k

242. Amin S, Barnett G V., Pathak JA, Roberts CJ, Sarangapani PS. Protein aggregation, particle formation, characterization & rheology. *Curr Opin Colloid Interface Sci*. 2014;19(5):438-449. doi:10.1016/j.cocis.2014.10.002

243. *CHRIS Hazardous Chemical Data Volume II*. Washington, D.C. : U.S Government Printing Office; 1985. http://hdl.handle.net/2027/uc1.32106021023764. Accessed March 24, 2019.

244. Kanellopoulos AG, Owen MJ. Adsorption of sodium dodecyl sulphate at the silicone fluid/water interface. *Trans Faraday Soc*. 1971;67(0):3127-3138. doi:10.1039/TF9716703127

245. Randolph TW, Jones LS. Surfactant-Protein Interactions. *Pharm Biotechnol*. 2002;13:159-175. doi:10.1007/978-1-4615-0557-0_7

246. Szebeni J. Complement activation-related pseudoallergy: A stress reaction in blood triggered by nanomedicines and biologicals. *Mol Immunol*. 2014;61(2):163-173. doi:10.1016/j.molimm.2014.06.038

247. Szebeni J. Hemocompatibility testing for nanomedicines and biologicals: Predictive assays for complement mediated infusion reactions. In: *European Journal of Nanomedicine*. Vol 4. ; 2012:33-53. doi:10.1515/ejnm-2012-0002

248. Moghimi SM, Andersen AJ, Ahmadvand D, Wibroe PP, Andresen TL, Hunter AC. Material properties in complement activation. *Adv Drug Deliv Rev*. 2011;63(12):1000-1007. doi:10.1016/J.ADDR.2011.06.002

249. Moghimi SM, Simberg D. Complement activation turnover on surfaces of nanoparticles. *Nano Today*. 2017;15:8-10. doi:10.1016/j.nantod.2017.03.001

250. Szebeni J, Storm G. Complement activation as a bioequivalence issue relevant to the development of generic liposomes and other nanoparticulate drugs. *Biochem Biophys Res Commun*. 2015;468(3):490-497. doi:10.1016/j.bbrc.2015.06.177

251. Ricklin D, Hajishengallis G, Yang K, Lambris JD. Complement: A key system for immune surveillance and homeostasis. *Nat Immunol*. 2010;11(9):785-797. doi:10.1038/ni.1923

252. Moghimi SM, Farhangrazi ZS. Nanomedicine and the complement paradigm. *Nanomedicine Nanotechnology, Biol Med*. 2013;9(4):458-460. doi:10.1016/j.nano.2013.02.011

253. Agbeko RS, Fidler KJ, Allen ML, Wilson P, Klein NJ, Peters MJ. Genetic variability in complement activation modulates the systemic inflammatory response syndrome in children*. *Pediatr Crit Care Med*. 2010;11(5):561-567. doi:10.1097/PCC.0b013e3181d900ba

254. Harris CL, Heurich M, Cordoba SR de, Morgan BP. The complotype: Dictating risk for inflammation and infection. *Trends Immunol*. 2012;33(10):513-521. doi:10.1016/j.it.2012.06.001

255. Szebeni J, Muggia F, Gabizon A, Barenholz Y. Activation of complement by therapeutic liposomes and other lipid excipient-based therapeutic products: Prediction and prevention. *Adv Drug Deliv Rev*. 2011;63(12):1020-1030. doi:10.1016/j.addr.2011.06.017

256. Can M, Alibaz-Öner F, Yılmaz-Öner S, Atagündüz P, İnanç N, Direskeneli H. Accelerated infusion rates of rituximab are well tolerated and safe in rheumatology practice: a single-centre experience. *Clin Rheumatol*. 2013;32(1):87-90. doi:10.1007/s10067-012-2094-1

257. Buch MH, Bryer D, Lindsay S, Rees-Evans B, Fairclough A, Emery P. Shortening infusion times for infliximab administration. *Rheumatology*. 2006;45(4):485-486. doi:10.1093/rheumatology/kei247

258. Callréus T. The precautionary principle and pharmaceutical risk management. *Drug Saf*. 2005;28(6):465-471. doi:10.2165/00002018-200528060-00001

Appendix

A.1 Particle Characterization Using the Shimadzu SALD-7500nano

Background:

The Shimadzu SALD-7500nano characterizes micro- and nanoparticles over a broad size range. According to the manufacturers specification this instrument can measure particles with sizes between 7 nm and 800 µm. This instrument utilizes the principal of laser diffraction, however the SALD-7500nano can measure concentrations as well as size distributions. Concentration data is calculated by applying Mie theory to deconvolute the angular dependence of light scattering data.

Aggregates sizer (left) and bubble sizer (right)

Instrument Set up:

Shimadzu has provided two versions of their SALD7500nano instrument. The “aggregate sizer” and “bubble sizer”. However, the only difference between these two instruments is the laser intensity, with the bubble sizer having a higher laser intensity and therefore greater sensitivity. As the intensity of the laser can always be reduced using filters, I recommend the use of the bubble sizer over the aggregates sizer for the majority of measurements especially if you have low particle concentrations.

After selecting the instrument, you would like to use for your measurement you can next select the sample holder. Shimadzu has provided again two options, a batch cell with a minimum volume of 7 mL and a micro cell with a minimum volume of 125 µL. The two holders can be easily swapped by pulling out the drawer and gently pulling out the unit. Note: when the batch cell is used without temperature control unsure that the metal shielding device is installed to minimize background light reaching the detector.

Instrument Initialization

Once you have selected your instrument and cell you can proceed to turn on the instrument using the rocker switch located on right side of the instrument. If you also plan to use the temperature control unit turn it on at this time using two switches located on the unit (make sure the temperature control unit is full of water)

After the unit has been turned on open the WingSALD bio software. You will be immediately prompted with the WingSALD II starting screen shown below. On this screen ensure you have correctly selected the cell type you plan to use for your measurement using the device composition dropdown menu. Then proceed to enter manual mode by entering the **administrator password 0000.** Note: this password is the same for both instruments and all versions of the software.

Once you enter the main measurement screen, if you plan on using temperature click on “Const Temp Ctrl” and input your desired temperature. Provide sufficient time for the instrument to equilibrate to your desired temperature before you begin measuring your samples.

Next click on the “Diag&Adjust button” and follow the instructions that will appear on the screen for initialization of the SALD7500-nano. Once you enter the diagnosis adjustment screen you will be shown the raw detector output from each sensor and the location of the laser on the sensor. This screen can be used to verify the initial cleanliness of the cell used for sample measurement as well as the location of the sensor relative to the laser beam.

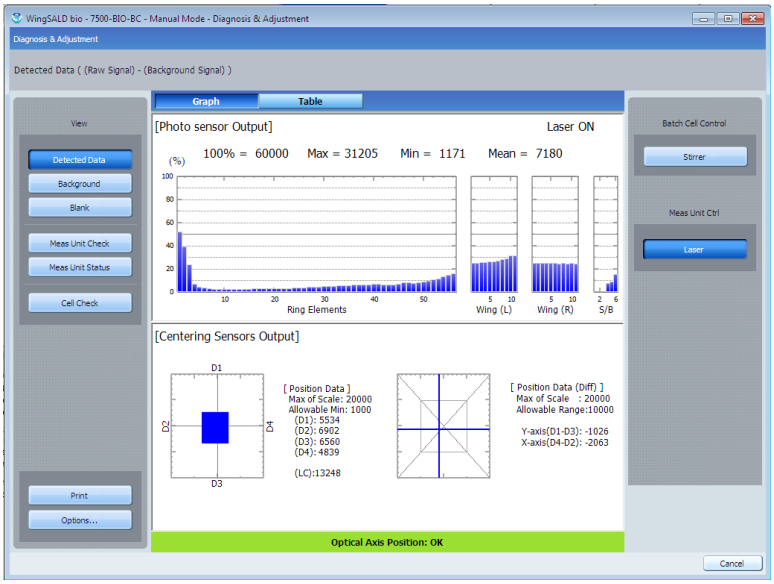

Fill your cell with either water of the buffer solution you will use for blanking the instrument and load it into the instrument. Shut the door and allow sufficient time for the sensor reading to settle. For a clean cell containing buffer or water the mean light intensity should be below 8,000. If the light intensity is greater than 8,000 than the cell must be cleaned. Clean the cells with water and Hellmanex detergent. Typically, cleaning the micro cell is more difficult than the micro cell. Depending on your sample more aggressive detergents may be required to reduce the background light intensity below 8,000.

Finally ensure the laser is centered on the sensor. The two outputs provided on this screen show you when the detector is centered. If the sensor is out of alignment open the door on the right side of the instrument and make the required adjustments. As shown below the sensor can be adjusted both up and down as well as left and right. Make sure to unclamp the desired adjustment direction before attempting to make any adjustments and only unclamp an adjust one side at a time. When the sensor is properly aligned the two blue lines will cross close to the middle of the square on the bottom right.

Once you have ensured that the cell is clean and that the laser is centered on the detector, exit the diagnosis and adjustment screen. Begin your measurement by clicking the manual button. Enter your sample information and the directory to which you would like to save your data and hit next. In the following screen you can modify the conditions for your measurement. Under measurement conditions, the default conditions are typically sufficient for most measurements. However, increase the signal average to the maximum value of 512 and the allowable range for blank light intensity to 150.

Under particle size distribution calculations provide the refractive index of the particles you will be measuring. This value will have a large impact on the results so ensure you have an accurate refractive index for your particles. Even small errors in this value can result in large errors in both the particle size distribution and concentration. Proceed to quantification conditions and provide the density of your particles and the filter attenuation if you are using a filter. If you are not using a filter enter a value of 1. If you are only interested in quantifying your particle size distribution in terms of counts an accurate value your particle density is not required. Particle density is only used to convert from counts to mass.

Hit next and begin your measurements. Before measuring your sample, you will need to blank the instrument with whatever medium your particles are dispersed in. After blanking you should not see any light intensities as shown in the image below.

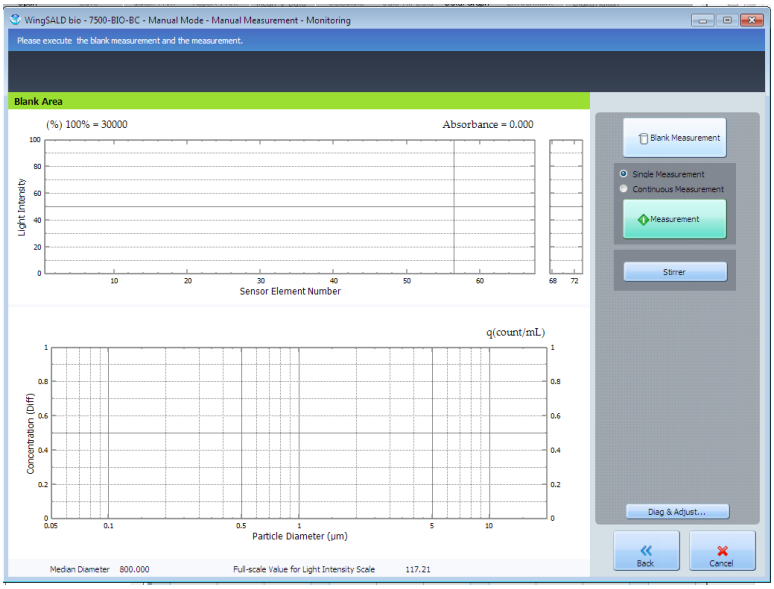

Remove the blank solution from the cell and replace it with your sample. Carefully add your sample to avoid forming any air bubbles and ensure you have sufficient sample volume so that the meniscus will not enter the measurement area. Next check that the light intensity from your sample is within the optimal range. After you place the cell containing your sample into the instrument the full-scale value for light intensity should be between 3,000 and 27,0000. If the light intensity is below 3,000 you do not have enough light intensity for a reliable measurement and your sample will need to be concentrated. However, if the light intensity is greater than 27,000 than the sensor is saturated.

There are two options if the light intensity from your sample exceeds 27,000. Either you can dilute your sample to lower the light intensity or you can use one of the light filters. The filters will reduce the laser light intensity by the factor printed on the filter. There were 3 filters provided with the instrument and the light attenuation factor for each filter is provided in the table below

Filter	Light Attenuation Factor
ND2	1.92
ND4	4.13
ND8	8.25

Once the light intensity is within the required range the measurement screen should look similar to that shown below. In the top figure the light intensity measured from each sensor element is plotted while the bottom figure provides a histogram with the particle size distribution. When you first place your sample in the instrument this distribution may fluctuate widely. Provide a few seconds for fluctuation to cease before clicking the measurement button. After the measurement is complete you must hit the save button for your measurement to be saved. You can then proceed to conduct additional measurements, cleaning and blanking between each measurement.

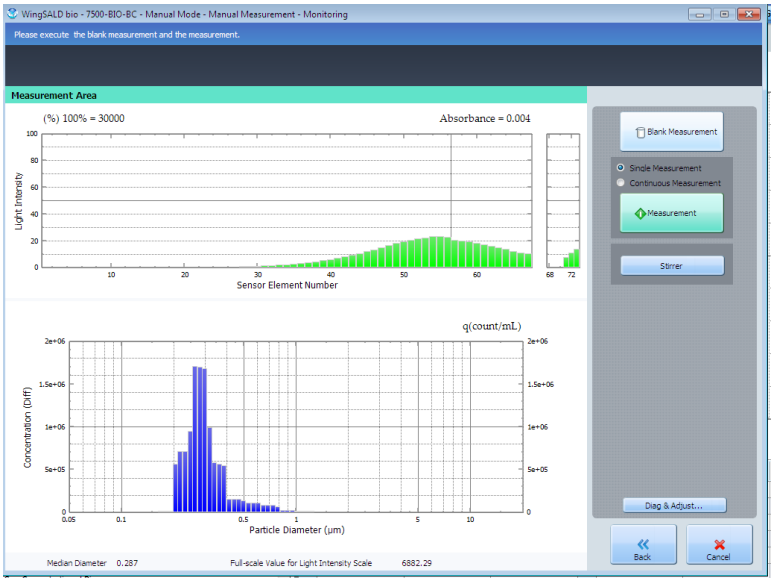

Data Analysis and Processing:

After you save your measurement it will be plotted in the main screen. Here you can analyze a single measurement or compare multiple measurements using the overlay graph tab. The plots shown in this screen can be modified using the Data/Graph button. Using this screen, you can change the size distribution from being plotted in terms of counts to particle mass. In addition, you can change the range of particle sizes displayed.

At any point the refractive index of the particles can be changed using the calculate button. Once a new refractive index is entered the software will recompute the size distribution and particle concentration.

The data can be exported from the software by selecting copy under the edit tab. You can then select if you would like to export summary, light or particle diameter data.

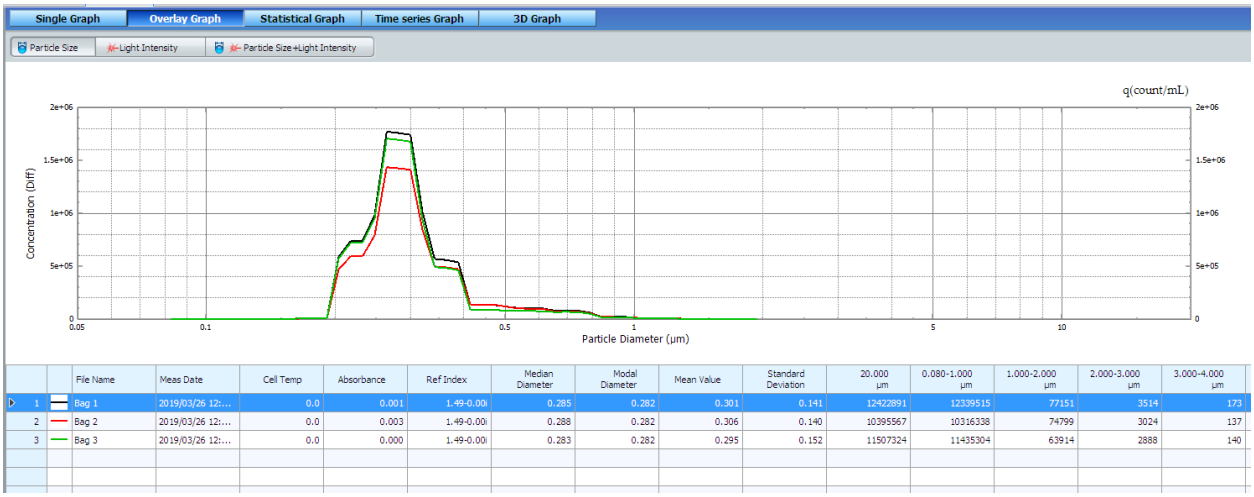

Additional Capabilities of the SALD-7500nano:

The SALD-7500nano can be used for single measurement as described in this protocol but also includes additional functionalities which may prove useful. Protein aggregation kinetics or colloidal stability can be monitored using the continuous measurement function. Under the manual measurement screen, you can select how many repeated measurements you would like to include and the time intervals between each. In addition, the software includes a trigger function so that the instrument will conduct a single measurement after a specified period has passed.

Important notes:

An adapter must be used with the micro cells. This black metal contraption can be difficult to open and close at first. Practice open and closing this adapter before attempting to use it with the micro cells or you may accidentally damage a cell.

The WingSALD Bio software was originally developed for use with the lower light intensity laser provided with the aggregates sizer instrument. However, it can still be used with the high intensity of laser of the bubble sizer but sometime gives error related to light intensity of the blank. This error can typically be ignored.

Clean up and Shutdown:

Once you have completed your final measurement thoroughly clean the cell ensuring that it will be ready for use by the next user. Close the software and turn off the instrument and temperature control unit.

Example Data:

Summary Data for PVC IV bags shaken at 350 rpm for 3 days at 25 °C

Bag	Ref. Index	Median Diameter (µm)	Mean Diameter (µm)	Concentration (#/mL)
Bag 1	1.49-0.00i	0.285	0.301	1.24E+07
Bag 2	1.49-0.00i	0.288	0.306	1.04E+07
Bag 3	1.49-0.00i	0.283	0.295	1.15E+07

Size distribution of droplets generated in a PVC IV bag during shaking

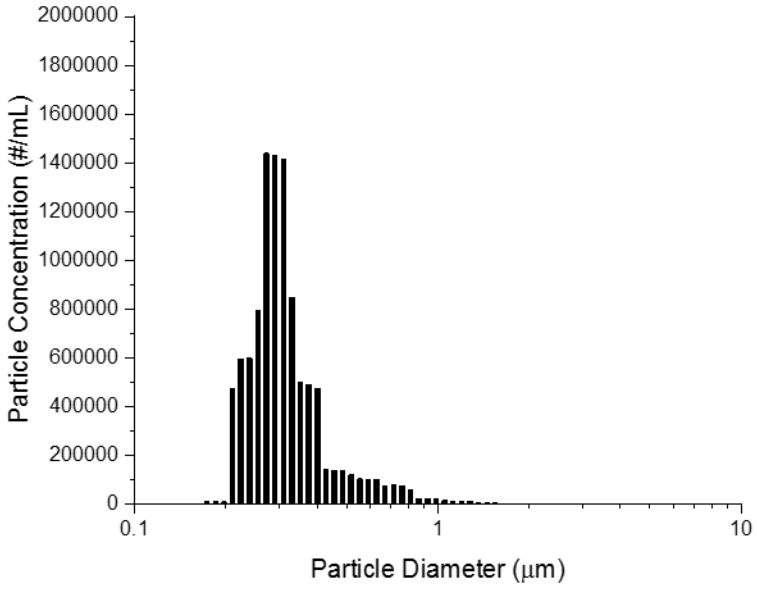

A.2 Measuring Nanoparticle Concentrations with Nanoparticle Tracking Analysis

Background:

Nanoparticle tracking analysis allows for the characterization of nanoparticles between 10 and 2000 nm. In this method each nanoparticle is tracked individually as points of scattered. From the diffusion rate of individual particle their size can be calculated using the Stoke-Einstein equation. This method allows for high resolution size distribution data as each particle is tracked individually

Note: This protocol is for operation of the NanoSight LM10 available in the Goodwin lab.

Protocol:

1. Remove the cover from the LM10 microscope and located the case containing the laser module
2. Carefully remove the laser module from the case and clean the upper and lower platforms using kim wipes, water and ethanol
3. Once both surfaces are clean attach the upper platform to the laser module using the four screws stored in the case.
4. As you install the screws apply pressure evenly and lightly to the laser module to avoid damage
5. Stand the unit up and slowly inject water thought the lower port using a syringe until it can be observed through the window and begins to exit through the upper port
6. Connect the laser module to the control unit and install the laser module on the microscope platform.
7. Open the NTA 3.0 software and hit the start camera button.
8. Ensure that the camera is located just to the right of the green line and that minimal particles are present. If particles are present rinse with ultrapure water.
9. Once the sample cell is clean inject your sample using a 1 mL syringe. Inject your sample until your particles are visible on the screen
10. Focus the microscope and select the light intensity best suited to your sample. Both light intensity and focus should be optimized to maximize the total number of particles that can be viewed while minimizing background scattering.
11. Select your measurement parameters using the standard measurement screen.
    a. Record at least three 60 second videos
    b. Maintain a constant temperature of 25 C
12. Select the directory and file name with which you would like to save your data
13. Click prepare script and run
14. Enter sample info and finalize camera settings
15. Follow scripts on screen, during measurement minimal any vibrations which could impact measurement
16. After data acquisition is complete you can proceed to data processing.
17. Select the optimal detection threshold by selecting the value which ensures that all particles are tracked while minimizing the effect of background noise

18. Once the analysis is complete hit end script and export data.
19. Between samples clean laser module with water, check after cleaning the particles from the previous measurement do not remain. If particle remaining dissemble laser module and clean thoroughly.
20. When measurements are complete dissemble and clean the laser module thoroughly. After cleaning return the laser module to the case.
21. Cover microscope and shutdown the computer.

Important Notes:

1. Using the LM10 available in the Goodwin lab each video will characterize the nanoparticles present only within the sample volume within view of the camera. For each video change the volume recorded by injecting addition sample. Be sure to select a random volume of your sample to analyze and not allow any user bias to influence results.
2. In the Carpenter lab on the Anschutz medical campus a NanoSight NS300 is available. This unit is interface with a syringe pump. Constantly injecting your sample during data acquisition will increase the total number of particle tracks recorded and is especially useful for low concentration samples.
3. Results obtained from the Nanosight NTA instrument can be subject to user bias as the user must select the optimal camera settings and focus for each individual sample. Therefore, for comparisons between samples the NTA should be operated by a single user.

Example report for a nanobubble suspension analyzed with nanoparticle tracking analysis

NANOSIGHT

Trehalose 24 hour anneal 4x diluted 2017-12-04 11-35-17

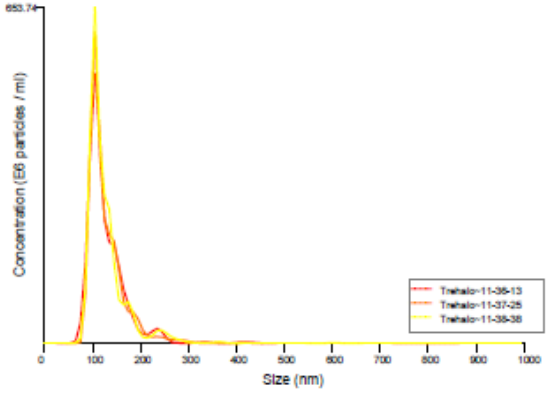

FTLA Size / Concentration graph for Experiment:
Trehalose 24 hour anneal 4x diluted 2017-12-04 11-35-17

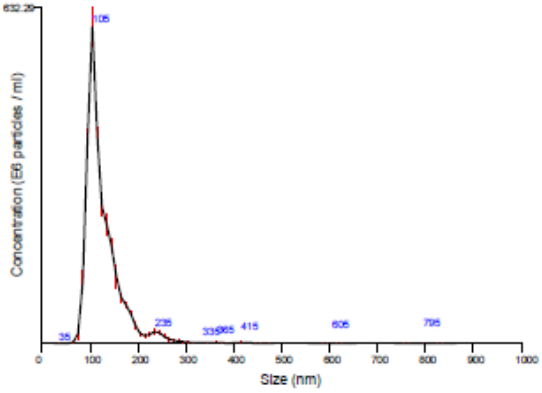

Averaged FTLA Size / Concentration
Red error bars indicate +/- 1 standard error of the mean

Included Files

Trehalose 24 hour anneal 4x diluted 2017-12-04 11-36-13
Trehalose 24 hour anneal 4x diluted 2017-12-04 11-37-25
Trehalose 24 hour anneal 4x diluted 2017-12-04 11-38-38

Details

NTA Version:	NTA 3.0 0069
Script Used:	SOP Standard Measurement 11-35-17AM 04Dec2017.txt
Time Captured:	11:35:17 04/12/2017
Operator:	Jared
Pre-treatment:	
Sample Name:	
Diluent:	PBS
Remarks:	

Capture Settings

Camera Type:	SCMOS
Camera Level:	13
Slider Shutter:	800
Slider Gain:	350
FPS	25.0
Number of Frames:	1498
Temperature:	25.0 - 25.0 °C
Viscosity:	1.2 cP
Dilution factor:	Dilution not recorded

Analysis Settings

Detect Threshold:	5
Blur Size:	Auto
Max Jump Distance:	Auto: 9.1 - 9.6 pix

Results

Stats: Merged Data

Mean:	122.6 nm
Mode:	105.0 nm
SD:	41.0 nm
D10:	83.4 nm
D50:	105.7 nm
D90:	164.4 nm

Stats: Mean +/- Standard Error

Mean:	122.6 +/- 0.3 nm
Mode:	105.1 +/- 0.3 nm
SD:	40.9 +/- 1.0 nm
D10:	83.3 +/- 0.8 nm
D50:	105.7 +/- 0.3 nm
D90:	164.4 +/- 0.7 nm
Concentration:	2.69e+009 +/- 3.97e+007 particles/ml
	136.4 +/- 2.0 particles/frame
	133.3 +/- 2.3 centres/frame

A.3 Zeta-Potential Measurements with the Litesizer 500

Background

The Anton Paar Litesizer 500 measures the zeta-potential of colloidal dispersion using the principal of phase analysis light scattering. This instrument can also be used for measuring particle size and molecular mass using light scattering methods.

Protocol

1. Open the Anton Paar Kalliope software and select Zeta-Potential measurement from the main menu.
2. Input the required measurement parameters. Typically, the default power and quality setting will be sufficient for most measurements.
3. Select the measurement temperature. If your measurement temperature differs significantly from the current temperature of your samples, make sure you provide enough time for sample equilibration before beginning your measurement.
4. Select your solvent from the drop-down menu ensuring that an accurate value of refractive index, viscosity and relative permittivity have been provided.
5. Load approximately 300-350 µL of your sample into a disposable omega cuvette using a 1 mL syringe. Begin loading with the cuvette upside down until your sample reaches the bottom of the cuvette. Then complete sample loading with the cuvette orientated normally.
6. After loading the sample ensure that your sample is in contact with the electrodes on both sides of the cuvette and that no bubbles are present. Remove air bubble by gently tapping the cuvette on hard surface.
7. Insert the omega cuvette into the sample chamber of the Litesizer 500 and begin measurement.
8. During the measurement ensure that your sample concentration is high enough by monitoring the filter optical density and mean intensity. If the filter optical density is 0 or the mean intensity is below 20 kcounts/s than your sample concentration is too low.
9. After the measurement is complete clean the omega cuvette with water and if necessary, detergents depending on your sample.
10. Dry the cuvette with ethanol and compressed air.

Recommendations

1. While the omega cuvettes are disposable replacement cuvettes are expensive. Therefore, continue to reuse the cuvettes for as long as possible. Over extended uses the electrodes will begin to degrade. When this corrosion become extensive dispose of the cuvette.
2. Verify omega cuvettes continue to function normally using the Zeta Potential standard provided by Anton Paar and stored in the drawer near the Litesizer 500.
3. Zeta-potential measurements with Litesizer 500 can be conducted with samples have conductivities as high as 200 mS/cm. However, for the most reliable and reproducible results minimize the conductivity of your sample. The omega cuvette electrodes degrade faster when measurements are taken at high ionic strengths.

Example Data:

Sample: Nanobubble Sample in 10% w/v trehalose and 10 mM sodium citrate buffer pH 6.6

Typical phase plot for zeta potential measurement. Significant change in phase should be observable during the measurement providing similar pattern to that shown below.

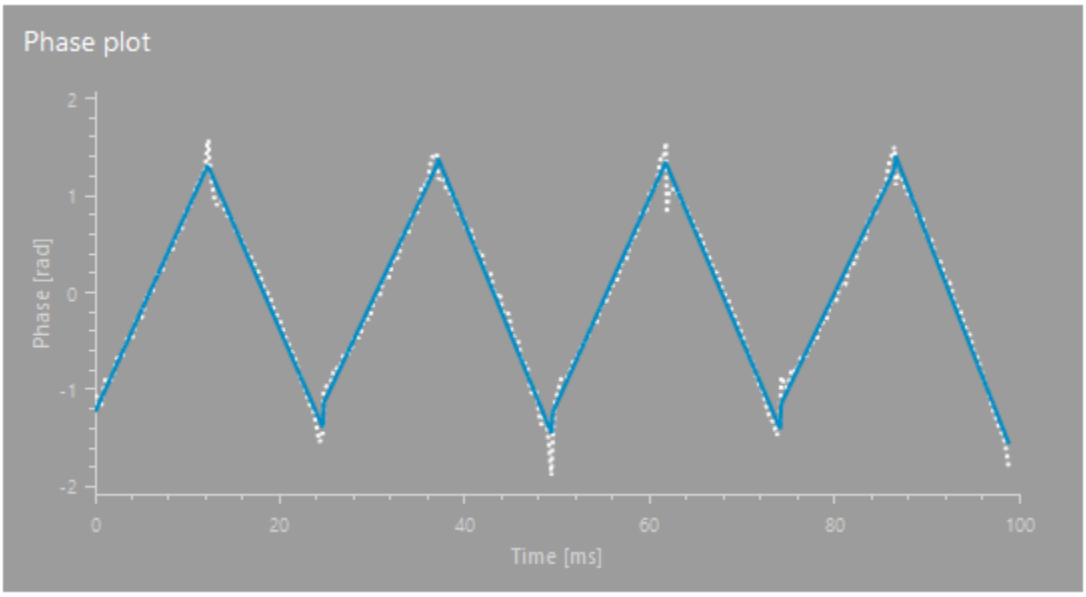

Zeta potential distribution for a nanobubble suspension

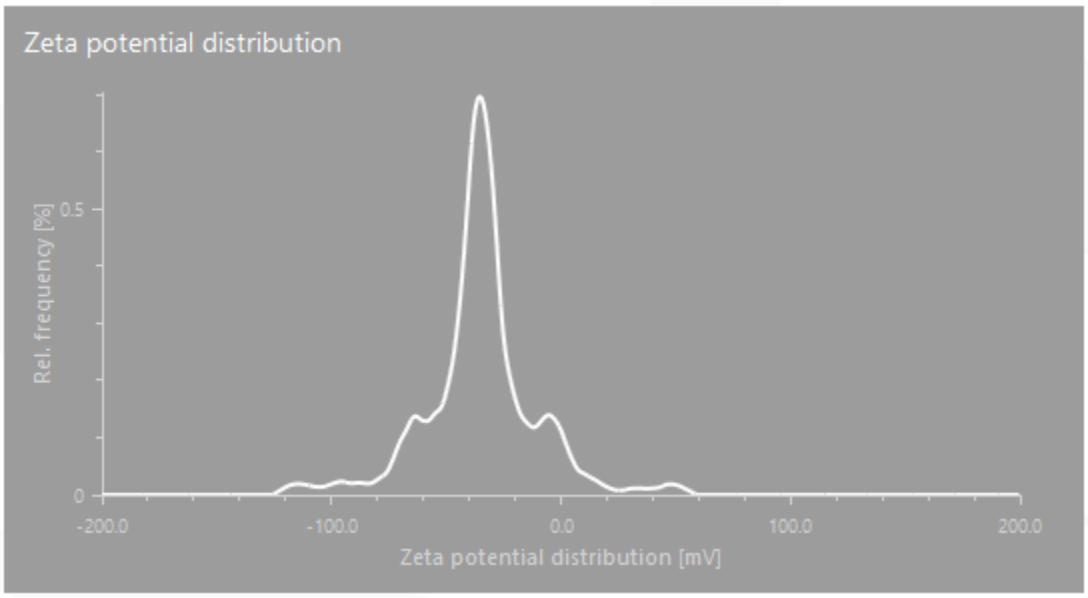

Triplicate Measurements for a Nanobubble Suspension

Sample	Zetapotential (mV)	Conductivity (mS/cm)	Electrophoretic Mobility (μm cm Vs^{-1})
1	-32.5	1.9	-1.88
2	-27.5	1.86	-1.59
3	-30.7	1.92	-1.78

A.4 Size Exclusion High Performance Liquid Chromatography

Operating parameters and example chromatogram for IVIG

SE-HPLC Operating Parameters for IVIG Formulations		
Pump	Elution	Isocratic
	Flow Rate	0.6 mL/min
	Seal Wash	10% Isopropyl Alcohol in Water
	Operating Pressure	~34 bar
	Pressure Limit	75 bar
Detector	Monitored Wavelength	280 nm
Autosampler/Injector	Injection Volume	50 µL
	Autosampler Temperature	4 °C
	Needle Wash	Water
	Draw Position	3 mm
	Injection Speed	200 µL/min
Column	Column Temperature	20 °C
	Column	TSKgel G3000SWXL
	Guard Column	TSKgel Guard Column
Mobile Phase	-	200 mM Sodium Phosphate buffer pH 7 with 400 mM NaCl

Example chromatogram for intravenous immunoglobulin (IVIG)

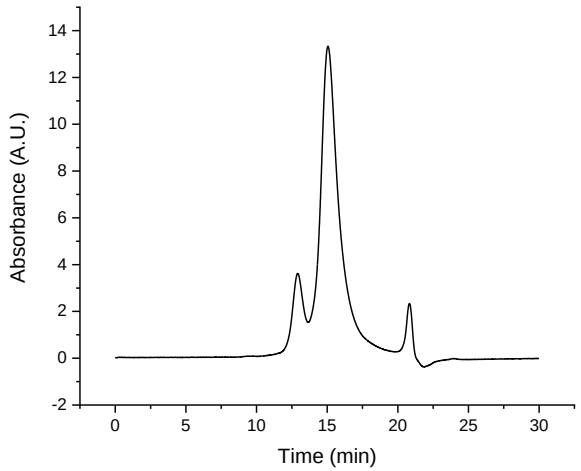

SE-HPLC chromatogram of Gammagard IVIG dilution to 0.5 mg/mL in 5 mM sodium citrate buffer pH 5 containing 154 mM sodium chloride. IVIG monomer eluted at approximately 15 minutes while the dimer eluted at 13 minutes. An additional buffer peak can be observed after 20 minutes. IVIG formulations contained approximately 14% dimer.

Operating parameters and example chromatogram for IL-1ra

SE-HPLC Operating Parameters for IL-1ra Formulations		
Pump	Elution	Isocratic
	Flow Rate	0.6 mL/min
	Seal Wash	10% isopropyl alcohol in water
	Operating Pressure	~30 bar
	Pressure Limit	75 bar
Detector	Monitored Wavelength	280 nm
Autosampler/Injector	Injection Volume	50 µL
	Autosampler Temperature	4 °C
	Needle Wash	Water
	Draw Position	3 mm
	Injection Speed	200 µL/min
Column	Column Temperature	20 °C
	Column	TSKgel G3000SWXL
	Guard Column	TSKgel Guard Column
Mobile Phase	-	10 mM sodium citrate buffer pH 6.6 with 140 mM NaCl

Example chromatogram for Interluekin-1 receptor antagonist (IL-1ra)

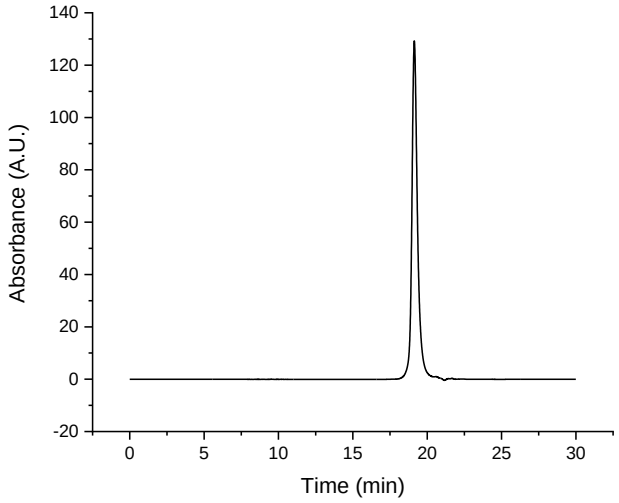

IL-1ra eluted after 19 minutes and showed no evidence of any higher order oligomers in the stock solution provided by Amgen and stored in the ultralow temperature freezer.

Note: All chromatograms were collected using an Agilent 1100 HPLC system with a variable wavelength detector.

A.5 Measuring Protein Concentrations with the Pierce 660 nm Protein Assay

Background

The Pierce 660 nm protein assay provides a simple and efficient microplate-based method for quickly determine the concentration of protein samples. This method is dependent on the binding of a dye-metal complex to proteins resulting in shift in the absorbance maxima of this complex from 450 to 600 nm. This method has proven especially useful for measuring protein binding isotherms where you may be only interested in protein concentration rather than the formation of insoluble oligomers.

Note: a distinct advantage of this method compare to other protein assays is its compatibility with a variety of detergents, chelating agents and reducing agents

Protocol

1. Prepare your samples and include protein standards with known concentrations. Ideally your standard curve should span the entire concentration range of your samples and include at least 5 points. Note the linear range of the 660 nm protein assay in a microplate formation is 25-2000 µg/mL
2. Add 10 ul of each sample and standard to a 96 well plate
3. As a blank add 10 µL of your buffer solution without protein 3-4 empty wells
4. Using a multichannel pipette added 150 µL of the 660 nm protein assay reagent to each well. As you add the reagent quickly mix the solution using the pipette.
5. After adding reagent to each well immediately cover the plate and mix for on a plate shaker for 1 minutes.
6. Incubate the plate for 5 minutes at room temperature before measuring the absorbance at 660 nm using a plate reader.
7. Average and subtract blank from absorbance measurements for both samples and standards
8. Plot protein standards and use relationship between protein concentration and absorbance to calculate the concentration of unknown samples.

Standard Curves for IVIG and IL-1ra

Standard curve for IVIG

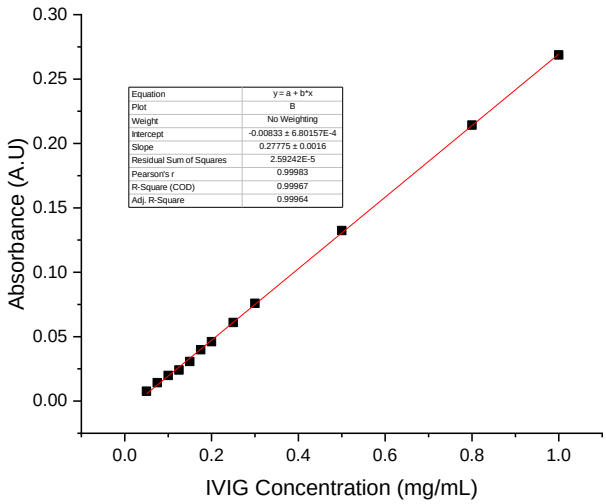

Standard Curve for IL-1ra